

# A BASIS FOR DISCRETIZATIONS

Robert Struijs\*

6 January 2010

**Abstract.** We discuss approximations of a given order of accuracy to first and higher derivatives on a structured grid in  $N$  dimensions using a basis of stencils. The basis of stencils follows from a truncated Taylor series expansion of the nodal values when the extent and the consistency of the approximation are imposed, together with the order of the error. The approximations include points which do not lie on grid lines passing through the point of discretization. Examples of such discretizations are diagonal discretizations, and a generalization of the formulation of Hildebrand. The basis of stencils is a convenient tool for generating and optimizing discretizations. The optimization is for the truncation error, or for stability and time step. In problems with a preferential direction such as the advection equation, the approximations are directional discretizations. The reduction of directional components of the truncation error leads to streamline approximations. Significant error reductions are possible, but they require a very regular grid. The stability and the time step in three dimensions increases threefold. The optimizations also apply to unstructured grids, but the computational advantage in three dimensions is marginal. The limiting functions for the grid-based derivatives are coupled, which complicates their solution.

**Key words:** Discretization, basis, streamline, limiter.

**AMS subject classification:** 65M06.

## 1. Introduction.

The subject of this paper is approximations to first and higher derivatives on a structured grid in  $N$  dimensions. The classical one-dimensional grid-aligned approximations restrict the nodes to the grid coordinate lines passing through the point where the approximation of the derivative is needed. The new approximations include nodes in the stencil beyond the grid coordinate lines, which improves accuracy and stability. Discretizations based on the same ideas are then developed for unstructured grids.

The search for improved discretizations has been going on for at least thirty years, see e.g. [1]–[6], and references therein. These efforts for the discretization of the advection equation are on structured and unstructured grids in the Finite Difference (FD), the Finite Volume (FV), the Finite Element (FE), and the Residual Distribution (RD) formulation.

The Flux Vector Distribution (FVD) approach is described in [7], with discretizations derived on unstructured and structured grids. Only distribution with the N scheme has been considered. This is an unnecessary restriction, and leads to inconsistent approximations on unstructured grids consisting of tetrahedra. The diagonal central second order discretization which has been found is an eye opener. Until now, it is tacitly assumed that only upwind discretizations can benefit from information supplied by the advection direction.

We start with a presentation of diagonal discretizations for the first derivative of any order of accuracy. Diagonal discretizations can also be obtained with a generalization of the formulation of Hildebrand. They form a class of one-dimensional approximations which in a natural way incorporate points which lie on diagonals of the grid. The theory of limiters is extended to directional discretizations. The limiting functions for the grid-based derivatives are coupled, which complicates their solution.

---

\*Dimitanis 14, 14564 N. Kifissia, Greece; robert.struijs@free.fr. ©Robert Struijs 2010.

A more general approach for an approximation is to consider a cluster of grid points going beyond the grid lines or diagonals passing through the point of approximation. The nodal values are developed in a truncated Taylor series expansion with respect to the point of discretization. The conditions of consistency of the approximation and the order of the error restrict the desired approximation to a basis of stencils. The basis of stencils represent degrees of freedom in the choice of the approximation of a derivative. With a basis of stencils, a systematic exploration of an approximation becomes possible. Various properties of the approximation are now easily accessible for optimization such as accuracy, stability, and the time step. The purpose is that the optimizations will lead to the use of coarser grids, or result in faster convergence, which translates into a reduction of the computational cost for the same quantitative result.

In problems with a preferential direction such as the advection equation, the approximations are directional discretizations. This application of a basis of stencils is the major subject of this paper. For optimization of the approximation, the error term is expressed in an axis system tied to the advection direction. We can obtain first and higher directional derivatives, both pure and mixed. The stencil of the approximation follows the flow direction, like the classical upwind discretizations, but now also for some central discretizations. An important constraint is continuity of the discretization when a variation of the flow direction triggers a change of stencil.

For the steady state solution of an advection equation, error terms which contain a streamline component are unimportant. The degrees of freedom of the basis of stencils can be used in some cases to eliminate the remaining low-order error terms which are normal to the streamline. The result is a streamline approximation to the derivative with an increased order of accuracy. This has been proposed by Sidilkover [8] for advection problems, but the approach has more general applications. For some central approximations the improvement is two orders of accuracy, with the additional advantage that for systems of equations no decomposition or wave model is needed. Following established practice, for unsteady problems we apply this method in a space of one lower dimension, and we interpret the suppressed space coordinate as the time axis.

However, this streamline error reduction is based on perfectly regular grids, and in practical applications the gains are limited, except for the FD formulation. Mapping to a uniform grid is possible, but only partly restores accuracy on a fairly smooth grid.

For adirectional problems, such as e.g. an approximation involving a Laplacian, the grid-based representation can be used for the error reduction. This has been exploited by Dahlquist and Bjork [9]. The error reductions can be important.

The analysis and optimization of the approximation can also take place in the Fourier domain. We consider stability properties and the time step, which are closely related to the propagation properties of waves. For an advection equation, the time step restriction is improved from  $\Delta t \sim (\sum |a_i|)^{-1}$  to  $\Delta t \sim (\max |a_i|)^{-1}$ , where  $a_i$  are the velocity components. In three dimensions, this improves the stability threefold. The gain in time step for both steady and unsteady problems is less sensitive to irregular grids. The amplification of error components can be reduced for the errors with high frequencies, which improves convergence when a multi-grid solver is used.

Optimization of the truncation error can entail improvement in the Fourier domain and vice versa. For a given application, a balance has to be struck between both types of optimization.

## 2. Directional discretizations.

We start by giving an expression of diagonal discretizations of the first derivative at point  $P$ . This point is situated at node  $(i, j, k, \dots)$  on a structured grid in  $N$  dimensions with basis  $G(\vec{x}, \vec{y}, \vec{z}, \dots)$  and grid spacings  $\Delta x, \Delta y, \Delta z, \dots$ . We wish to approximate a first derivative of  $u$  in a preferential direction. The preferential direction is e.g. the advection direction of a flow,  $\vec{a} = (a_x, a_y, a_z, \dots)^T$ . Therefore, we define a directional local basis  $B(\vec{e}_1, \vec{e}_2, \vec{e}_3, \dots)$  of curvilinear coordinates which has the unit vector  $\vec{e}_1$  along the preferential direction, i.e.  $\vec{e}_1 = \vec{a}/a$ , where  $a$  is the magnitude of the velocity. In an advection equation, we encounter the stream-wise derivative  $\vec{a} \cdot \vec{\nabla} u = a\vec{e}_1 \cdot \vec{\nabla} u = a\partial u/\partial e_1$ . The approximation of the derivative  $\partial u/\partial e_1$  is expressed in grid-based derivatives  $u_x, u_y, u_z, \dots$ . The purpose is to choose each of the derivatives  $u_x, u_y, u_z, \dots$  in such a way that the error in the discretization of the combination  $\partial u/\partial e_1$  is reduced for certain advection directions.

### 2.1. A general diagonal discretization.

In the one-dimensional grid-aligned approximation, the error is least when the flow is along a grid line. The reason is that the approximation is then based on nodes along a streamline. This eliminates the presence of cross-wind error terms. The idea behind diagonal discretizations is to extend this property for flow along diagonals of the grid. We choose the following combination of  $u_x, u_y, u_z, \dots$  for the approximation of  $\partial u/\partial e_1$ .

Consider the case that the flow is along the  $x$ -axis,  $\vec{e}_1 = (1, 0, 0, \dots)^T$ . Since  $\partial u/\partial e_1 = \vec{e}_1 \cdot \vec{\nabla} u = u_x$  we look for a discretization of  $u_x$  which only uses nodes on the  $x$ -axis,

$$(u_x)_{i,j,k,\dots} = \frac{1}{\Delta x} \left\{ a_{-m} u_{i-m,j,k,\dots} + a_{-m+1} u_{i-m+1,j,k,\dots} + \dots + a_{n-1} u_{i+n-1,j,k,\dots} + a_n u_{i+n,j,k,\dots} \right\}. \quad (2.1)$$

Equation (2.1) represents a general approximation of a first derivative taking a stencil on the  $x$ -axis with an extent of  $(i-m, \dots, i+n)$  using coefficients  $a_{-m}, \dots, a_n$ . This is shown in Fig. 2.1, where the nodes with their respective weights are indicated, omitting the part  $j, k, \dots$  in the nodal indices. The position of point  $P$  is at node  $i$  as indicated in this, and in the following figures.

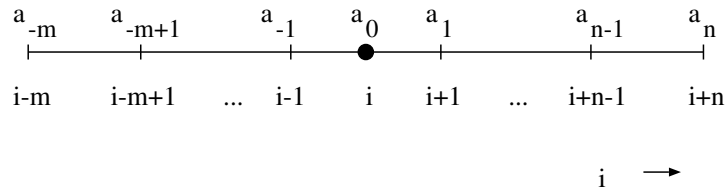


Figure 2.1. The nodes on the  $x$ -axis involved in the derivative  $u_x$  of (2.1) with their respective weights.

Next, consider the case that the flow is along the diagonal in the  $x$ - $y$  plane. This means that  $\vec{e}_1 = (\Delta x, \Delta y, 0, \dots)^T/\Delta d_1$ , with  $\Delta d_1^2 = \Delta x^2 + \Delta y^2$ , and  $\vec{e}_1 \cdot \vec{\nabla} u = (u_x \Delta x + u_y \Delta y)/\Delta d_1$ .

We take now a discretization which only uses nodes on that diagonal,

$$\frac{u_x \Delta x + u_y \Delta y}{\Delta d_1} = \frac{1}{\Delta d_1} \left\{ a_{-m} u_{i-m, j-m, k, \dots} + a_{-m+1} u_{i-m+1, j-m+1, k, \dots} + \dots \right. \\ \left. + a_{n-1} u_{i+n-1, j+n-1, k, \dots} + a_n u_{i+n, j+n, k, \dots} \right\}. \quad (2.2)$$

The discretization uses for the points on the diagonal the same coefficients as in (2.1). This is shown in Fig. 2.2, where the nodes with their respective weights are indicated, omitting the part  $k, \dots$  in the nodal indices.

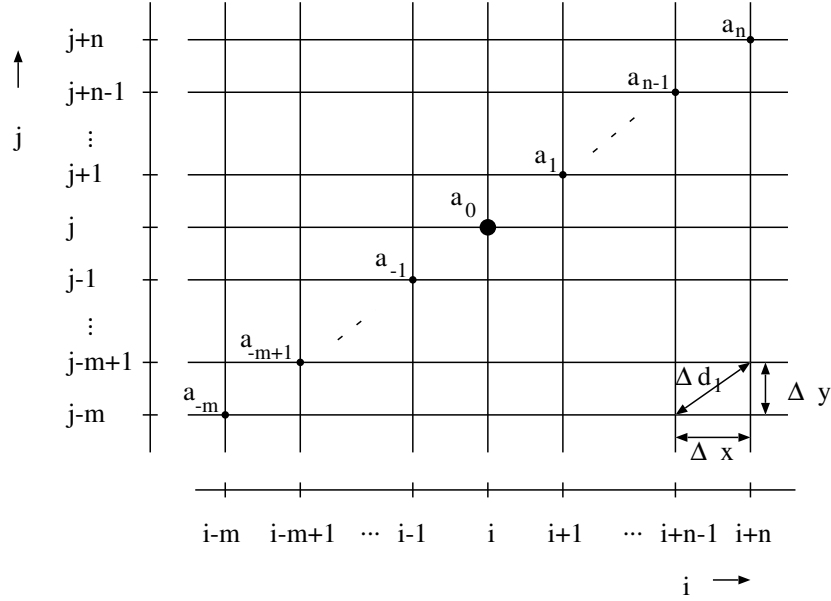


Figure 2.2. The nodes in the  $x$ - $y$ -plane along the diagonal involved in the derivative of (2.2) with their respective weights.

Since  $u_x$  is defined by (2.1), a subtraction gives

$$(u_y)_{i,j,k,\dots} = \frac{1}{\Delta y} \left\{ \begin{aligned} & a_{-m} (u_{i-m, j-m, k, \dots} - u_{i-m, j, k, \dots}) \\ & + a_{-m+1} (u_{i-m+1, j-m+1, k, \dots} - u_{i-m+1, j, k, \dots}) \\ & + \dots \\ & + a_{n-1} (u_{i+n-1, j+n-1, k, \dots} - u_{i+n-1, j, k, \dots}) \\ & + a_n (u_{i+n, j+n, k, \dots} - u_{i+n, j, k, \dots}) \end{aligned} \right\}. \quad (2.3)$$

This derivative is schematically indicated in Fig. 2.3, where the coefficient  $a_n$  is the weight which is applied to the difference of the points  $i+n, j+n, k, \dots$  and  $i+n, j, k, \dots$ , and so on.

This procedure can be repeated for the body diagonal in  $x$ - $y$ - $z$  space, which gives

$$(u_z)_{i,j,k,\dots} = \frac{1}{\Delta z} \left\{ \begin{aligned} & a_{-m} (u_{i-m, j-m, k-m, \dots} - u_{i-m, j-m, k, \dots}) \\ & + a_{-m+1} (u_{i-m+1, j-m+1, k-m+1, \dots} - u_{i-m+1, j-m+1, k, \dots}) \\ & + \dots \end{aligned} \right\}$$

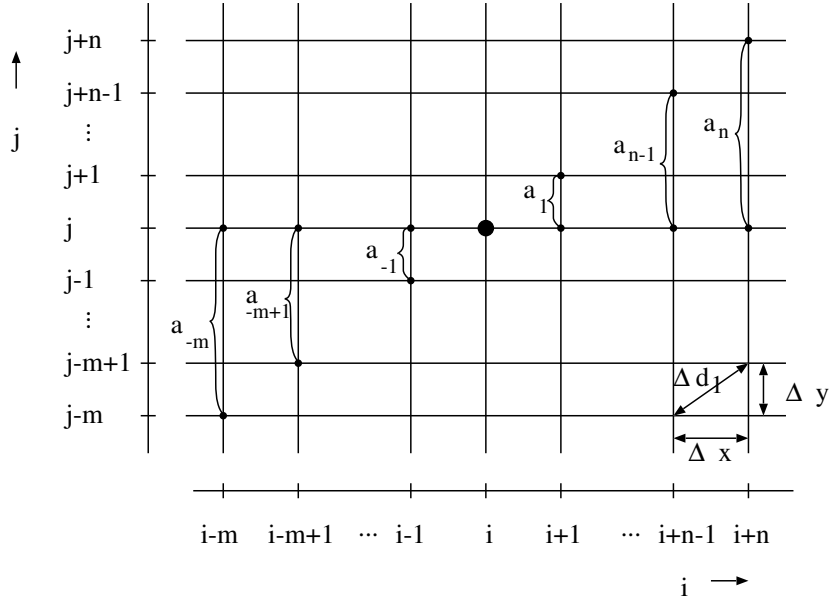


Figure 2.3. The nodes in the  $x$ - $y$ -plane involved in the  $u_y$  derivative of (2.3), which is the difference between the value on the diagonal and the  $x$ -axis, multiplied by their respective weights.

$$\begin{aligned}
 & + a_{n-1}(u_{i+n-1,j+n-1,k+n-1,\dots} - u_{i+n-1,j+n-1,k,\dots}) \\
 & + a_n(u_{i+n,j+n,k+n,\dots} - u_{i+n,j+n,k,\dots}) \quad \Bigg\}, \quad (2.4)
 \end{aligned}$$

and so on for each additional dimension.

The effect of this choice of stencils is that the approximation becomes one-dimensional when the flow is aligned with the  $x$ -axis or with one of the diagonals mentioned. The error term contains then only the stream-wise derivatives along  $\vec{e}_1$ , while the other derivatives are absent. This reduces the error in the approximation in a significant way compared to one-dimensional discretizations along grid lines only. Later on we will show that diagonal discretizations are applied with the optimal time step. Note that the node of discretization  $(i, j, k, \dots)$  appears only in  $u_x$ .

This discretization can be used for any flow direction, but its principal range of application is  $a_x/\Delta x \geq a_y/\Delta y \geq a_z/\Delta z \geq \dots \geq 0$ , and permutations thereof for other directions.

It is possible to create discretizations which are one-dimensional in other directions, e.g. the direction  $(2, 1)^T$  in the  $x$ - $y$ -plane. The condition is now that  $a_i = 0$  for  $i$  odd, since we want to use the same coefficients  $a_i$  both on the  $x$ -axis and on the nodes defined by the direction  $(2, 1)^T$ . This extra condition will have the effect that it lowers the maximum order of accuracy which can be obtained on a stencil of a given extent.

The diagonal discretization has the peculiarity that the stencil contains only points on grid lines and on diagonals, but not in between. The effect of inclusion of other points in the stencil will be discussed in §4. It is possible to construct approximations with the diagonal property which contain points outside diagonals and grid lines.

In the following, we will give some examples of diagonal discretizations, where again the position of point  $P$  is emphasized in the drawings.

### 2.2. A first order upwind diagonal discretization.

A first order diagonal upwind discretization in  $N$  dimensions is given by

$$\begin{aligned}
 (u_x)_{i,j,k,\dots} &= \frac{1}{\Delta x} (u_{i,j,k,\dots} - u_{i-1,j,k,\dots}), \\
 (u_y)_{i,j,k,\dots} &= \frac{1}{\Delta y} (u_{i-1,j,k,\dots} - u_{i-1,j-1,k,\dots}), \\
 (u_z)_{i,j,k,\dots} &= \frac{1}{\Delta z} (u_{i-1,j-1,k,\dots} - u_{i-1,j-1,k-1,\dots}), \\
 &\vdots
 \end{aligned} \tag{2.5}$$

This discretization is a special case of (2.1), (2.3), and (2.4), with  $m = 1$ ,  $n = 0$ ,  $a_{-1} = -1$ , and  $a_0 = 1$ . The stencils for this discretization in two dimensions are shown in Fig. 2.4, and in three dimensions in Fig. 2.5 for the case  $a_x/\Delta x \geq a_y/\Delta y \geq a_z/\Delta z \geq \dots \geq 0$ .



Figure 2.4. The stencils for the derivatives  $u_x$  and  $u_y$  of (2.5) in two dimensions.

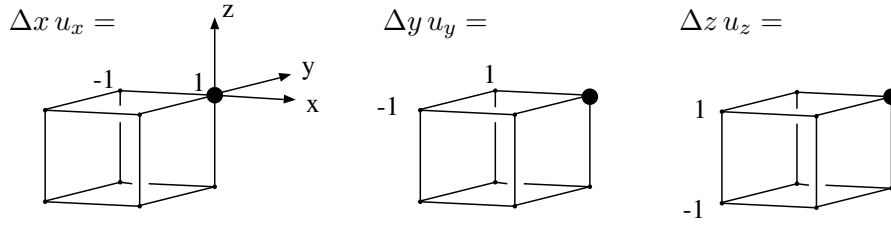


Figure 2.5. The stencils for the derivatives  $u_x$ ,  $u_y$ , and  $u_z$  of (2.5) in three dimensions.

This discretization has a history of some twenty years [4, 8] and is nowadays called the N scheme. Of the above class of discretizations, it is the only one which is currently known. An analysis of this discretization is presented in [10].

### 2.3. A second order central diagonal discretization.

A second order diagonal central discretization in  $N$  dimensions is given by

$$\begin{aligned}
 (u_x)_{i,j,k,\dots} &= \frac{1}{2\Delta x} (u_{i+1,j,k,\dots} - u_{i-1,j,k,\dots}), \\
 (u_y)_{i,j,k,\dots} &= \frac{1}{2\Delta y} (u_{i+1,j+1,k,\dots} - u_{i+1,j,k,\dots} + u_{i-1,j,k,\dots} - u_{i-1,j-1,k,\dots}), \\
 (u_z)_{i,j,k,\dots} &= \frac{1}{2\Delta z} (u_{i+1,j+1,k+1,\dots} - u_{i+1,j+1,k,\dots} + u_{i-1,j-1,k,\dots} - u_{i-1,j-1,k-1,\dots}), \\
 &\vdots
 \end{aligned} \tag{2.6}$$

This discretization is a special case of (2.1), (2.3), and (2.4), with  $m = n = 1$ ,  $a_{-1} = -1/2$ ,  $a_0 = 0$ , and  $a_1 = 1/2$ . This discretization has been derived in two dimensions in [7]. It is

the average of two first order upwind discretizations, (2.5), for advection speeds  $\vec{a}$  and  $-\vec{a}$ . The stencils for this discretization in two dimensions are shown in Fig. 2.6, and in three dimensions in Fig. 2.7.

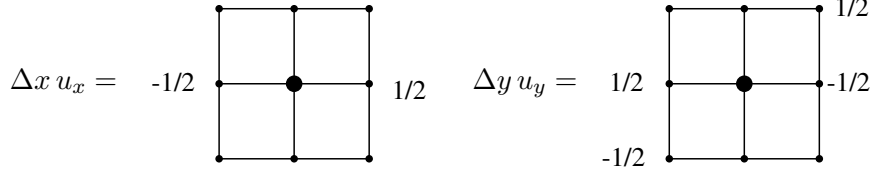


Figure 2.6. The stencils for the derivatives  $u_x$  and  $u_y$  of (2.6) in two dimensions.

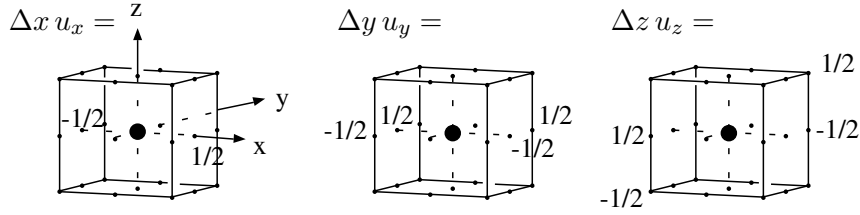


Figure 2.7. The stencils for the derivatives  $u_x$ ,  $u_y$ , and  $u_z$  of (2.6) in three dimensions.

#### 2.4. A second order upwind diagonal discretization.

A second order diagonal upwind discretization is given by

$$\begin{aligned}
 (u_x)_{i,j,k,\dots} &= \frac{1}{\Delta x} \left( \frac{3}{2} u_{i,j,k,\dots} - 2u_{i-1,j,k,\dots} + \frac{1}{2} u_{i-2,j,k,\dots} \right), \\
 (u_y)_{i,j,k,\dots} &= \frac{1}{\Delta y} \left( -2(u_{i-1,j-1,k,\dots} - u_{i-1,j,k,\dots}) + \frac{1}{2}(u_{i-2,j-2,k,\dots} - u_{i-2,j,k,\dots}) \right), \\
 (u_z)_{i,j,k,\dots} &= \frac{1}{\Delta z} \left( -2(u_{i-1,j-1,k-1,\dots} - u_{i-1,j-1,k,\dots}) + \frac{1}{2}(u_{i-2,j-2,k-2,\dots} - u_{i-2,j-2,k,\dots}) \right), \\
 &\vdots
 \end{aligned} \tag{2.7}$$

This discretization is a special case of (2.1), (2.3), and (2.4), with  $m = 2$ ,  $n = 0$ ,  $a_{-2} = 1/2$ ,  $a_{-1} = -2$ , and  $a_0 = 3/2$ . The stencils for this discretization in two dimensions are shown in Fig. 2.8, and in three dimensions in Fig. 2.9.

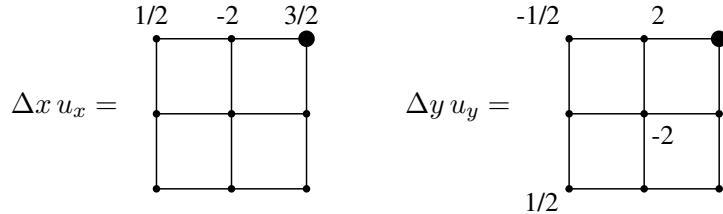


Figure 2.8. The stencils for the derivatives  $u_x$  and  $u_y$  of (2.7) in two dimensions.

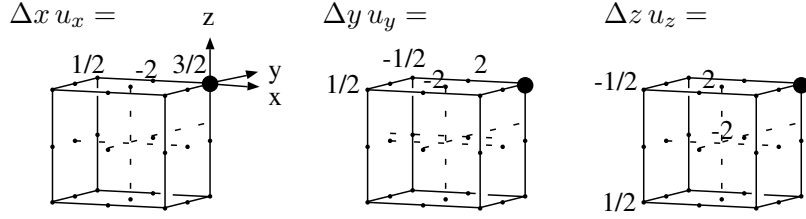


Figure 2.9. The stencils for the derivatives  $u_x$ ,  $u_y$ , and  $u_z$  of (2.7) in three dimensions.

### 2.5. A third order upwind biased diagonal discretization.

A third order diagonal upwind biased discretization is given by

$$\begin{aligned}
 (u_x)_{i,j,k,\dots} &= \frac{1}{6\Delta x} \left( u_{i-2,j,k,\dots} - 6u_{i-1,j,k,\dots} + 3u_{i,j,k,\dots} + 2u_{i+1,j,k,\dots} \right), \\
 (u_y)_{i,j,k,\dots} &= \frac{1}{6\Delta y} \left( \begin{aligned} &u_{i-2,j-2,k,\dots} - u_{i-2,j,k,\dots} \\ &-6(u_{i-1,j-1,k,\dots} - u_{i-1,j,k,\dots}) \\ &+3(u_{i,j,k,\dots} - u_{i,j,k,\dots}) \\ &+2(u_{i+1,j+1,k,\dots} - u_{i+1,j,k,\dots}) \end{aligned} \right), \\
 (u_z)_{i,j,k,\dots} &= \frac{1}{6\Delta z} \left( \begin{aligned} &u_{i-2,j-2,k-2,\dots} - u_{i-2,j-2,k,\dots} \\ &-6(u_{i-1,j-1,k-1,\dots} - u_{i-1,j-1,k,\dots}) \\ &+3(u_{i,j,k,\dots} - u_{i,j,k,\dots}) \\ &+2(u_{i+1,j+1,k+1,\dots} - u_{i+1,j+1,k,\dots}) \end{aligned} \right), \\
 &\vdots
 \end{aligned} \tag{2.8}$$

This discretization is a special case of (2.1), (2.3), and (2.4), with  $m = 2$ ,  $n = 1$ ,  $a_{-2} = 1/6$ ,  $a_{-1} = -1$ ,  $a_0 = 1/2$ , and  $a_1 = 1/3$ . The stencils for this discretization in two dimensions are shown in Fig. 2.10.

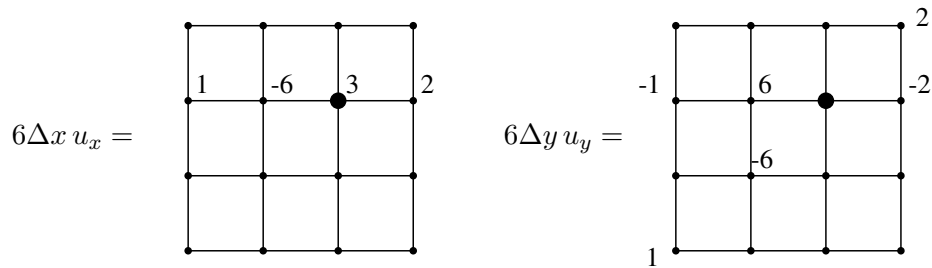


Figure 2.10. The stencils for the derivatives  $u_x$  and  $u_y$  of (2.8) in two dimensions.

**2.6. A fourth order central diagonal discretization.**

$$\begin{aligned}
 (u_x)_{i,j,k,\dots} &= \frac{1}{12\Delta x} \left( u_{i-2,j,k,\dots} - 8u_{i-1,j,k,\dots} + 8u_{i+1,j,k,\dots} - u_{i+2,j,k,\dots} \right), \\
 (u_y)_{i,j,k,\dots} &= \frac{1}{12\Delta y} \left( \begin{aligned} &u_{i-2,j-2,k,\dots} - u_{i-2,j,k,\dots} \\ &-8(u_{i-1,j-1,k,\dots} - u_{i-1,j,k,\dots}) \\ &+8(u_{i+1,j+1,k,\dots} - u_{i+1,j,k,\dots}) \\ &-(u_{i+2,j+2,k,\dots} - u_{i+2,j,k,\dots}) \end{aligned} \right), \\
 (u_z)_{i,j,k,\dots} &= \frac{1}{12\Delta z} \left( \begin{aligned} &u_{i-2,j-2,k-2,\dots} - u_{i-2,j-2,k,\dots} \\ &-8(u_{i-1,j-1,k-1,\dots} - u_{i-1,j-1,k,\dots}) \\ &+8(u_{i+1,j+1,k+1,\dots} - u_{i+1,j+1,k,\dots}) \\ &-(u_{i+2,j+2,k+2,\dots} - u_{i+2,j+2,k,\dots}) \end{aligned} \right), \\
 &\vdots
 \end{aligned} \tag{2.9}$$

This discretization is a special case of (2.1), (2.3), and (2.4), with  $m = n = 2$ ,  $a_{-2} = 1/12$ ,  $a_{-1} = -8/12$ ,  $a_0 = 0$ ,  $a_1 = 8/12$ , and  $a_2 = -1/12$ . The stencils for this discretization in two dimensions are shown in Fig. 2.11.

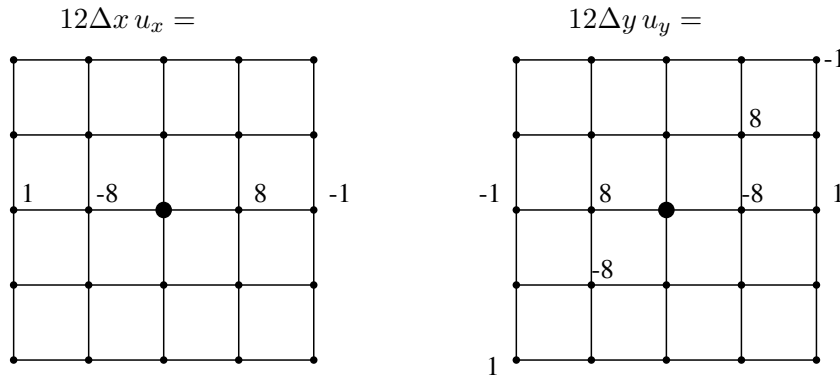


Figure 2.11. The stencils for the derivatives  $u_x$  and  $u_y$  of (2.9) in two dimensions.

**2.7. Other diagonal discretizations.**

From these few examples, the general idea will be clear. The formulation allows to extend a one-dimensional discretization to a diagonal directional discretization. The list of possible candidates is long, which is why we have limited ourselves to those few examples. The discretizations can be used in any scheme.

Further on, we will analyze the discretizations given above as example, and we will look at the degrees of freedom which appear when we include nodes outside the axis and diagonals. The Lax-Wendroff scheme will be treated separately.

The higher order discretizations can be limited to the monotone first order diagonal discretization, as described in appendix A.

### 3. A generalization of the formulation of Hildebrand.

A formulation which generates one-dimensional discretizations has been given by Hildebrand [11], which we can generalize to  $N$  dimensions as follows.

The starting point is a Taylor series expansion [12], which expresses the unknown  $u(\vec{r} + \Delta\vec{r})$  in  $u(\vec{r})$ , the displacement  $\Delta\vec{r}$  and space derivatives,

$$u(\vec{r} + \Delta\vec{r}) = \left(1 + \nabla_r + \frac{\nabla_r^2}{2!} + \frac{\nabla_r^3}{3!} + \dots\right)u(\vec{r}). \quad (3.1)$$

The projection of the gradient  $\vec{\nabla} = (\partial/\partial x, \partial/\partial y, \partial/\partial z, \dots)^T$  on the displacement vector  $\Delta\vec{r}$  is  $\nabla_r = \Delta\vec{r} \cdot \vec{\nabla}$ . We restrict the displacement vector  $\Delta\vec{r}$  to discrete jumps between nodes  $(i, j, k, \dots)$  and  $(l, m, n, \dots)$  on the grid. The grid difference vector  $\vec{g}_d = (l - i, m - j, n - k, \dots)^T$  of the grid indices will be used to express the displacement vector. We introduce the grid spacing diagonal matrix  $D_g = \text{diag}(\Delta x, \Delta y, \Delta z, \dots)$  to write  $\Delta\vec{r} = D_g \cdot \vec{g}_d = ((l - i)\Delta x, (m - j)\Delta y, (n - k)\Delta z, \dots)^T$ , and  $\nabla_r$  as  $\nabla_r = (l - i)\Delta x \partial/\partial x + (m - j)\Delta y \partial/\partial y + (n - k)\Delta z \partial/\partial z + \dots$ . Remark that  $\nabla_r$  is a function of all the space derivatives.

In operator form, the displacement is represented by  $E_{\Delta\vec{r}}u(\vec{r}) = u(\vec{r} + \Delta\vec{r})$ . On the grid, this means that  $E_{\Delta\vec{r}}u_{i,j,k,\dots} = u_{l,m,n,\dots}$ . The Taylor series (3.1) can be condensed to  $E_{\Delta\vec{r}} = e^{\nabla_r}$ , which leads to

$$\nabla_r = \ln E_{\Delta\vec{r}} = -\ln E_{-\Delta\vec{r}}, \quad (3.2)$$

since  $E_{\Delta\vec{r}} = E_{-\Delta\vec{r}}^{-1}$ .

We need at least  $N$  different vectors  $\vec{g}_d$  or  $\Delta\vec{r}$  in order to obtain all the  $N$  space derivatives present in  $\nabla_r$  of (3.2). In the one-dimensional case, the choice of vectors  $\vec{g}_d^{1D}$  is the set of axes,  $(1, 0, 0, \dots)^T$ ,  $(0, 1, 0, \dots)^T$ , etc, which decouples the space derivatives in (3.2). For diagonal directional discretizations, the choice of vectors  $\vec{g}_d^{diag}$  is the  $x$ -axis and diagonals,  $(1, 0, 0, \dots)^T$ ,  $(1, 1, 0, \dots)^T$ , etc, and the various space derivatives are found by subtraction, like in §2.

The next step is to write the displacement operator  $E_{\Delta\vec{r}}$  in (3.2) as a function of a difference operator in the direction  $\Delta\vec{r}$ . The difference operator can be e.g. a forward difference operator, a backward difference operator or a central difference operator. In the one-dimensional case, the difference operators generate differences along the various axes; for the diagonal case, the differences are along the  $x$ -axis and diagonals. As an example, consider the vectors of backward differences

$$\vec{d}_{1D}^- = \begin{pmatrix} u_{i,j,k,\dots} - u_{i-1,j,k,\dots} \\ u_{i,j,k,\dots} - u_{i,j-1,k,\dots} \\ u_{i,j,k,\dots} - u_{i,j,k-1,\dots} \\ \vdots \end{pmatrix} \quad \text{and} \quad \vec{d}_{diag}^- = \begin{pmatrix} u_{i,j,k,\dots} - u_{i-1,j,k,\dots} \\ u_{i-1,j,k,\dots} - u_{i-1,j-1,k,\dots} \\ u_{i-1,j-1,k,\dots} - u_{i-1,j-1,k-1,\dots} \\ \vdots \end{pmatrix}, \quad (3.3)$$

where for the diagonal differences we have taken the differences of (2.5). The difference operator is  $d^- = \vec{g}_d \cdot \vec{d}^-$ , where  $\vec{g}_d$  is one of the  $N$  vectors which are needed to find the  $N$  space derivatives, and  $\vec{d}^-$  is one of the expressions of (3.3). Then, we have  $E_{-\Delta\vec{r}} = 1 - d^-$ . The logarithm of (3.2) can be expanded in the series  $-\ln(1 - d) = d + d^2/2 + d^3/3 + \dots$ , and the approximation for  $\nabla_r$  becomes

$$\nabla_r = d^- + \frac{(d^-)^2}{2} + \frac{(d^-)^3}{3} + \dots. \quad (3.4)$$

To the lowest order, we have for the diagonal case  $\nabla_r u_{i,j,k,\dots} = d_{diag}^- u_{i,j,k,\dots}$ , which gives us back the discretization of (2.5). Including the second term in eq. (3.4) gives the second order upwind discretization of (2.7).

The generalization of the formalism of Hildebrand can be extended with the diagonal forward difference,

$$\vec{d}^+ = \begin{pmatrix} u_{i+1,j,k,\dots} - u_{i,j,k,\dots} \\ u_{i+1,j+1,k,\dots} - u_{i+1,j,k,\dots} \\ u_{i+1,j+1,k+1,\dots} - u_{i+1,j+1,k,\dots} \\ \vdots \end{pmatrix}, \quad (3.5)$$

the diagonal central difference  $\vec{d}^c = 1/2(\vec{d}^+ + \vec{d}^-)$ ,

$$\vec{d}^c = \frac{1}{2} \begin{pmatrix} u_{i+1,j,k,\dots} - u_{i-1,j,k,\dots} \\ u_{i+1,j+1,k,\dots} - u_{i+1,j,k,\dots} + u_{i-1,j,k,\dots} - u_{i-1,j-1,k,\dots} \\ u_{i+1,j+1,k+1,\dots} - u_{i+1,j+1,k,\dots} + u_{i-1,j-1,k,\dots} - u_{i-1,j-1,k-1,\dots} \\ \vdots \end{pmatrix}, \quad (3.6)$$

and the diagonal half-integer formulations

$$\vec{d}^{h-} = \begin{pmatrix} u_{i,j,k} - u_{i-1/2,j,k} \\ u_{i-1/2,j,k} - u_{i-1/2,j-1/2,k} \\ u_{i-1/2,j-1/2,k} - u_{i-1/2,j-1/2,k-1/2} \\ \vdots \end{pmatrix}, \quad (3.7)$$

and similar for the diagonal forward and central differences  $\vec{d}^{h+}$  and  $\vec{d}^{hc}$ . The abbreviations  $E = E_{\Delta\vec{r}}$ ,  $E^- = E_{-\Delta\vec{r}} = E^{-1}$ , and powers of  $E$  such as  $E^{-1/2}$  are used in relations between the difference operators,

$$\begin{aligned} d^+ &= E - 1, & d^c &= \frac{1}{2}(E - E^{-1}), \\ d^- &= 1 - E^{-1}, & d^+ d^- &= d^- d^+ = d^+ - d^- = (d^{hc})^2, \\ d^- &= E^{-1} d^+, & d^{hc} &= d^c \left\{ 1 + \frac{1}{4} (d^{hc})^2 \right\}^{-1/2}, \end{aligned} \quad (3.8)$$

which are the one-dimensional relations.

The generalization of the formalism of Hildebrand amounts to extending the difference operators and the shift operator to more dimensions. To obtain the  $N$  individual derivatives, the formulation has to be applied  $N$  times with the complete set of grid differences  $\vec{g}_d$ . Instead of using diagonal differences, other differences can be applied which incorporate nodes which do not lie on grid axes or diagonals. Examples of such approximations are given in §5 and §6.

The first derivatives of the previous section have been found with the generalization of the formulation of Hildebrand. We can use the new formulation also to generate higher directional derivatives. For mixed derivatives we use permutations of (3.3), (3.5), (3.6), and (3.7) since we need derivatives along  $e_2, e_3, \dots$ . When using the half-integer differences, the resulting derivative can be transferred to the nodes by the use of interpolations. Some examples of higher derivatives are given in §5 and §6.

#### 4. Derivatives devised with a basis of stencils.

The idea of directional discretizations is to reduce for certain preferential directions some error terms in the approximation, or to optimize in the Fourier domain. The previous two sections gave prescriptions how to generate such discretizations in a somewhat abstract and formal way. A more general approach is to use the error in the discretization as a tool to find and analyze discretizations, directional or adirectional. This includes diagonal discretizations.

The present approach exploits a basis of stencils to describe all the possible discretizations which approximate a certain derivative. The basis of stencils follows from a truncated Taylor series expansion on a cluster of nodes. The extent and the consistency of the approximation is imposed together with the order of the error. The basis of stencils which is used in the approximation of a derivative is a convenient tool for generating and optimizing discretizations. The method applies also to higher derivatives.

The Taylor series expansion (3.1) is a standard tool to analyze and generate one-dimensional discretizations, without the invocation of a basis of stencils. The concept of a basis, even if not explicitly mentioned, can be discerned in numerical literature. This is mostly for first order upwind discretizations in two or three dimensions, or second order approximations in two space dimensions. The absence of a basis of stencils in more than one dimension may be an explanation that with few exceptions the Taylor series has been used to analyze a given discretization, instead of being involved in the generation of multi-dimensional approximations. Sidilkover [8] discusses limited upwind discretizations on a small stencil in two dimensions, and later with Roe in three dimensions [10]. Hirsch [13] applies the Taylor series to analyze a nine point stencil. Koren [14] has used the basis on a  $2 \times 2$  grid to generate and analyze upwind discretizations. They all come close to the concept of a basis of stencils in more than one dimension. These publications focus on reducing the cross wind derivatives in the error of the approximation, since this improves the accuracy of the solution of an advection equation.

##### 4.1. The derivative expressed in a series related to the preferential direction.

In the Finite Difference method, a general expression for the approximation  $D_p$  of a  $p^{\text{th}}$  derivative at the node with indices  $(i, j, k, \dots)$  is

$$D_p = \sum_{l,m,n,\dots \in S} C_{l,m,n,\dots} u_{l,m,n,\dots} . \quad (4.1)$$

The approximation of the derivative is a linear combination of the values  $u_s$  at the points of the stencil  $S$  with weights  $C_{l,m,n,\dots}$ . We develop each of the values  $u_s$  into a truncated Taylor series with respect to the point  $P$  where the approximate derivative is sought. The series is expressed in the local orthogonal basis  $B$ , showing clearly various contributions of derivatives along the local axes. This enables us to choose a combination of points and weights which minimizes certain error terms. For approximations to derivatives which do not depend on a preferential direction, we take the basis  $B$  aligned with the grid axes.

The expansion of the nodal values in a series takes place in two steps. First, we apply the Taylor series expansion of (3.1) to the nodes  $u_s$  of the stencil in the grid-based coordinate system  $G$ . Then, we apply a coordinate transformation to the local basis  $B$ . This means

that for a certain point  $u_s$  with indices  $(l, m, n, \dots)$  in (4.1), we write

$$u_{l,m,n,\dots} = u_{i,j,k,\dots} + \sum_{r=1}^{r_{\max}} \frac{1}{r!} \left( (l-i)\Delta x \frac{\partial}{\partial x} + (m-j)\Delta y \frac{\partial}{\partial y} + (n-k)\Delta z \frac{\partial}{\partial z} + \dots \right)^r u, \quad (4.2)$$

where the error in  $u_{l,m,n,\dots}$  depends on the last term in the series, which is determined by the upper limit in the summation,  $r_{\max}$ . The term between brackets in (4.2) can be written as

$$(q_1 + q_2 + q_3 + \dots)^r = \sum_{n_1, n_2, n_3, \dots} \frac{r!}{n_1! n_2! n_3! \dots} q_1^{n_1} q_2^{n_2} q_3^{n_3} \dots, \quad (4.3)$$

where the sum is over all non-negative integers  $n_1, n_2, n_3, \dots$  for which  $n_1 + n_2 + n_3 + \dots = r$ .

The partial derivatives appearing in the truncated Taylor series expansions can be rewritten in derivatives of the local basis  $B$ . We consider here a rotation between  $B$  and  $G$ , with the linear coordinate transformation

$$\begin{aligned} x &= t_{1,1}e_1 + t_{1,2}e_2 + t_{1,3}e_3 + \dots, \\ y &= t_{2,1}e_1 + t_{2,2}e_2 + t_{2,3}e_3 + \dots, \\ z &= t_{3,1}e_1 + t_{3,2}e_2 + t_{3,3}e_3 + \dots, \\ &\vdots \end{aligned}, \quad (4.4)$$

where the coefficients  $t_{\alpha,\beta}$  depend on the angles between the two coordinate systems. The derivative of  $u$  with respect to both systems is derived from (4.4) as

$$\begin{aligned} \frac{\partial u}{\partial x} &= t_{1,1} \frac{\partial u}{\partial e_1} + t_{1,2} \frac{\partial u}{\partial e_2} + t_{1,3} \frac{\partial u}{\partial e_3} + \dots, \\ \frac{\partial u}{\partial y} &= t_{2,1} \frac{\partial u}{\partial e_1} + t_{2,2} \frac{\partial u}{\partial e_2} + t_{2,3} \frac{\partial u}{\partial e_3} + \dots, \\ \frac{\partial u}{\partial z} &= t_{3,1} \frac{\partial u}{\partial e_1} + t_{3,2} \frac{\partial u}{\partial e_2} + t_{3,3} \frac{\partial u}{\partial e_3} + \dots, \\ &\vdots \end{aligned}, \quad (4.5)$$

which can be used in (4.2). Finally, the expansion can be substituted in (4.1), and the coefficients  $C_{l,m,n,\dots}$  are adjusted such that  $D_p$  approximates the  $p^{\text{th}}$  derivative.

The choice of  $C_{l,m,n,\dots}$  is not unique. There are many criteria, of which the extent of the stencil, the desired truncation error, a specific behavior in the Fourier domain for stability and wave propagation properties, and computational cost are the most common. The art of designing numerical discretizations consists in finding the optimum for a given application among sometimes conflicting constraints. The extent of the stencil is especially important for multi-block solvers where a small stencil reduces data transfer between blocks.

For directional discretizations, an additional constraint is imposed: optimize the discretization by reducing for certain preferential directions unwanted terms in the error expressed in the local basis  $B$  of the approximation, or optimize in the Fourier domain. E.g. for a second order accurate approximation of the first derivative  $\partial u / \partial e_1$ , we will eliminate other terms than  $\partial^3 u / \partial e_1^3$  for the case that the flow is along the  $x$ -axis or diagonals, as described in §2.1.

The systematic way of the construction of discretizations for first and higher derivatives as described above is very well suited for implementation in a computer program. Given that manual analysis becomes very error-prone and tedious in three or more dimensions on grids which go beyond  $2^3$  points, the use of a computer program which handles symbolic manipulation is indispensable. The discussion in this paper is based on the output of such a program, called Generate Directional Discretizations (GDD). This program for various approximations to derivatives is written in MuPAD [15].

The solution by GDD of (4.1) together with (4.2)–(4.5) is a consistent approximation of the derivative under consideration, characterized by the extent of the stencil and the order of accuracy. The result is in the form of a fixed stencil with a basis of stencils. The basis of stencils represent the degrees of freedom in the approximation. This is similar to describing a plane in space by a vector from the origin to the plane, together with two degrees of freedom, which are the two basis vectors in the plane. The fixed stencil in the approximation, like the vector from the origin to the plane, can be chosen with freedom. Transformations such as symmetry operations and orthogonalization improve the simplicity and beauty of a basis. The idea of a basis of stencils is the cardinal point in formulating discretizations, and the generation of the basis by means of a computer program is instrumental. The basis of stencils with its degrees of freedom constitute a formal and systematic extension of the work of Sidilkover [8], Hirsch [13], and Koren [14]. Appendix B contains an overview of the number of stencils for the first, second, and third stream-wise derivatives in one, two and three dimensions for different extent of the stencils.

On a structured grid in any number of dimensions, the surrounding of each node is similar to another. A consistent approximation with a basis of stencils can be expressed in a FD, FV or other formulation. On unstructured grids, the number of elements surrounding a node may be different. A consistent approximation is possible in a FD formulation. A discontinuous flux computation in a FV formulation, or a RD or FVD distribution based on the N scheme may lead to an inconsistent approximation [7].

In the following sections, we will focus on directional discretizations of up to fourth order accuracy. Emphasis will be on structured grids in two and in three dimensions. We will also consider a node surrounded by triangles in two dimensions and by tetrahedra in three dimensions with low order approximations. For simplicity of notation, we take the point for the discretization of the derivative at the origin, i.e.  $i = j = k = \dots = 0$ .

## 5. Directional discretizations of derivatives in two dimensions.

We start with low order directional discretizations of  $\partial u / \partial e_1$  in two dimensions. The bases are manageable small and easy to draw and comprehend. The directional approximation can be used for the scalar advection equation in nonlinear or linear form,

$$\frac{\partial u}{\partial t} + \frac{\partial f}{\partial x} + \frac{\partial g}{\partial y} = 0, \quad \text{or} \quad \frac{\partial u}{\partial t} + a_x \frac{\partial u}{\partial x} + a_y \frac{\partial u}{\partial y} = 0, \quad (5.1)$$

with  $a_x = \partial f / \partial u$ ,  $a_y = \partial g / \partial u$ , and the velocity  $a = \sqrt{a_x^2 + a_y^2}$ .

### 5.1. Directional first order upwind discretizations of the first derivative in two dimensions on a $2 \times 2$ grid.

We start with the lowest order directional discretization of  $\partial u / \partial e_1$ . The number of basis stencils on the  $2 \times 2$  stencil is small. This simplifies a detailed exposition of the different steps in the analysis of the discretization and its various optimizations.

This stencil has been the subject of much investigation. Two papers are relevant to our discussion. Koren [14] effectively uses a basis of stencils to generate discretizations with certain properties. Sidilkover [8] does not use a basis, but introduces a limiter for a more accurate compact discretization. The discussion below uses the basis of stencils to generalize their results, and to prepare the stage for higher order discretizations, also in three dimensions.

*The basis of stencils.* From the space of all possible discretizations on a  $2 \times 2$  grid, we will consider the subspace of consistent first order approximations of the first derivative  $\partial u / \partial e_1$  expressed in grid-based derivatives  $u_x$  and  $u_y$ . The consistent discretization of  $u_x$  and  $u_y$  can be written as

$$\begin{aligned} \Delta x u_x &= \Delta x u_{x,f} + \Delta x u_{x,b}(k_x) = u_{0,0} - u_{-1,0} + k_x \{u_{0,0} - u_{-1,0} - u_{0,-1} + u_{-1,-1}\} , \\ \Delta y u_y &= \Delta y u_{y,f} + \Delta y u_{y,b}(k_y) = u_{0,0} - u_{0,-1} + k_y \{u_{0,0} - u_{-1,0} - u_{0,-1} + u_{-1,-1}\} . \end{aligned} \tag{5.2}$$

This solution comprises two parts. The first part of (5.2), symbolically indicated by  $u_{x,f}$  and  $u_{y,f}$ , is the fixed stencil. The second part indicated by  $u_{x,b}$  and  $u_{y,b}$  involves the parameters  $k_x$  and  $k_y$ . The parameters represent two degrees of freedom due to the basis of stencils. These parameters correspond to the parameters  $\delta_1$  and  $\delta_2$  of Koren [14]. The stencils are shown in Fig. 5.1 for  $u_x$  and  $u_y$  respectively, where the basis consists of one stencil  $b$ . The scaling of the basis stencils is such that the nodal values are integers. The smallest non-zero value is  $\pm 1$ .

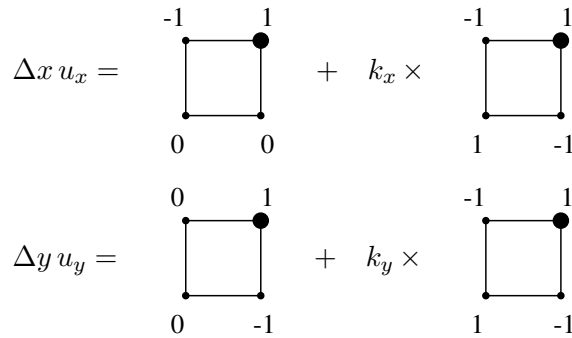


Figure 5.1. The fixed stencil and the basis stencils used in the discretization of  $u_x$  and  $u_y$  of (5.2).

The application of a grid-based Taylor series expansion shows that the fixed stencils are first order approximations to the first derivative, and the part involving the parameters  $k$  is an approximation to the mixed second derivative  $\partial^2 u / \partial x \partial y$ . The appearance of degrees of freedom represented by stencils of higher derivatives multiplied by parameters is typical of discretizations in more than one dimension. The second derivative takes more than two points in one dimension. Here, we find a mixed derivative ; the pure second derivative is also absent.

The parameters can be constants or a function of the preferential direction  $\alpha$ ,  $k = k(\alpha)$ , which will make the discretization of  $\partial u / \partial e_1$  also dependent on the angle. This is accepted practice in distribution discretizations, but in a FD context Koren [14] has been perhaps the first to consider angle dependent discretizations in two dimensions. In the following, the notation  $k$  will be used as a shorthand for  $k(\alpha)$ . The one-dimensional grid-aligned

discretization is obtained with  $k_x = k_y = 0$  while the diagonal approximation of (2.5) has  $k_x = 0$ ,  $k_y = -1$ . This confirms that the choice of the fixed stencil is free. We have chosen the fixed stencil in (5.2) such that the  $x$  and  $y$  derivatives are their mirror image with respect to the diagonal. Another possibility for a symmetric fixed stencil is the choice  $k_x = k_y$ , e.g.  $k_x = k_y = -1/2$ , see Fig. 5.2.

$$\Delta x u_{x,f} = \begin{array}{cc} -1/2 & 1/2 \\ \bullet & \bullet \\ \hline \bullet & \bullet \\ -1/2 & 1/2 \end{array} \quad \Delta y u_{y,f} = \begin{array}{cc} 1/2 & 1/2 \\ \bullet & \bullet \\ \hline \bullet & \bullet \\ -1/2 & -1/2 \end{array}$$

Figure 5.2. Alternative fixed stencils for the approximations of  $u_x$  and  $u_y$ .

We continue the discussion with the stencils of (5.2). Other choices of fixed stencils give similar results, sometimes more elaborate or more compact.

*The approximation in stream-wise coordinates.* We use the coordinate transformation of (4.4) in two dimensions. For a preferential direction with angle  $\alpha$ ,  $\vec{e}_1 = (\cos \alpha, \sin \alpha)^T$ , and the transformation is a rotation over the angle  $\alpha$  from the fixed axes to the local basis,

$$\begin{array}{l} e_1 = x \cos \alpha + y \sin \alpha \\ e_2 = -x \sin \alpha + y \cos \alpha \end{array} \quad \text{or} \quad \begin{array}{l} x = e_1 \cos \alpha - e_2 \sin \alpha \\ y = e_1 \sin \alpha + e_2 \cos \alpha \end{array} . \quad (5.3)$$

This transformation is used in (4.5).

We will consider the principal region,  $0 \leq \alpha \leq \pi/4$ , where  $\cos \alpha \geq \sin \alpha \geq 0$ , and  $a_x/\Delta x \geq a_y/\Delta y \geq a_z/\Delta z \geq \dots \geq 0$ . For other flow angles we will use a permutation of the discretization.

On a regular grid with  $\Delta x = \Delta y = h$ , the approximation to the first stream-wise derivative is

$$\frac{\partial u}{\partial e_1} = \vec{e}_1 \cdot \vec{\nabla} u = \frac{1}{h} \left\{ \begin{array}{l} u_{0,0} \{ (1 + k_x) \cos \alpha + (1 + k_y) \sin \alpha \} \\ -u_{-1,0} \{ (1 + k_x) \cos \alpha + k_y \sin \alpha \} \\ -u_{0,-1} \{ k_x \cos \alpha + (1 + k_y) \sin \alpha \} \\ +u_{-1,-1} \{ k_x \cos \alpha + k_y \sin \alpha \} \end{array} \right\}. \quad (5.4)$$

The coefficients  $k_x$  and  $k_y$  appear only in the combination  $k = k_x \cos \alpha + k_y \sin \alpha$ , and we can write

$$\frac{\partial u}{\partial e_1} = \frac{1}{h} \{ (k + \cos \alpha + \sin \alpha) u_{0,0} - (k + \cos \alpha) u_{-1,0} - (k + \sin \alpha) u_{0,-1} + k u_{-1,-1} \}. \quad (5.5)$$

The coefficient  $k$  is therefore the central parameter which determines the properties of the approximation. This is reflected in the analysis of the discretization where the monotonicity and stability will depend only on  $k$ . The individual parameters  $k_x$  and  $k_y$  are important when considering the continuity of the approximation, and above all for coding the discretization.

*Monotonicity of the approximation.* First order discretizations are commonly used as a fall-back. When a higher-order discretization generates an oscillatory solution near a discontinuity, a limiting function reduces the discretization to a monotonic first order one.

The standard approach to obtain a monotonic scheme is to ensure that  $u^{n+1}$  is a convex average of the nodal values. For the advection equation, (5.1), where  $a_x = a \cos \alpha$ ,  $a_y = a \sin \alpha$ , the Euler backward scheme is  $u_{0,0}^{n+1} = u_{0,0}^n - a\Delta t \partial u / \partial e_1$ . The monotonicity conditions for the discretization of (5.5) are therefore

$$1 - \frac{a\Delta t}{h}(k + \cos \alpha + \sin \alpha) \geq 0, \quad k + \cos \alpha \geq 0, \quad k + \sin \alpha \geq 0, \quad \text{and} \quad k \leq 0. \quad (5.6)$$

For sufficiently small  $\Delta t$  and on the principal region where  $\cos \alpha \geq \sin \alpha \geq 0$ , this reduces to

$$0 \geq k \geq -\sin \alpha. \quad (5.7)$$

The monotonicity domain for  $k$  is given as the shaded region in Fig. 5.3.

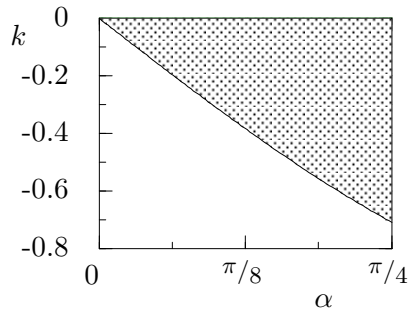


Figure 5.3. The region of  $k$  which satisfies the monotonicity conditions of (5.7).

The one-dimensional grid-aligned discretization has  $k = 0$  which is the upper limit, and the diagonal discretization of (2.5) has  $k = -\sin \alpha$ , the lower limit. The latter exhibits also the maximum time step,  $\Delta t \leq h/(a \cos \alpha) = h/a_x$ . For  $\alpha = 0$  they meet at  $k(0) = 0$ .

*Finite Difference and Finite Volume formulations.* In a FD formulation, the derivatives of (5.2) are used in the approximation of  $\partial u / \partial t$  of (5.1).

The FV discretization in a cell-vertex formulation uses fluxes through the edges which make up the dual cell around the nodes which are positioned at the vertices of the grid. For node  $(0,0)$ , the dual cell is indicated in Fig. 5.4 by the dashed edges. In a cell-centered perspective, the grid edges form the cells with the nodes at the centers. The flux balance through these edges generates the variation of the nodal values  $\partial u / \partial t$ , when (5.1) is integrated over the dual volume.

The approximation of (5.2) translates into the edge fluxes  $f_{i\pm 1/2,j}$  and  $g_{i,j\pm 1/2}$  as follows.

In a Flux Vector Splitting (FVS) context, the fluxes are in the linear case, for  $a_x \geq a_y \geq 0$ ,

$$\begin{aligned} f_{i-1/2,j} &= a_x \{ (1 + k_x) u_{i-1,j} - k_x u_{i-1,j-1} \}, \\ g_{i,j-1/2} &= a_y \{ (1 + k_y) u_{i,j-1} - k_y u_{i-1,j-1} \}, \end{aligned} \quad (5.8)$$

and in the non-linear case

$$\begin{aligned} f_{i-1/2,j} &= (1 + k_x) f(u_{i-1,j}) - k_x f(u_{i-1,j-1}), \\ g_{i,j-1/2} &= (1 + k_y) g(u_{i,j-1}) - k_y g(u_{i-1,j-1}). \end{aligned} \quad (5.9)$$

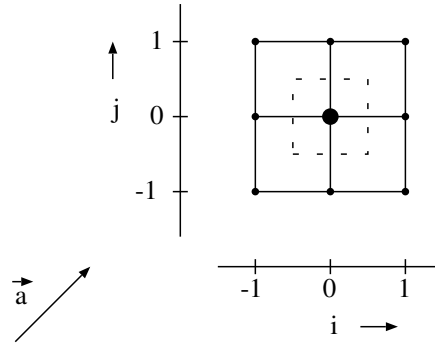


Figure 5.4. The edges which make up the dual cell surrounding node  $(0,0)$  in a vertex-centered Finite Volume formulation.

The standard FVS interpretation is that the fluxes of (5.8) or (5.9) are the result of the nodal split fluxes

$$\begin{aligned}
 f_{i,j}^+ &= \begin{cases} (1+k_x)f(u_{i,j}) \rightarrow \text{edge } i+1/2, j \\ -k_x f(u_{i,j}) \rightarrow \text{edge } i+1/2, j+1 \end{cases} \\
 g_{i,j}^+ &= \begin{cases} (1+k_y)g(u_{i,j}) \rightarrow \text{edge } i, j+1/2 \\ -k_y g(u_{i,j}) \rightarrow \text{edge } i+1, j+1/2 \end{cases} .
 \end{aligned} \tag{5.10}$$

The distribution of these split fluxes is shown in Fig. 5.5.

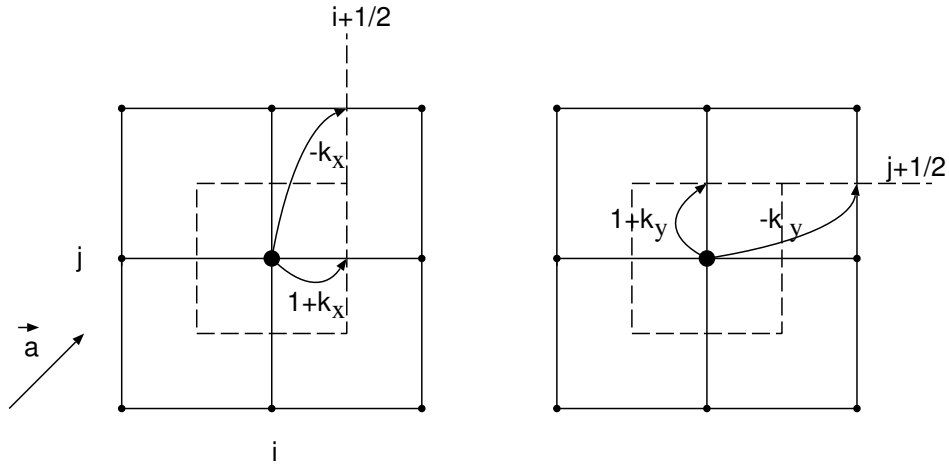


Figure 5.5. The nodal splitting of the flux and distribution to the edges according to (5.10). Left: the contribution to  $u_x$  ( $f_{i+1/2,j}$  and  $f_{i+1/2,j+1}$ ), right: to  $u_y$  ( $g_{i,j+1/2}$  and  $g_{i+1,j+1/2}$ ).

The FVS formulation means distributing the nodal flux over the dual edges of the grid, while the Flux Vector Distribution method described in [7] amounts to distributing the edge fluxes over the nodes. In the non-linear case, the fluxes are split and distributed according to the nodal advection speed,  $a_x = \partial f / \partial u$ ,  $a_y = \partial g / \partial u$ .

Remark that the directional computation of an interface flux amounts to a directional extrapolation, and the approximations in this paper lend themselves for directional extrapolations.

In a Flux Difference Splitting (FDS) context, computation of the fluxes is based on an edge averaged state. The edge based average advection speeds  $\vec{a}_e = (a_{x,e}, a_{y,e})^T$  decide which nodes contribute to the edge flux. In Harten et al. [16], an average state is used in the construction of the flux difference. In their one-dimensional context, the average is a function of the two states adjacent to the edge. Here, there are six nodes which may contribute to the edge flux, and the average is of those six nodes. The flux computation is now according to (5.8), where the velocities  $a_x$  and  $a_y$  are a function of the average of the six nodes surrounding the dual edge.

The extension to fluxes for systems of equations is the standard one-dimensional grid-aligned one, where averages and matrices matrices now may be a function the unknowns of more than two nodes.

*Continuity of the approximation.* The stencil of the discretization uses certain nodes for flow angles  $0 \leq \alpha \leq \pi/4$ . For the remaining angles, a permutation is used. It is important that the approximation of  $\partial u / \partial e_1$  depends continuously on the unknowns when the changing flow angle forces a change of stencil.

In the FD context, this means that for  $\alpha = 0$  the stencil of  $\partial u / \partial e_1$  should have a mirror symmetry with respect to the  $x$ -axis, while for  $\alpha = \pi/4$  the mirror symmetry of the stencil has to be with respect to the diagonal in the  $x$ - $y$  plane.

This is respected by the one-dimensional grid-aligned approximation. Also the diagonal discretizations of §2 satisfy the above requirements, and are continuous by construction. Consider e.g. a flow almost parallel with the  $x$ -axis. For both  $\alpha \downarrow 0$  and  $\alpha \uparrow 0$ , the approximation of  $\partial u / \partial e_1$  uses only nodes on the  $x$ -axis. A similar diagonal one-dimensional approximation results when the flow is aligned with a diagonal of the grid, such as shown in Fig. 5.4. For  $\alpha \downarrow \pi/4$ , the node  $(0, -1)$  vanishes from the discretization, while for  $\alpha \uparrow \pi/4$ , the node  $(-1, 0)$  disappears. When  $\alpha = \pi/4$ , the approximation uses  $u_{0,0} - u_{-1,-1}$ .

The use of the basis of stencils obliges us to impose continuity explicitly. For the present degrees of freedom, described by the flow direction dependent coefficients  $k_x(\alpha)$  and  $k_y(\alpha)$ , this means that  $k_x(0) = 0$ . There is no constraint for  $\alpha = \pi/4$  since the stencils associated with the degrees of freedom are symmetric with respect to the diagonal.

Continuity of the solution is a more severe constraint in the FV context. In a FV discretization, the nodal values are updated using the flux balance through the edges which make up the dual cell volume, as described by (5.8)–(5.10), and by Fig. 5.5. The edge fluxes used in this balance should be continuously dependent on the nodal values when  $\alpha$  leaves the domain  $[0, \pi/4]$ , and a different stencil is used for the flux approximation. Continuity is now individually imposed on the  $u_x$  and  $u_y$  derivatives. If this is not the case, the fluxes computed with FVS may be inconsistent, and with FDS the discontinuity may introduce wiggles.

For  $\alpha = 0$ ,  $a_y = 0$ , the  $g$ -flux ( $u_y$  derivative) is absent from the approximation. The continuity condition is the same as in the FD case.

When the flow is along a diagonal of the grid,  $\alpha = \pi/4$ , the conditions become more severe. In the approximation of  $\partial u / \partial e_1$ , the transition from  $\alpha < \pi/4$  to  $\alpha > \pi/4$  amounts to swapping the  $x$  and  $y$  axes. The continuity of the approximation means that at  $\alpha = \pi/4$  the  $x$  and  $y$  derivatives should be their mirror image with respect to the diagonal. In terms of the basis of stencils, this implies that  $k_x(\pi/4) = k_y(\pi/4)$ .

Remark that the latter condition is not satisfied by the diagonal discretization of §2,  $k_x = 0$ ,  $k_y = -1$ . The FV implementation of a diagonal discretization gives indeed incorrect

solutions when the advection direction is close to the diagonal. Concerning continuity, the FV method is for diagonal discretizations an exception to the FD and distribution methods. Since the discretizations of §2 cannot be used in a FV context, we need to make the degrees of freedom a function of the advection direction for the diagonal discretizations.

Some simple continuous monotone diagonal discretizations with the optimal time step,  $k = -\sin \alpha$ , are obtained with e.g.

$$k_x = \frac{1}{2}(\cos(2\alpha) - 1), \quad k_y = \frac{1}{2}\sin(2\alpha) - 1, \quad (5.11)$$

or with

$$k_x = k_y = -\frac{\sin \alpha}{\cos \alpha + \sin \alpha}. \quad (5.12)$$

In both cases, at  $\alpha = \pi/4$  the grid-based derivatives reduce to the stencils with  $k_x = k_y = -1/2$ , which are the fixed stencils of Fig. 5.2. The approximations for  $u_x$  and  $u_y$  are their mirror image for  $\alpha = \pi/4$ , and the swapping of both derivatives which takes place when the advection direction passes the diagonal has no effect.

The approximation of (5.11) emphasizes the  $i = -1$  nodes in the computation of  $u_y$ , and is the diagonal approximation for  $\alpha = 0$ . In (5.12), the  $i = 0$  nodes have greater weight in the computation of  $u_y$ , and we find for  $\alpha = 0$  the one-dimensional grid-aligned approximation. The treatment of  $u_x$  is not vastly different between the two discretizations. The approximations are identical for  $\alpha = \pi/4$ .

Both approximations satisfy the previously mentioned continuity and monotonicity constraints, and have the optimal time step. We have an example of two different discretizations which are indistinguishable in the analysis of their numerical behavior. Yet, they may give different results, e.g. in the presence of a discontinuity.

Continuity is also important when the time step is computed. The one-dimensional grid-aligned time step  $\Delta t = h/(a_x + a_y)$  or the diagonal optimal time step  $\Delta t = h/a_x$  can be computed directly at the node in a FD fashion. Alternatively, during the computation of the fluxes, the term  $a_x + a_y$  or  $a_x$  which is used in the time step calculation can be accumulated in parallel with the flux computation. This has then to be done in a way which ensures continuity when the stencil changes.

*Computing the flow angle.* The dependence on the flow angle increases the computational cost, but not excessively so. A reasonably economic way to compute the coefficients of (5.11) and (5.12) on an irregular grid is to make use of  $\tan \alpha$ . Given a diagonal vector  $\vec{v}_1$  and a grid vector  $\vec{v}_2$ , Fig. 5.6, a convenient definition of  $\alpha$  is that  $\alpha = 0$  for  $\vec{a} // \vec{v}_2$ , and that  $\alpha = \pi/4$  for  $\vec{a} // \vec{v}_1$ .

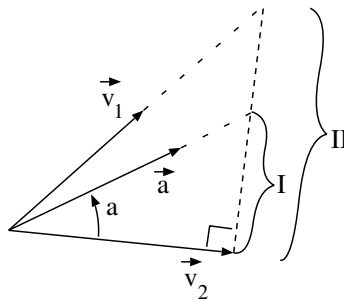


Figure 5.6. Computing  $\tan \alpha$ , given the advection vector  $\vec{a}$ , and two grid-related vectors  $\vec{v}_1$  and  $\vec{v}_2$ .

With the configuration of Fig. 5.6, and writing  $\vec{a} = a\vec{e}_1$ ,

$$\tan \alpha = \frac{\text{I}}{\text{II}} = \frac{\vec{e}_1 \cdot \vec{v}_{2\perp}}{\vec{v}_1 \cdot \vec{v}_{2\perp}} \frac{\vec{v}_1 \cdot \vec{v}_2}{\vec{e}_1 \cdot \vec{v}_2}, \quad (5.13)$$

where  $\vec{v}_2 \cdot \vec{v}_{2\perp} = 0$ . In a numerical code, the dot products involving  $\vec{e}_1$  are already computed in order to find the nodes which are used in the computation of the fluxes. The remaining geometric factors  $\vec{v}_2 \cdot \vec{v}_{2\perp}$  and  $\vec{v}_1 \cdot \vec{v}_2$  can be stored.

The factors of (5.10) expressed in terms of  $t_\alpha = \tan \alpha$  using the option of (5.11) are then  $1/(1+t_\alpha^2)$  and  $t_\alpha^2/(1+t_\alpha^2)$ . With the choice of (5.12), the factors are  $1/(1+t_\alpha)$  and  $t_\alpha/(1+t_\alpha)$ .

An alternative to this computation of the angle on an irregular grid is a transformation to a uniform  $(\xi, \eta)$  grid with  $x = x(\xi, \eta)$  and  $y = y(\xi, \eta)$ . In the  $\xi - \eta$  plane we find the angle simply by  $\arctan(\eta/\xi)$ . This transformation, while simplifying the angle evaluation, only partly restores accuracy in a FV context on a fairly smooth grid.

*Optimizing the directional error.* The directional error in the approximation of  $\partial u / \partial e_1$ , (5.4), is obtained with a Taylor series expansion expressed in the local basis,

$$\vec{e}_1 \cdot \vec{\nabla} u = \frac{\partial u}{\partial e_1} + h \left\{ c_{20} \frac{\partial^2 u}{\partial e_1^2} + c_{11} \frac{\partial^2 u}{\partial e_1 \partial e_2} + c_{02} \frac{\partial^2 u}{\partial e_2^2} \right\} + O(h^2), \quad (5.14)$$

where  $c_{mn}$  is the coefficient of  $\partial^2 u / \partial e_1^m \partial e_2^n$ , excluding the factor  $h$ . The coefficients  $c_{mn}$  are (see also Koren [14])

$$\begin{aligned} c_{20} &= \frac{1}{2}k \sin(2\alpha) + \frac{1}{4}(\cos \alpha + \sin \alpha)(\sin(2\alpha) - 2), \\ c_{11} &= k \cos(2\alpha) + \frac{1}{2} \sin(2\alpha)(\cos \alpha - \sin \alpha), \\ c_{02} &= -\frac{1}{4} \sin(2\alpha)(2k + \cos \alpha + \sin \alpha), \end{aligned} \quad (5.15)$$

which depend on the coefficient  $k$ . With the fixed stencil of Fig. 5.2, the coefficients are  $c_{20} = 1/2(k \sin(2\alpha) - \cos \alpha - \sin \alpha)$ ,  $c_{11} = 1/2(2k \cos(2\alpha) - \cos \alpha + \sin \alpha)$  and  $c_{02} = -1/2 k \sin(2\alpha)$ . A pure one-dimensional approximation for a given angle  $\alpha^*$  has  $c_{02}(\alpha^*) = c_{11}(\alpha^*) = 0$ , but these constraints can only be met for certain angles  $\alpha^*$ .

A measure of the error of the discretizations is the average value  $I_{mn}$ , the scaled norm over the domain  $(0, \pi/4)$ ,

$$I_{mn} = \frac{4}{\pi} |c_{mn}|_{L_1} = \frac{4}{\pi} \int_0^{\pi/4} |c_{mn}| d\alpha. \quad (5.16)$$

The degrees of freedom give the opportunity to reduce some, but not all, of these error terms.

A major error reduction is obtained with directional discretizations when the pure normal derivative term in the error is eliminated. According to (5.14), this is obtained by taking the degrees of freedom such that  $c_{02} = 0$ . This approach has been advocated by Sidilkover [8] since this increases the accuracy for steady state approximations with one order, and is further elaborated by Hirsch [13]. We can rewrite the error part  $\epsilon$  of (5.14) as

$$\epsilon = h \left\{ \left( c_{20} \frac{\partial}{\partial e_1} + c_{11} \frac{\partial}{\partial e_2} \right) \frac{\partial u}{\partial e_1} + c_{02} \frac{\partial^2 u}{\partial e_2^2} \right\} + O(h^2). \quad (5.17)$$

The reason for the error reduction is that a smooth steady solution of the advection equation contains no stream-wise derivative terms, since the numerical approximation

of  $\partial u/\partial e_1$  is of  $O(h)$ . This implies that also  $\partial^2 u/\partial e_1^2$  and  $\partial^2 u/\partial e_1 \partial e_2$  are of  $O(h)$ , and the terms with coefficients  $c_{20}$  and  $c_{11}$  become irrelevant in the error of (5.17). A first order approximation of  $\partial u/\partial e_1$  which sets  $c_{02} = 0$  (or of  $O(h)$ ) then takes care of  $\partial^2 u/\partial e_2^2$  and gives a solution which is second order accurate at steady state. When  $c_{02} = 0$ , the coefficient  $c_{11}$  cannot be eliminated simultaneously according to (5.15), see also Koren [14], but this is not needed as explained above.

We will indicate by a *streamline approximation* an approximation which eliminates the pure normal derivative in the error term.

If the flow is near steady state, the most important variations are normal to the advection direction. The most important coefficient is therefore  $c_{02}$ , then  $c_{11}$  and  $c_{20}$ .

The case of an equation with a source term is discussed by Sidilkover [8], while Hirsch [13] considers more accurate time discretizations in a Lax-Wendroff type of development.

For the unsteady case we cannot obtain a second order solution with the approximation of (5.2). This can easily be seen when we consider a simple wave solution in the stream-wise direction  $\vec{a}$  of the form

$$U(x, y, t) = U_a \cos(\omega t - x \cos \alpha - y \sin \alpha). \quad (5.18)$$

With this solution, the error in (5.14) becomes  $\epsilon = [1/2 \cos \alpha (1 + 2 \sin \alpha \sin(2\alpha)(\sin \alpha - \cos \alpha)) - 1/2 k \sin(4\alpha)] hU$ . For  $\alpha = 0$ ,  $\epsilon = 1/2 hU$ . Also for other angles a nonzero error remains.

It is possible to construct approximations with an increased order of the error for unsteady problems. We take in the approximation of  $\partial u/\partial e_1$  the  $y$ -axes as the time variable. This is an established practice for one-dimensional grid-aligned discretizations, and works also for directional discretizations like the above with  $c_{02} = 0$ . We obtain an approximation in one space dimension which is second order in time and space when the time step  $\Delta t$  is proportional to  $h$ . This is explained in more detail for the central approximations later in this paper.

The error term  $c_{02}$  is eliminated by choosing  $k = -1/2 (\cos \alpha + \sin \alpha)$ , or  $k_x = -1/2 (1 + (1 + 2k_y) \tan \alpha)$ . First of all, this is incompatible for  $\alpha = 0$  with the continuity condition  $k_x(0) = 0$  for the FD and FV formulations. Also the monotonicity condition (5.7) is breached with this choice everywhere on the principal region  $0 \leq \alpha \leq \pi/4$ .

The monotonicity condition is assuming constant coefficients, i.e. it is linear, or independent of the unknowns (but dependent on  $\alpha$ ). The solution  $k = -1/2 (\cos \alpha + \sin \alpha)$  can be rendered monotone by making the discretization non-linear using the unknowns and limiters. The solution is monitored for oscillations, and when they appear, the condition  $c_{02} = 0$  is relaxed in order to revert to a monotone approximation. The practice of limiters has been mentioned before when a higher order discretizations is limited to a first order approximation. An example is given in appendix A where limiters are discussed for diagonal discretizations. The present application of limiters is different in that the oscillatory higher order approximation is not an approximation on a larger stencil, but an approximation with  $c_{02} = 0$ .

This type of limiting has a long history, and the procedure is effectively present in the Stream-wise Upwind Petrov-Galerkin method (SUPG) in the Finite Element (FE) formulation [17, 18].

On structured grids, Sidilkover [8] has analyzed discretizations with coefficients  $k$  which are independent of the flow angle in a FV context. This limited version of the N scheme

is named the S scheme. He continued his analysis with Roe in [10] and [19], extending the stencil with one point.

The unstructured limited discretizations appeared in the Residual Distribution formulation [20] with the NN scheme of Deconinck, the PSI scheme of Struijs, and the Level scheme of Roe. Shortly after, Sidilkover showed that the PSI scheme is a minmod limited N scheme on triangles. The PSI scheme has an order of accuracy of about 1.6 [21], similar to the SUPG FE discretizations. It has the property of preserving a linear solution, which is the equivalent on unstructured grids of the increased accuracy of structured grids when  $c_{02} = 0$ . The non monotonic discretizations reach an order of accuracy of 2.

An approach slightly different from [8] is to write the discretization with  $c_{02} = 0$  as the monotone directional discretization of (5.11) or (5.12) plus a correction term. The limiting is based on restricting the new value of node  $(0,0)$ ,  $u_{0,0}^{n+1}$ , to the range  $[u_{-1,0}, u_{-1,-1}]$ . These two nodes are the upstream nodes in the diagonal discretization. For the optimal time step,  $\Delta t = h/a_x$ , the monotone solution is  $u_{0,0,\text{mon}}^{n+1} = a_y/a_x u_{-1,-1} + (a_y - a_x)/a_x u_{-1,0}$ . The correction term for  $k = 0$  is  $u_c = 1/2 (1 - a_y/a_x) [(u_{0,0} - u_{-1,0}) - (u_{0,-1} - u_{-1,-1})]$ . The limiting is simply restricting  $u_{0,0,\text{mon}}^{n+1} + u_c$  to the range  $[u_{-1,0}, u_{-1,-1}]$ . To this can be added a limiting of  $u_c$  such that  $k \rightarrow 0$  for  $\alpha \rightarrow 0$  for continuity in a FVS formulation.

*The Fourier components.* For the analysis in the Fourier domain we use components of the form

$$U_{i,j}^n = U_0 \rho^n e^{I(i\phi_x + j\phi_y)}, \quad (5.19)$$

where  $U_0 \rho^n$  is the amplitude of the component at time level  $n$ ,  $\phi_x$  and  $\phi_y$  are the phase angles in  $x$  and  $y$  direction, and  $I$  is the imaginary unit,  $I^2 = -1$ . We take as grid size  $\Delta x = \Delta y = h$ , and  $\phi_x = h \kappa_x$  and  $\phi_y = h \kappa_y$  where  $\kappa_x$  and  $\kappa_y$  are the wave numbers in the two grid directions. The amplification factor for the discretization of (5.4) in an Euler backward scheme is

$$G = \frac{U_{i,j}^{n+1}}{U_{i,j}^n} = \mathcal{R}(G) + \mathcal{I}(G) = g_r + I g_i, \quad (5.20)$$

with

$$\begin{aligned} G &= 1 - \nu \left\{ \cos \alpha (1 - e^{-I\phi_x}) + \sin \alpha (1 - e^{-I\phi_y}) \right. \\ &\quad \left. + k(\alpha) (e^{-I(\phi_x + \phi_y)} - e^{-I\phi_y} - e^{-I\phi_x} + 1) \right\}, \\ g_r &= 1 - \nu \left\{ \cos \alpha (1 - \cos \phi_x) + \sin \alpha (1 - \cos \phi_y) \right. \\ &\quad \left. + k(\alpha) (\cos(\phi_x + \phi_y) - \cos \phi_y - \cos \phi_x + 1) \right\}, \\ g_i &= -\nu \left\{ \cos \alpha \sin \phi_x + \sin \alpha \sin \phi_y \right. \\ &\quad \left. + k(\alpha) (\sin \phi_x + \sin \phi_y - \sin(\phi_x + \phi_y)) \right\}, \end{aligned} \quad (5.21)$$

where  $\nu = a\Delta t/h$ . We use the notation  $k(\alpha)$  to show explicitly the dependence on  $\alpha$ . The dissipation and dispersion depend on this parameter and can therefore be optimized, but this will not be explored further here.

For arbitrary  $k$  and for  $\phi_x = \pi$ ,  $\phi_y = 0$ , stability imposes that  $\Delta t \leq h/(a \cos \alpha) = h/a_x$ . This is the optimal step for stability which we encountered for the diagonal directional approximation with  $k = -\sin \alpha$  ensuring monotonicity.

For the one-dimensional grid-aligned approximation with  $k = 0$  and for the reduced diffusion approximation with  $k = -1/2(\cos \alpha + \sin \alpha)$ , the time step based on stability is  $\Delta t \leq h/\{a(\cos \alpha + \sin \alpha)\} = h/(a_x + a_y)$ . For arbitrary flow angle the optimal and one-dimensional time step limitations generalize to  $h/\max(|a_x|, |a_y|)$  and  $h/(|a_x| + |a_y|)$  respectively.

In the case of the diagonal discretization,  $k_x = 0$ ,  $k_y = -1$ , the discretization is one-dimensional for  $\alpha = 0$  and for  $\alpha = \pi/4$ . The amplification of (5.21) is in the first case  $g_r = 1 + \nu(\cos \phi_x - 1)$  and  $g_i = -\nu \sin \phi_x$ . In the second case,  $g_r = 1 + 1/2\sqrt{2}\nu(\cos(\phi_x + \phi_y) - 1)$  and  $g_i = -1/2\sqrt{2}\nu \sin(\phi_x + \phi_y)$ . Since the wave numbers transform according to (5.3), we can rewrite the latter in a stream-wise wave number  $\kappa_{e_1}$ ,  $g_r = 1 + \nu_e(\cos \phi_{e_1} - 1)$  and  $g_i = -\nu_e \sin \phi_{e_1}$  where  $\nu_e = a\Delta t/h\sqrt{2}$  and  $\phi_{e_1} = h\sqrt{2}\kappa_{e_1}$ . The behavior in both cases is similar, as expected. The degrees of freedom can be used to aim for isotropy in the behavior in the Fourier domain, that is to reduce the dependence of the amplification or the dispersion on the flow angle.

On this small grid, we have revisited the one-dimensional grid-aligned approximation, the diagonal approximation (the N scheme), and the streamline approximation. A continuous diagonal approximation is necessary for the FV approximation. The properties of these discretizations are summarized in Table 5.1.

Table 5.1. Numerical properties of the one-dimensional grid-aligned approximation, the diagonal approximation, the continuous diagonal approximation, and the streamline approximation.

discretization	continuity	monotonicity	streamline	switching	time step
one-dimensional	y	y	n	$\pi/2$	$h/(a_x + a_y)$
diagonal	y(FD), n(FV)	y	n	$\pi/4$	$h/a_x$
cont. diagonal	y	y	n	$\alpha$	$h/a_x$
streamline	n	n	y	$\alpha$	†

The symbol  $\alpha$  in the column *switching* indicates a discretization which depends continuously on the flow angle  $\alpha$ .

†: to be determined with the stability of the space operator.

We compare in Fig. 5.7 the coefficients  $c_{mn}$  and the average error values  $I_{mn}$  in Table 5.2. The limited discretization will have errors somewhere between the diagonal discretization and the streamline discretization.

Table 5.2. The average error values  $I_{mn}$  for discretizations of Table 5.1.

discretization	$I_{20}$	$I_{11}$	$I_{02}$
one-dimensional	0.424	0.124	0.212
diagonal	0.574	0.052	0.062
streamline, $k = -1/2(\cos \alpha + \sin \alpha)$	0.637	0.264	0.0

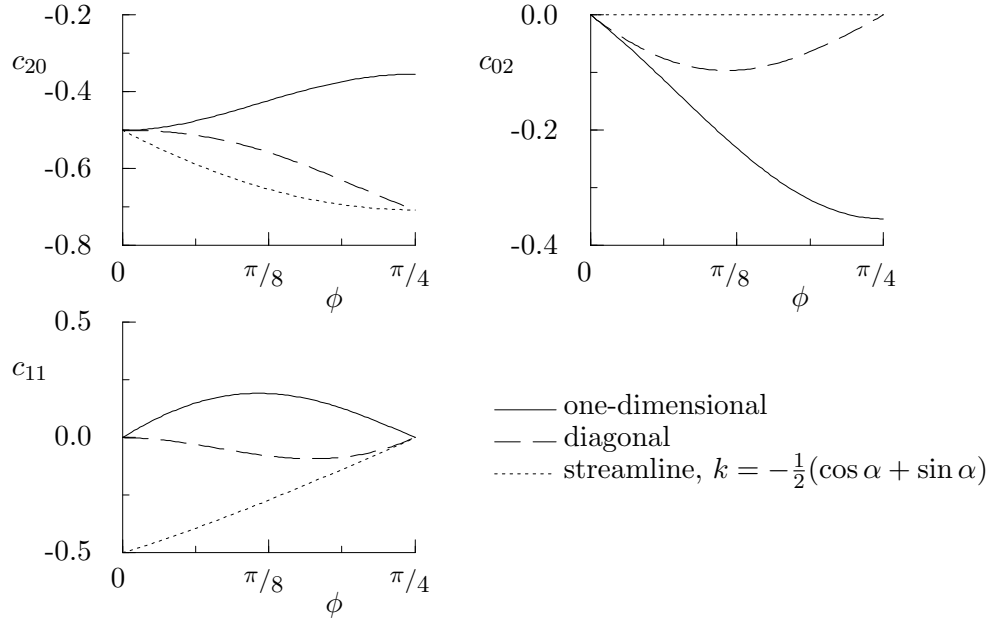


Figure 5.7. The error coefficients  $c_{mn}$  for discretizations of Table 5.1.

## 5.2. Directional second order discretizations of the first derivative in two dimensions on a $3 \times 3$ grid.

This is the  $[-1, 1]^2$  nine-point stencil considered by Hirsch [13]. We will analyze the discretizations from the viewpoint of a basis of stencils. Special attention will be given to the continuity of the approximation, using where necessary coefficients  $k$  which depend on the flow angle  $\alpha$ .

*The basis of stencils.* Our starting point will be the subspace of consistent second order approximations of the first derivative on a  $3 \times 3$  grid as generated by the program GDD,

$$\begin{aligned} \Delta x u_x &= \Delta x u_{x,f} + \Delta x u_{x,b}(k_{x1}, k_{x2}, k_{x3}) = \frac{1}{2} (u_{1,0} - u_{-1,0}) + k_{x1}b^1 + k_{x2}b^2 + k_{x3}b^3, \\ \Delta y u_y &= \Delta y u_{y,f} + \Delta y u_{y,b}(k_{y1}, k_{y2}, k_{y3}) = \frac{1}{2} (u_{0,1} - u_{0,-1}) + k_{y1}b^1 + k_{y2}b^2 + k_{y3}b^3, \end{aligned} \quad (5.22)$$

where  $b^i$  is the basis stencil  $i$ , see Fig. 5.8,

$$\begin{aligned} b^1 &= u_{-1,0} - 2u_{0,0} + u_{1,0} - u_{-1,-1} + 2u_{0,-1} - u_{1,-1}, \\ b^2 &= -u_{-1,1} + 2u_{-1,0} - u_{-1,-1} + u_{0,1} - 2u_{0,0} + u_{0,-1}, \\ b^3 &= -u_{-1,1} + u_{1,1} + 4u_{-1,0} - 4u_{0,0} - 3u_{-1,-1} + 4u_{0,-1} - u_{1,-1}. \end{aligned} \quad (5.23)$$

This solution comprises two parts. The first part of (5.22), symbolically indicated by  $u_{x,f}$  and  $u_{y,f}$ , is the fixed stencil. We have taken for the fixed stencil the one-dimensional discretization in the  $x$  and  $y$  directions. The second part indicated by  $u_{x,b}$  and  $u_{y,b}$  involves the parameters  $k_{xi}$  and  $k_{yi}$ ,  $i = 1 \dots 3$ . The parameters represent six degrees of freedom due to the basis of stencils  $b = \{b^1, b^2, b^3\}$ , (5.23). The stencils of the basis  $b$  are approximations of mixed third derivatives; the grid is too small for pure third derivatives. In the space of consistent second order approximations of the first derivative, approximations to the

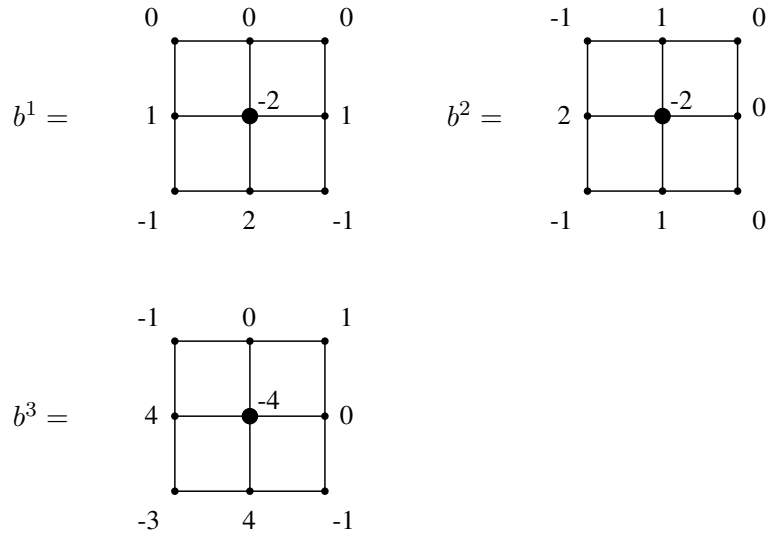


Figure 5.8. The basis of stencils  $b = \{b^1, b^2, b^3\}$  of (5.23), corresponding to the degrees of freedom for  $u_x$  and  $u_y$  of (5.22).

second derivative are by definition absent. It is of course possible to add an artificial viscosity term separately. Such discretizations are discussed in §5.4.

The basis stencils are the same for  $u_x$  and for  $u_y$ . The coefficients  $k_{xi}$  and  $k_{yi}$  appear in the approximation of  $\partial u / \partial e_1$  in the combination  $k_i = k_{xi} \cos \alpha + k_{yi} \sin \alpha$  as before. The diagonal approximation of (2.6) has  $k_{xi} = 0$ ,  $k_{y1} = k_{y2} = -1/2$ , and  $k_{y3} = 1/2$ .

In the previous section we had a basis of only one stencil; we now have a basis of three stencils. A particular approximation of a grid-based derivative of (5.22), e.g.  $u_x$ , is therefore given by a fixed stencil and the vector  $\vec{k}_x = (k_{x1}, k_{x2}, k_{x3})^T$  with respect to a basis  $b$ .

The upper triangle of the basis stencils in figure Fig. 5.8 consists of the three nodes  $(1,0)$ ,  $(0,1)$ , and  $(1,1)$ . The weight of these nodes is  $w_1, w_2$ , and  $w_3$  respectively, and has a value of either 0 or 1, depending on  $b^i$ . This means that the vector  $\vec{k}_x$  corresponds to the weights of the upper triangle. The program GDD generates the basis in such a way that there is always an upper triangle which has this property.

We can orthogonalize the basis  $b$  when we have an inner product. Also an orthonormal basis is possible, using the normalization procedure of Gram-Schmidt.

Let us denote by  $b_{pq}^i$  the value of stencil  $b^i$  at the node  $(p, q)$ , and take as inner product the Hadamard product  $b^i \cdot b^j = \sum_{p,q=-1}^1 b_{pq}^i b_{pq}^j$ , which satisfies the common requirements of an inner product. The basis  $b$  of stencils of Fig. 5.8 is not orthogonal since  $b^1 \cdot b^2 = 0$ , but  $b^1 \cdot b^3 \neq 0$ , and  $b^2 \cdot b^3 \neq 0$ .

The orthogonalization procedure does not produce a beautiful basis, but applying symmetry does. We obtain a convenient orthogonal basis by splitting the stencils of the basis  $b$  in their antisymmetric and symmetric parts  ${}^a b^i$  and  ${}^s b^i$  respectively, as described in [13], see Fig. 5.9.

By itself, the antisymmetric stencils  ${}^a b^i$  of Fig. 5.9 do not form a basis. In the  $\vec{k}$  notation,  ${}^a b^1 = (0, -2, 1)^T$ ,  ${}^a b^2 = (-2, 0, 1)^T$ ,  ${}^a b^3 = (-1, -1, 1)^T$ , and the antisymmetric stencils are dependent since  $2 {}^a b^3 = {}^a b^1 + {}^a b^2$ . Also the node  $(0,0)$  is by definition absent in an asymmetric stencil. We need to include the symmetric stencil to form the orthogonal

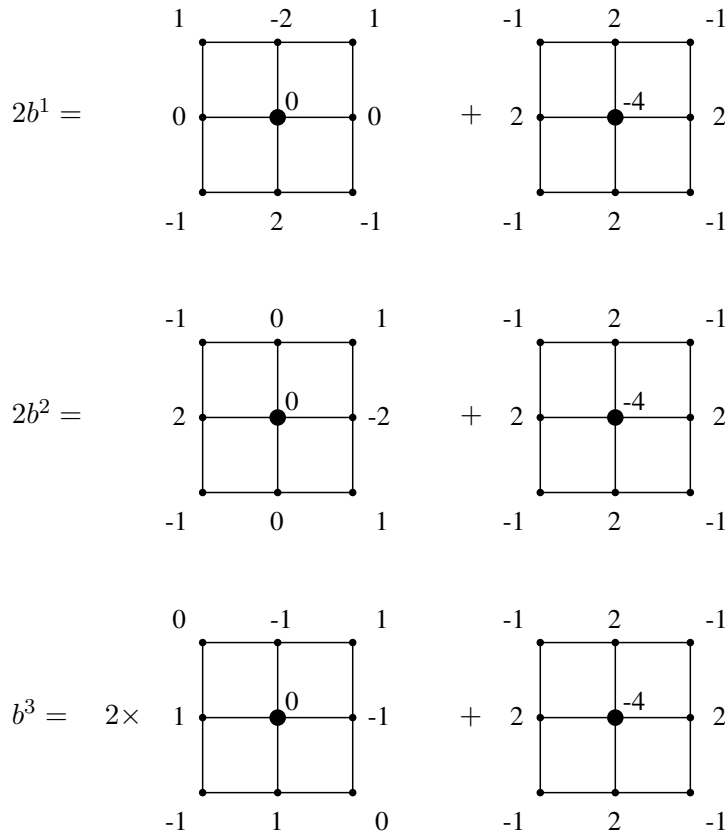


Figure 5.9. The basis stencils  $b^1$ ,  $b^2$ , and  $b^3$  of (5.23), split in an antisymmetric part  ${}^a b^i$ , left, and a symmetric part  ${}^s b^i$ , right.

basis  $B = \{{}^a b^2, {}^a b^1, {}^s b^3\}$ , used with parameters  $K_{xi}$  and  $K_{yi}$ , combined in  $K_i$ .

We have inverted in this basis the order of  ${}^a b^1$  and  ${}^a b^2$  for reasons of symmetry. The stencil  $B^2 = {}^a b^1$  is symmetric in  $x = 0$  and antisymmetric in  $y = 0$ . This asymmetry in the  $y$  direction leads to a skewness in the stencil of the  $u_x$ -derivative. Likewise, the stencil  $B^1 = {}^a b^2$  creates an asymmetry in the  $x$  direction and a skewness in the derivative  $u_y$ . It is an approximation to the mixed third derivative  $2\Delta x^2 \Delta y \partial^3 u / \partial x^2 \partial y$ .

We will use the term *regular* for approximations where the stencil of  $u_y$  is the stencil of  $u_x$  mirrored in the  $x = y$  diagonal. A *straight* approximation of a derivative in the  $x$ -direction indicates that the stencil is antisymmetric in  $x = 0$  and symmetric in  $y = 0$ , and similar for a derivative along  $y$ . This is an approximation without skewness.

The basis stencil  $B^2$  is  $B^1$  mirrored in the  $x = y$  diagonal, and a regular approximation has

$$K_{y2} = K_{x1} \quad \text{and} \quad K_{x2} = K_{y1}, \quad \text{or} \quad K_2 = K_{y1} \cos \alpha + K_{x1} \sin \alpha. \quad (5.24)$$

Remark that  $K_{x2} \neq 0$  or  $K_{y1} \neq 0$  introduces a skewness in the approximation.

The choice  $K_x = (0, 0, 0)^T$ ,  $K_y = (1/4, 1/4, 0)^T$  gives the diagonal approximation of (2.6).

The symmetric stencil  $B^3 = {}^s b^3$  is an approximation to the mixed fourth derivative  $-\Delta x^2 \Delta y^2 \partial^4 u / \partial x^2 \partial y^2$ , but it is the sum of basis stencils approximating third derivatives since  $B^3 = (2, 2, -1)^T$ . The error of the stencil is one order higher than the truncation

error, and the symmetric stencil is therefore of secondary importance in the approximation. Concerning the truncation error, a reduced basis which is sufficient to describe second order accurate approximations to the first derivative is therefore  $b' = \{^a b^2, ^a b^1\}$ . This basis will generate asymmetric (central) approximations.

The diagonal discretizations of §2 are designed to reduce the approximation to a purely one-dimensional discretization which uses only nodes on the diagonal when  $\alpha = \pi/4$  with the idea to eliminate the coefficients  $c_{mn}$  with  $m+n = 3$ ,  $m < 3$  for that direction. However, the restriction to use only nodes on the diagonal is unnecessary. When we impose in GDD the condition that at  $\alpha = \pi/4$ ,  $c_{mn} = 0$  with  $m+n = 3$ ,  $m < 3$ , we get the solution of (2.6) with the basis  $\{B^3\}$ . The additional constraint therefore reduces the basis, but permits approximations which use nodes outside the diagonal.

*Monotonicity of the approximation.* The update using (5.22) is not monotone.

*Continuity of the approximation.* We will consider the principal region,  $0 \leq \alpha \leq \pi/4$ , where  $\cos \alpha \geq \sin \alpha \geq 0$ , and  $a_x/\Delta x \geq a_y/\Delta y \geq a_z/\Delta z \geq \dots \geq 0$ . For other flow angles we will use a permutation of the discretization.

For the central discretizations we have two types of stencils. The fixed stencils such as the one-dimensional grid-aligned central approximation do not change when the flow angle changes. For these fixed stencils we will mainly consider regular approximations. This is effectively the continuity condition for all flow angles. Breaking the symmetry between  $u_y$  and  $u_x$  is possible, but this will not improve the accuracy or the stability.

On the other hand, there are central flow-angle dependent discretizations. The stencils can change when the flow angle passes a grid line or a diagonal. This is the case for the diagonal discretization of §2.3. The central stencils can also be continuous functions of the flow angle. They behave like the upwind approximations of the previous section, and continuity conditions apply for the discretization with respect to the flow angle. This means that the symmetry is imposed at only two flow angles,  $\alpha = 0$  and  $\alpha = \pi/4$ . They are  $k_1(0) = -2k_3(0)$  and  $k_1(\pi/4) = k_2(\pi/4)$ . For the FV formulation, the conditions  $k_{x1}(0) = -2k_{x3}(0)$ ,  $k_{x1}(\pi/4) = k_{y2}(\pi/4)$ ,  $k_{x2}(\pi/4) = k_{y1}(\pi/4)$  and  $k_{x3}(\pi/4) = k_{y3}(\pi/4)$  apply, which are not satisfied by (2.6) in FV form. When we use the orthogonal basis  $B$ , the FD conditions are  $K_2(0) = 0$  and  $K_1(\pi/4) = K_2(\pi/4)$ , and for the FV formulation the conditions are  $K_{x2}(0) = 0$ ,  $K_{x1}(\pi/4) = K_{y2}(\pi/4)$ ,  $K_{x2}(\pi/4) = K_{y1}(\pi/4)$  and  $K_{x3}(\pi/4) = K_{y3}(\pi/4)$ . Since the discretization of (2.6) is not continuous in the FV formulation, we construct a continuous version with (5.11) or (5.12) in an average of the velocities  $\vec{a}$  and  $-\vec{a}$ .

*Flow-angle dependent approximations for systems of equations.* The easiest way to apply the central discretizations which depend on flow angles to system of equations is to consider the approximation as a sum of upwind discretizations with opposite speeds, and to apply FVS or FDS according to preference.

*Optimizing the directional error.* The directional error in the approximation of  $\partial u/\partial e_1$  of (5.22) is given by

$$\begin{aligned} \vec{e}_1 \cdot \vec{\nabla} u &= \frac{\partial u}{\partial e_1} + h^2 \left\{ c_{30} \frac{\partial^3 u}{\partial e_1^3} + c_{21} \frac{\partial^3 u}{\partial e_1^2 \partial e_2} + c_{12} \frac{\partial^3 u}{\partial e_1 \partial e_2^2} + c_{03} \frac{\partial^3 u}{\partial e_2^3} \right\} \\ &+ h^3 \left\{ \sum_{k,l}^{k+l=4} d_{k,l} \frac{\partial^4 u}{\partial e_1^k \partial e_2^l} \right\} + O(h^4), \end{aligned} \quad (5.25)$$

where  $c_{mn}$  is the coefficient of  $\partial^3 u / \partial e_1^m \partial e_2^n$ , excluding the factor  $h^2$ , and similar  $d_{kl}$ . In basis  $B$ , the coefficients  $c_{mn}$  take the form

$$\begin{aligned} c_{30} &= \frac{1}{6}(\cos^4 \alpha + \sin^4 \alpha) + \sin(2\alpha)(K_1 \sin \alpha + K_2 \cos \alpha), \\ c_{21} &= -\frac{1}{4} \sin(2\alpha) \cos(2\alpha) + K_1(3 \cos(2\alpha) + 1) \sin \alpha + K_2(3 \cos(2\alpha) - 1) \cos \alpha, \\ c_{12} &= \frac{1}{4} \sin^2(2\alpha) + K_1(3 \cos(2\alpha) - 1) \cos \alpha - K_2(3 \cos(2\alpha) + 1) \sin \alpha, \\ c_{03} &= \sin(2\alpha)\left(\frac{1}{12} \cos(2\alpha) - K_1 \cos \alpha + K_2 \sin \alpha\right). \end{aligned} \quad (5.26)$$

The coefficients  $d_{kl}$  are proportional to  $K_3$ ; taking  $K_3 = 0$  eliminates the terms  $d_{kl}$ . We have the parameters  $K_1$  and  $K_2$  to optimize the leading error terms between brackets of (5.25), where the parameters are constants or a function of the flow direction  $\alpha$ .

A streamline approximation eliminates the term  $c_{03}$  altogether in (5.26). If we cast (5.25) in a form similar to (5.17), we see that this means that the steady solution of the advection problem, (5.1) will be fourth order accurate when  $K_3 = 0$ .

A solution is  $K_1(\alpha) = 1/12 \cos \alpha$  and  $K_2(\alpha) = 1/12 \sin \alpha$ , with e.g.  $K_{x2} = K_{y1}(\alpha) = 0$  and  $K_{x1}(\alpha) = K_{y2}(\alpha) = 1/12$ . This corresponds to the stencils

$$\begin{aligned} \Delta x u_x &= \frac{1}{12} (u_{1,1} + 4u_{1,0} + u_{1,-1} - u_{-1,1} - 4u_{-1,0} - u_{-1,-1}), \\ \Delta y u_y &= \frac{1}{12} (u_{-1,1} + 4u_{0,1} + u_{1,1} - u_{-1,-1} - 4u_{0,-1} - u_{1,-1}), \end{aligned} \quad (5.27)$$

which are shown in Fig. 5.10.

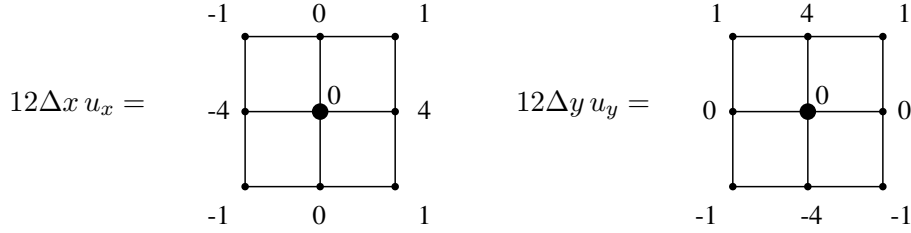


Figure 5.10. The stencils  $u_x$  and  $u_y$  of (5.27) which eliminate the term  $c_{03}$  in (5.26).

These stencils are regular since they are their mirror image with respect to the diagonal. They can be applied in a FV context, e.g. as fixed stencils  $u_{x,f}$  and  $u_{y,f}$  in the approximation of (3.6). The approximation for  $u_x$  can be interpreted as the average of  $1/2(u_{i+1,j} - u_{i-1,j})$  with weights  $1/6$ ,  $4/6$ , and  $1/6$  for  $j = 1, 0, -1$  respectively.

For a general approximation it is convenient to use the fixed stencils of (5.27) together with the orthogonal basis  $B$ . With this representation the choice  $K_x = (-1/12, 0, 0)^T$ ,  $K_y = (0, -1/12, 0)^T$  gives the one-dimensional grid-aligned discretization, and  $K_x = (-1/12, 0, 0)^T$ ,  $K_y = (1/4, 1/6, 0)^T$  produces the diagonal approximation of (2.6). Due to the symmetry of the new fixed stencils, the continuity conditions are unaffected. The directional errors reduce to

$$\begin{aligned} c_{30} &= \frac{1}{6} + \sin(2\alpha)(K_1 \sin \alpha + K_2 \cos \alpha), \\ c_{21} &= K_1(3 \cos(2\alpha) + 1) \sin \alpha + K_2(3 \cos(2\alpha) - 1) \cos \alpha, \\ c_{12} &= \frac{1}{6} + K_1(3 \cos(2\alpha) - 1) \cos \alpha - K_2(3 \cos(2\alpha) + 1) \sin \alpha, \\ c_{03} &= \sin(2\alpha)(-K_1 \cos \alpha + K_2 \sin \alpha). \end{aligned} \quad (5.28)$$

The general streamline approximation, i.e. the solution  $c_{03} = 0$  in (5.28) is

$$K_1 \cos \alpha = K_2 \sin \alpha \quad \text{or} \quad K_{x1} \cos^2 \alpha - K_{y2} \sin^2 \alpha + (K_{y1} - K_{x2}) \sin \alpha \cos \alpha = 0. \quad (5.29)$$

This relation reduces the number of undetermined parameters with one, and has to be combined with the continuity conditions.

An approximation with flow-angle independent stencils is

$$K_{x1} = K_{y2} = 0, \quad K_{y1} = K_{x2} \quad \text{or} \quad K_1 = K_{x2} \sin \alpha, \quad K_2 = K_{x2} \cos \alpha, \quad (5.30)$$

which is not subject to the continuity constraints. The stencil is regular, but the parameter  $K_{x2}$  introduces a skewness to the stencils.

The parameter  $K_2$  can be used to reduce the remaining error terms, or to optimize in the Fourier domain. We can substitute (5.29) in (5.28) to obtain the terms

$$c_{03} = 0, \quad c_{12} = \frac{1}{6} - 2K_2 \sin \alpha, \quad c_{21} = 2K_2 \frac{\cos(2\alpha)}{\cos \alpha}, \quad c_{30} = \frac{1}{6} + 2K_2 \sin \alpha. \quad (5.31)$$

The parameter  $K_3$  is present in the coefficient  $c_{04} = 1/8 K_3 (\cos(4\alpha) - 1)$ , which can therefore be eliminated by taking  $K_3 = 0$ . The coefficient  $c_{05}$  can only be minimized, but not eliminated.

A pure one-dimensional approximation for a given angle  $\alpha^*$  has to satisfy  $c_{03}(\alpha^*) = c_{12}(\alpha^*) = c_{21}(\alpha^*) = 0$ , but these constraints can only be met for certain angles  $\alpha^*$ . We note that for  $\alpha = 0$ ,  $c_{12}$  and  $c_{21}$  cannot both be zero, and the streamline approximation with  $c_{03} = 0$  is not one-dimensional along the  $x$  axis. For  $\alpha = \pi/4$ , a pure one-dimensional approximation needs  $K_2(\pi/4) = 1/12\sqrt{2}$ .

For the unsteady problem in one dimension we use the  $y$ -axis as the time variable. With an advection speed of  $\vec{a} = (a, 1)^T$  and  $\vec{\nabla}u = (\partial/\partial x, \partial/\partial t)^T$ , the steady approximation  $a\vec{e}_1 \cdot \vec{\nabla}u = 0$  now represents  $u_t + au_x = 0$ , and the angle  $\alpha$  is between 0 and  $\pi$ .

The fixed stencil of (5.27) translates to

$$\begin{aligned} \Delta x u_x &= \frac{1}{12} (u_{i+1}^{n+1} + 4u_{i+1}^n + u_{i+1}^{n-1} - u_{i-1}^{n+1} - 4u_{i-1}^n - u_{i-1}^{n-1}), \\ \Delta t u_t &= \frac{1}{12} (u_{i+1}^{n+1} + 4u_i^{n+1} + u_{i-1}^{n+1} - u_{i+1}^{n-1} - 4u_i^{n-1} - u_{i-1}^{n-1}), \end{aligned} \quad (5.32)$$

The error of this scheme follows from the truncated Taylor series expansion in  $x$  and  $t$ ,

$$\vec{e}_1 \cdot \vec{\nabla}u = \frac{\partial u}{\partial t} + a \frac{\partial u}{\partial x} + \frac{1}{6} \left( \Delta x^2 \frac{\partial^2}{\partial x^2} + \Delta t^2 \frac{\partial^2}{\partial t^2} \right) \left( \frac{\partial u}{\partial t} + a \frac{\partial u}{\partial x} \right) + O(\Delta x^4, \Delta x^2 \Delta t^2, \Delta t^4). \quad (5.33)$$

The term  $u_t + au_x$  between brackets is at least of  $O(\Delta x^2, \Delta t^2)$ , and we obtain an approximation which is fourth order in time and space when the time step  $\Delta t$  is proportional to  $\Delta x$ .

We use the Fourier components of the previous section to obtain an expression for the amplification factor of (5.32),

$$G^2 (I \sin \phi_x + \nu(\cos \phi_x + 2)) + 4GI \sin \phi_x + I \sin \phi_x - \nu(\cos \phi_x + 2) = 0. \quad (5.34)$$

Both roots of this quadratic expression for  $G(\nu, \phi_x)$  have a magnitude of one for all values of  $\nu$  and  $\phi_x$ .

The steady two-dimensional or unsteady one-dimensional analysis is valid for a perfectly regular grid. When this is not the case, the cancellation of terms, which is at the basis of the error reduction, is not valid anymore. The solutions revert to second order on a distorted grid. On a reasonably smooth grid an important reduction of the error can still be observed. In a FD context, the grid coordinates can be included in the derivations of this section directly, and the approximation retains the accuracy. In a FV method where the edge flux is used in two neighboring cells, a full grid correction is theoretically not possible. A coordinate transformation to a uniform  $\xi$ - $\eta$  plane only partly restores accuracy on a fairly smooth grid.

A similar observation holds for the diagonal approximations of §2, but these discretizations are less sensitive to grid quality.

*The Fourier components.* The stability analysis for central discretizations takes place in two steps. First, the stability domain of the space operator  $\Omega$  is determined. The complex eigenvalues  $\Omega_j$  should satisfy the condition  $Re(\Omega_j) \leq 0 \forall j$ .

Then, a suitable time integration method is chosen. An Euler backward scheme is not stable for a central discretization, but e.g. a four-step Runge-Kutta or an implicit time integration leads to a stable solution. The stability region of the four step Runge-Kutta method in the  $\Omega\Delta t$  plane includes the imaginary axis until the value 2.78, and the real axes until the value -1.

We use the Fourier components to find the eigenvalues of the space operator for the discretization of (5.22) when the approximation is based on the fixed stencil of (5.27) together with the basis  $B$ . The use of Fourier components corresponds to periodic boundary conditions for the space operator. The eigenvalues are then

$$\begin{aligned} \Omega_{l,m} = -4\frac{a}{h} & \left( \frac{1}{12}I(\cos\alpha\sin\phi_x(\cos\phi_y+2) + \sin\alpha\sin\phi_y(\cos\phi_x+2)) \right. \\ & + K_1I\sin\phi_x(\cos\phi_y-1) + K_2I\sin\phi_y(\cos\phi_x-1) \\ & \left. - K_3(\cos\phi_x-1)(\cos\phi_y-1) \right), \end{aligned} \quad (5.35)$$

where  $\phi_x = \Delta x k_x = l\pi/N$ ,  $l = 0 \dots N$ , and  $\phi_y = \Delta y k_y = m\pi/N$ ,  $m = 0 \dots N$ , with  $N$  the number of points in one direction.

The general expression for the eigenvalues, (5.35), includes a real part related to the parameter  $K_3$ . This parameter is associated with the symmetric stencil which represents a Laplacian smoother. The Runge-Kutta time integration method accommodates space operators with eigenvalues which have a negative real part. This implies that we need  $K_3 \leq 0$ . A quick investigation reveals that  $|\Re(\Omega)| \leq 1$  for  $-3/5 \lesssim K_3 \leq 0$ . However, a full analysis of the discretizations with the eigenvalues of (5.35) permitting the optimal time step with a real part within the stability domain of the Runge-Kutta time integration is beyond the scope of this paper. We restrict ourselves to imaginary eigenvalues,  $K_3 = 0$ .

For the one-dimensional grid-aligned discretizations with  $K_x = (-1/12, 0, 0)^T$ ,  $K_y = (0, -1/12, 0)^T$ , the eigenvalues of the space operator are

$$\Omega_{l,m} = -\frac{a}{h}I(\cos\alpha\sin\phi_x + \sin\alpha\sin\phi_y). \quad (5.36)$$

The largest eigenvalues  $\Omega_{\max}$  are obtained for  $\sin\phi_x = \sin\phi_y = 1$ ,  $\phi_x = \phi_y = \pi/2$  with the value  $\Omega_{\max}(\alpha) = -a/hI(\cos\alpha + \sin\alpha)$ . This eigenvalue restricts the time step of the time integration.

For the diagonal approximation of (2.6),  $K_x = (-1/12, 0, 0)^T$ ,  $K_y = (1/4, 1/6, 0)^T$ , the eigenvalues are

$$\Omega_{l,m} = -\frac{a}{h}I((\cos \alpha - \sin \alpha) \sin \phi_x + \sin \alpha \sin(\phi_x + \phi_y)). \quad (5.37)$$

For angles  $0 \leq \alpha \leq \pi/4$ , the largest eigenvalue  $\Omega_{\max}(\alpha) = -a/hI \cos \alpha$  appears when  $\phi_x = \pi/2$  and  $\phi_y = 0$ . For these phase angles, the eigenvalues of (5.35) with  $K_3 = 0$  coincide, and the time step which is associated with these eigenvalues is therefore the optimal time step. The allowable time step is larger by a factor  $(\cos \alpha + \sin \alpha)/\cos \alpha$  than the one-dimensional grid-aligned discretization. This is similar to the first order upwind discretization. The time step restriction  $\Delta t \sim h/(a \cos \alpha) = h/a_x$  is typical for diagonal discretizations.

The general streamline approximation with flow-angle independent stencils of (5.30),  $c_{03} = 0$ , taking  $K_3 = 0$ , has the eigenvalues

$$\Omega_{l,m} = -\frac{a}{3h}I \left\{ \cos \alpha \sin \phi_x (\cos \phi_y + 2) + \sin \alpha \sin \phi_y (\cos \phi_x + 2) \right. \\ \left. + 12K_{x2} \left[ \cos \alpha \sin \phi_y (\cos \phi_x - 1) + \sin \alpha \sin \phi_x (\cos \phi_y - 1) \right] \right\}. \quad (5.38)$$

The streamline stencil of (5.27) has  $K_{x2} = 0$ , and the eigenvalues in (5.38) attain a maximum at  $\alpha = \pi/4$  and  $\phi_x = \phi_y$ ,  $\cos \phi_x = 1/2(\sqrt{3} - 1)$ , of  $\Omega_{\max}(\pi/4) = -a/3hI\sqrt{2} \sin \phi_x (2 + \cos \phi_x) \approx 1.04$ . The expression of  $\Omega_{\max}$  as function of the flow angle is complicated, but  $\Omega_{\max}$  smoothly increases between 1 and 1.04 for angles  $0 \leq \alpha \leq \pi/4$ . The streamline stencil of (5.27) also has the optimal stability. The skewness introduced by  $K_{x2}$  is detrimental to stability. The approximations with  $K_{x2} = \pm 1/12$  have a maximum of the one-dimensional grid-aligned stability.

The optimal time step can be an additional design criterion for flow-angle dependent approximations. Assume that we are interested in purely imaginary eigenvalues, and that the parameters  $K_1(\alpha)$  and  $K_2(\alpha)$  are expressed in a sum of associated Legendre polynomials, using sets of parameters  $\kappa_1$  and  $\kappa_2$ . For any flow angle  $\alpha$ , we try to minimize the magnitude of  $\Omega$  computed with these values of  $\kappa$ . In the optimal case, this should not exceed  $a/h \cos \alpha$ . An analytical solution to this problem is difficult to formulate due to the large number of parameters involved. For a given flow angle  $\alpha$  we can use an optimization procedure to determine the parameters  $\kappa$ . This procedure is then repeated for some angles between 0 and  $\pi/4$ , and an analytic expression for the  $\kappa$ 's can be fitted to this data. A detailed analysis and exploration of this method is outside the scope of this paper.

Instead, we will consider briefly the optimal time step of (5.35) for the streamline discretization with  $c_{03} = 0$ , (5.29). The most simple expression for  $K_2$  which satisfies the continuity constraint  $K_2(0) = 0$  is  $K_2 = f \sin \alpha$ , where the factor  $f$  remains to be determined. A brute force approach consists in computing  $\Omega$  for a large number of the combinations of  $\phi_x$ ,  $\phi_y$ , and  $\alpha$ , and verifying for which values of  $f$  the condition  $\Omega = a/h \cos \alpha$  is respected. The result is

$$f = \frac{1}{6}, \quad K_2 = \frac{1}{6} \sin \alpha, \quad (5.39)$$

and we can take for  $K_{x2}$  and  $K_{y2}$  the coefficients of (5.11) or (5.12) multiplied by  $-1/6$ . Then  $K_1$  follows from (5.29), e.g.  $K_{x1} = K_{x2} \tan \alpha$  and  $K_{y1} = K_{y2} \tan \alpha$  which satisfy also the continuity constraints. At  $\alpha = 0$  we start with the streamline approximation of (5.27),

while at  $\alpha = \pi/4$ ,  $K_{x1} = K_{y1} = K_{x2} = K_{y2} = 1/12$ . The stencils of  $u_x$  and of  $u_y$  for flow along the diagonal are shown in Fig. 5.11. The sum of  $u_x$  and  $u_y$  is  $1/2(u_{11} - u_{-1-1})$ , the diagonal approximation for  $\partial u/\partial e_1$ .

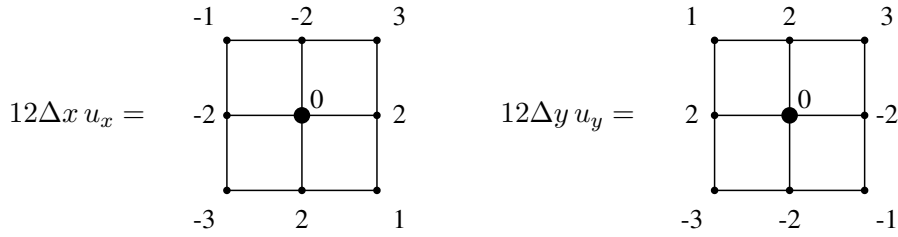


Figure 5.11. The stencils for  $u_x$  and  $u_y$  at  $\alpha = \pi/4$  which eliminate the term  $c_{03}$  while permitting the optimal time step due to a maximum amplification  $\Omega = a/h \cos \alpha$ .

The eigenvalues of this discretization are

$$\Omega_{l,m} = -\frac{a}{h} I \left\{ \frac{1}{3} \cos \alpha \sin \phi_x (\cos \phi_y + 2) + \sin \alpha \cos \phi_x \sin \phi_y + \frac{2 \sin^2 \alpha}{3 \cos \alpha} \sin \phi_x (\cos \phi_y - 1) \right\}, \quad (5.40)$$

and the maxima correspond to the optimal time step of the diagonal discretization.

The streamline approximation of (5.27) is slightly less optimal in stability, but it has the advantage of avoiding the dependence on the flow angle. For systems of equations a decomposition with FVS or FDS in traveling waves is avoided. Furthermore, while the application in FD of the stencils of Fig. 5.11 is straightforward, the implementation in FV is not. This is due to the presence of stencil  $B^2$  in  $u_x$  and of  $B^1$  in  $u_y$ . A solution is to incorporate the first in the  $g$ -flux and the second in the  $f$ -flux. There is no streamline optimal time step solution with  $K_{y1} = 0$  and  $K_{x1} = 0$  which is at the same time continuous.

The diagonal approximation of (2.6) and the streamline stencil of (5.39) are both dependent on the flow angle. The first changes stencil each  $\pi/4$ , the second modifies the approximation continuously. It is possible to get the optimal stability of the diagonal approximation with fixed stencils, but then we have to drop the streamline condition. We examine the regular approximations, condition (5.24), at angles  $\alpha = 0$  and  $\alpha = \pi/4$  to find  $K_{x1} = 1/6$  with the stencils of Fig. 5.12.

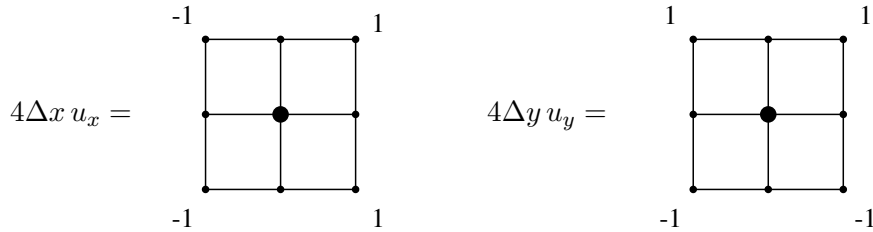


Figure 5.12. The stencils for  $u_x$  and  $u_y$  which give an approximation of  $\partial u/\partial e_1$  with the optimal stability of the diagonal approximation.

Remark that the approximation for  $\partial u/\partial e_1$  using the stencils of Fig. 5.12 is one-dimensional along the diagonals, but not along the grid axes. The improvement in stability

compared to the one-dimensional grid-aligned approximation has a price of double the truncation error. Compared to the diagonal discretization it removes the flow dependency, but quadruples the error. The eigenvalues of the space operator of this discretization are

$$\Omega_{l,m} = -\frac{a}{h}I(\cos \alpha \sin \phi_x \cos \phi_y + \sin \alpha \cos \phi_x \sin \phi_y). \quad (5.41)$$

The maximum eigenvalue of  $\Omega$ , excluding the scaling factor  $a/h$  as a function of the flow angle  $\alpha$  is given in Fig. 5.13 for the above approximations.

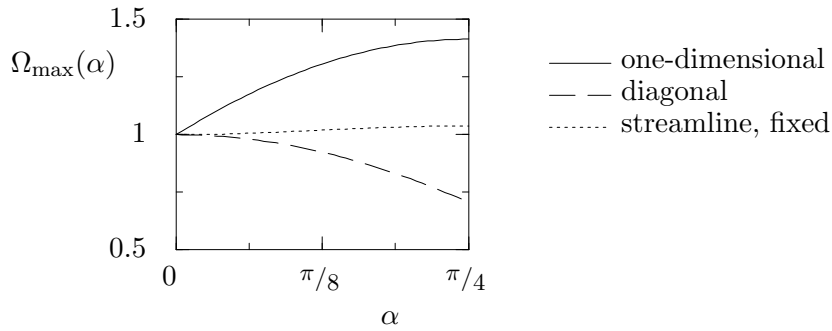


Figure 5.13. The maximum eigenvalue of  $\Omega$ , excluding the scaling factor  $a/h$ , as a function of the flow angle  $\alpha$  for the three approximations: one-dimensional grid-aligned (5.36), diagonal (5.37) and streamline (5.38) with  $K_{x2} = 0$ . The flow-angle dependent streamline approximation (5.39), and the fixed stencil with optimal stability, Fig. 5.12, share the curve of the diagonal approximation.

For a time-accurate numerical simulation, the global time step is determined by the maximum value of  $\Omega_{\max}$ , and the streamline approximation is almost as good as the diagonal approximation. With a local time step, the streamline approximation is somewhere in between the diagonal and the one-dimensional grid-aligned approximation.

For multi-grid solvers, the amplification of the high frequency components is of importance. We show in Fig. 5.14 the behavior of  $\Omega_{\max}$  for  $\pi/2 \leq |\phi_x|, |\phi_y| \leq \pi$  of the above approximations.

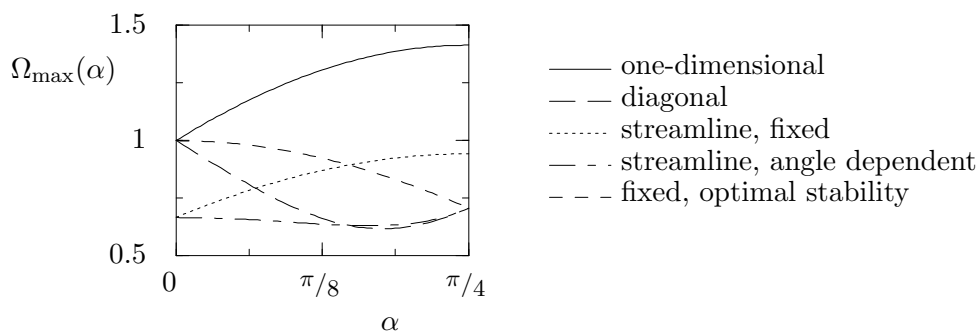


Figure 5.14. The maximum eigenvalue of  $\Omega$  in the high frequency domain  $\pi/2 \leq |\phi_x|, |\phi_y| \leq \pi$ , excluding the scaling factor  $a/h$ , as a function of the flow angle  $\alpha$  for the five approximations: one-dimensional grid-aligned (5.36), diagonal (5.37), streamline (5.38) with  $K_{x2} = 0$ , the flow-angle dependent streamline approximation (5.39), and the fixed stencil with optimal stability Fig. 5.12.

The degrees of freedom of the stability in (5.35) permit also optimization for this type of application, but this is not explored in this paper.

The error of the directional discretizations is significantly smaller than for the one-dimensional grid-aligned discretizations, for which

$$\begin{aligned} c_{30} &= \frac{1}{24}(3 + \cos(4\alpha)), & c_{03} &= \frac{1}{24} \sin(4\alpha), \\ c_{21} &= \frac{1}{8}(1 - \cos(4\alpha)), & c_{12} &= -\frac{1}{8} \sin(4\alpha). \end{aligned} \quad (5.42)$$

We have used the basis of stencils to add new central approximations to the previously known one-dimensional grid-aligned approximation and the diagonal approximation. They are a continuous diagonal approximation, a fixed streamline approximation, a streamline angle-dependent approximation, and a fixed approximation with optimal stability. The properties of these discretizations are summarized in Table 5.3.

Table 5.3. Numerical properties of the central one-dimensional grid-aligned approximation, the diagonal approximation, the fixed streamline approximation, the streamline angle-dependent approximation, and the fixed approximation with optimal stability.

discretization	continuity	streamline	switching	$\Omega_{max}$
one-dimensional	y	n	fixed	$(a_x + a_y)/h$
diagonal	y(FD), n(FV)	n	$\pi/4$	$a_x/h$
continuous diagonal	y	n	$\alpha$	$a_x/h$
streamline, fixed	y	y	fixed	$1.04 a/h^\dagger$
streamline, angle	y	y	$\alpha$	$a_x/h$
fixed, opt. stability	y	n	fixed	$a_x/h$

In the column *switching*, the symbol  $\alpha$  indicates a discretization which depends continuously on the flow angle  $\alpha$ .

†: the stability of the streamline discretization varies little with the flow angle  $\alpha$ .

We compare for the above discretizations the coefficients  $c_{mn}$  in Fig. 5.15, and the average error values  $I_{mn}$  in Table 5.4.

Table 5.4. The average values  $I_{mn}$  for the discretizations of  $\partial u / \partial e_1$  of Table 5.3.

discretization	$I_{30}$	$I_{21}$	$I_{12}$	$I_{03}$
one-dimensional	0.125	0.080	0.125	0.0265
diagonal	0.227	0.057	0.068	0.0073
streamline, fixed	0.167	0.0	0.167	0.0
streamline, angle-dep., $K_2 = 1/6 \sin \alpha$	0.227	0.065	0.106	0.0
fixed, optimal stability	0.250	0.159	0.250	0.0531

The reduction in the error  $c_{03}$  for the diagonal discretization compared to the one-dimensional grid-aligned discretization is 3.65. This reduction is of the same order as for the first order discretization. The fixed stencil with optimal time step doubles this error.

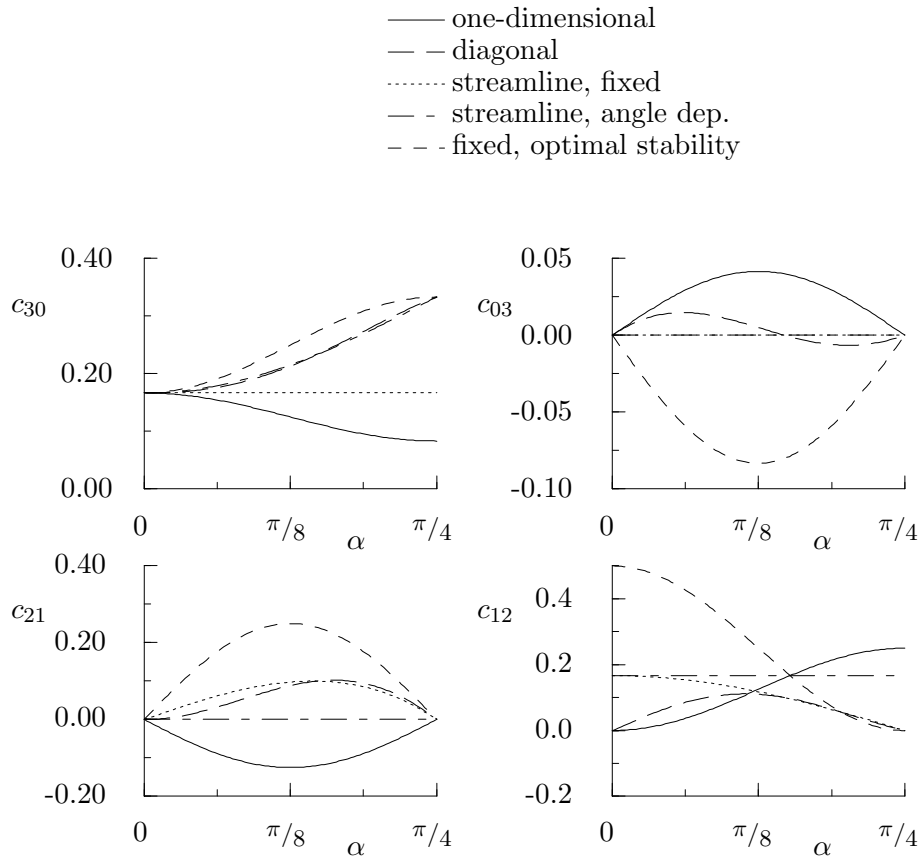


Figure 5.15. The coefficients of the error terms for the approximations of Table 5.3.

### 5.3. Directional first order discretizations of the first derivative in two dimensions on a $3 \times 3$ grid.

The first order upwind discretizations discussed by Sidilkover [8] and by Koren [14] occupy a stencil which fits in a  $3 \times 3$  grid. Their considerations are to improve multi-grid properties.

The basis for a first order discretization of the first derivative is given by

$$\begin{aligned}
 \Delta x u_x &= \Delta x u_{x,f} + \Delta x u_{x,b}(k_{x1}, \dots, k_{x6}) = (u_{0,0} - u_{-1,0}) + \sum_{i=1}^6 k_{xi} b^i, \\
 \Delta y u_y &= \Delta y u_{y,f} + \Delta y u_{y,b}(k_{y1}, \dots, k_{y6}) = (u_{0,0} - u_{0,-1}) + \sum_{i=1}^6 k_{yi} b^i,
 \end{aligned} \tag{5.43}$$

where  $b^i$  is the basis stencil  $i$ , see Fig. 5.16.

The nodes on the extended upper triangle are  $(1,-1)$ ,  $(0,0)$ ,  $(1,0)$ ,  $(-1,1)$ ,  $(0,1)$ , and  $(1,1)$ , and have a weight 1 or 0 in the basis stencils  $b^1 \dots b^6$  respectively.

When we enforce the diagonal condition, i.e. at  $\alpha = \pi/4$  we set  $c_{mn} = 0$  with  $m+n = 2$ ,

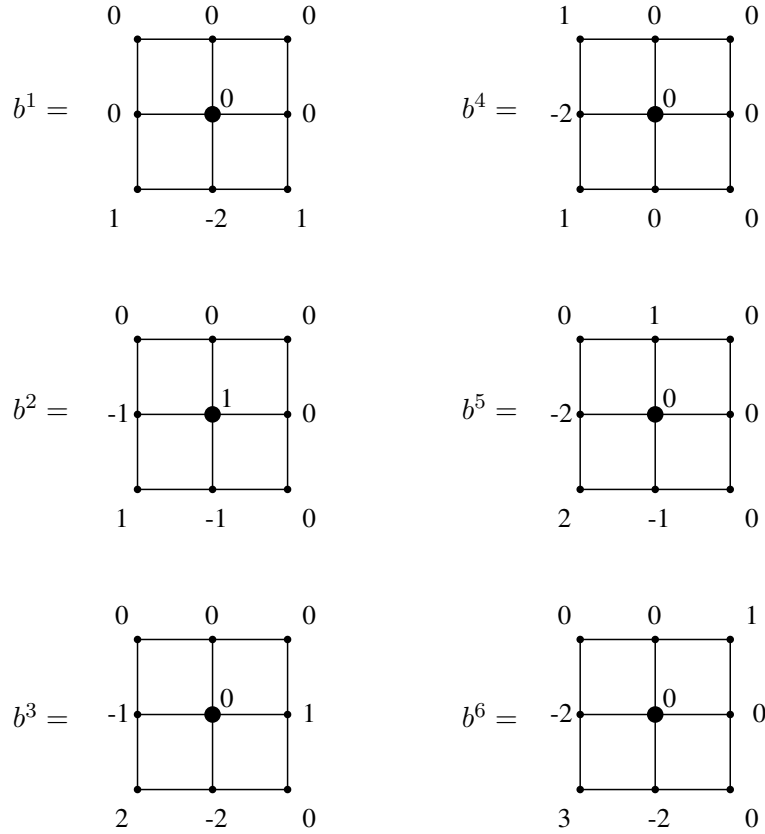


Figure 5.16. The stencils of the basis of (5.43).

$m < 2$ , the program GDD gives the solution

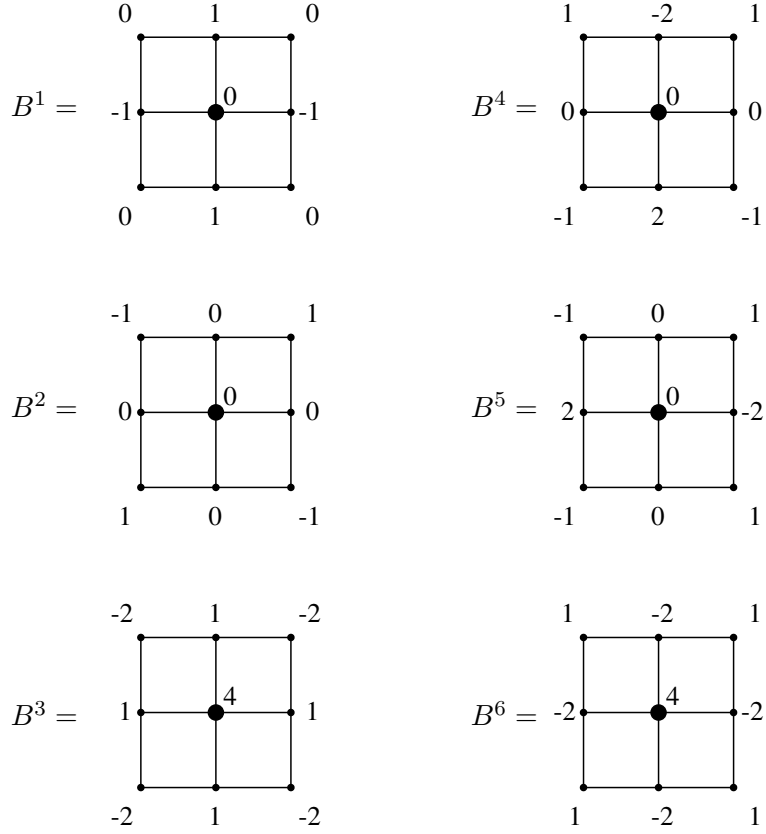
$$\begin{aligned} \Delta x u_x &= \Delta x u_{x,f} + \Delta x u_{x,b}(k_{y1}, \dots, k_{y4}) = (u_{0,0} - u_{-1,0}) + (k_{y3} + k_{y4} - k_{y1} - k_{y2})b^1, \\ \Delta y u_y &= \Delta y u_{y,f} + \Delta y u_{y,b}(k_{y1}, \dots, k_{y5}) = (u_{0,0} - u_{0,-1}) + \sum_{i=1}^5 k_{yi}b^i, \end{aligned} \quad (5.44)$$

where  $b^i$  is the basis stencil  $i$ ,

$$b'^1 = b^1, \quad b'^2 = b^3 - 2b^2, \quad b'^3 = b^4 + 2b^2, \quad b'^4 = b^5, \quad \text{and} \quad b'^5 = b^6 - 2b^2. \quad (5.45)$$

The diagonal constraint has reduced the basis of stencils of Fig. 5.16 to five stencils. Furthermore, the approximations of the derivatives  $u_x$  and  $u_y$  are now linked via the parameters  $k_{y1} \dots k_{y4}$ .

The splitting of the basis stencils  $b$  in symmetric and antisymmetric stencils as described in §5.2 leads to the basis  $B' = \{^a b^1, ^a b^2, ^s b^1, ^s b^2, ^s b^3, ^s b^4\}$ . This basis is neither orthogonal nor really beautiful, and we impose some more conditions of symmetry to arrive at the orthogonal basis  $B$  with coefficients  $K$  of Fig. 5.17. Only the first three stencils appear in the truncation error as lowest order contribution.

Figure 5.17. An orthogonal basis  $B$  of stencils for (5.43).

*Monotonicity of the approximation.* The expression for  $\partial u / \partial e_1$  using (5.43) based on  $k_i$  leads to the monotonicity constraints on the principal region

$$\begin{aligned}
 k_1 \leq 0, k_3 \leq 0, k_4 \leq 0, k_5 \leq 0, k_6 \leq 0, & \quad k_2 + k_3 + 2k_4 + 2k_5 + 2k_6 + \cos \alpha \geq 0, \\
 k_1 + k_2 + 2k_3 + k_4 + 2k_5 + 3k_6 \leq 0, & \quad 2k_1 + k_2 + 2k_3 + k_5 + 2k_6 + \sin \alpha \geq 0, \\
 k_2 + \cos \alpha + \sin \alpha \leq \frac{h}{a\Delta t}. & \quad (5.46)
 \end{aligned}$$

The monotonicity conditions in basis  $B$  are

$$\begin{aligned}
 K_2 - 2K_3 - K_4 - K_5 + K_6 \leq 0, & \quad -K_1 + K_3 + 2K_5 - 2K_6 - \cos x \leq 0, \\
 -K_2 - 2K_3 + K_4 - K_5 + K_6 \leq 0, & \quad K_1 + K_3 + 2K_4 - 2K_6 - \sin x \leq 0, \\
 4K_3 + 4K_6 + \cos \alpha + \sin \alpha \leq \frac{h}{a\Delta t}, & \quad K_1 + K_3 - 2K_4 - 2K_6 \leq 0, \\
 -K_2 - 2K_3 - K_4 + K_5 - 2K_6 \leq 0, & \quad -K_1 + K_3 - 2K_5 - 2K_6 \leq 0, \\
 & \quad K_2 - 2K_3 + K_4 + K_5 + K_6 \leq 0. \quad (5.47)
 \end{aligned}$$

For the optimal time step,  $\Delta t \leq h / (a \cos \alpha) = h / a_x$ ,  $k_2 = -\sin \alpha$ , and  $k_1 = k_3 = k_5 = k_6 = 0$ , and  $0 \geq k_4 \geq -1/2(\cos \alpha + \sin \alpha)$ . The more general monotone solution which involves the six basis stencils does not have the optimal time step.

*Continuity of the approximation.* The FD conditions for continuity of the discretization with respect to the flow angle for  $\alpha = 0$  are  $K_2 = 0$ ,  $K_4 = 0$ . In a FV formulation they are  $K_{x2} = 0$  and  $K_{x4} = 0$ . At the diagonal,  $\alpha = \pi/4$ , the conditions are for the FD method  $K_1 = 0$ ,  $K_4 = K_5$ , and for the FV method  $K_{x1} = -K_{y1}$ ,  $K_{x2} = K_{y2}$ ,  $K_{x3} = K_{y3}$ ,  $K_{x4} = K_{y5}$ ,  $K_{x5} = K_{y4}$ , and  $K_{x6} = K_{y6}$ . Similar conditions hold in basis  $b$ .

*Optimizing the directional error.* In basis  $B$ , the error  $c_{02}$  in the approximation of  $\partial u / \partial e_1$  is

$$c_{02} = -\frac{1}{4} \sin(2\alpha)(\cos \alpha + \sin \alpha) + K_1 \cos(2\alpha) - 2K_2 \sin(2\alpha) - 3K_3. \quad (5.48)$$

The streamline solution  $c_{02} = 0$  follows from (5.48) and can be combined with the continuity constraints; a particular upwind solution which is continuously dependent on  $\alpha$  for  $0 \leq \alpha \leq \pi/4$  is given in [14]. It is also possible to have  $c_{03} = 0$  and  $c_{04} = 0$ , but not  $c_{05} = 0$ .

To see if there is a monotone discretization with  $c_{02} = 0$ , substitute the solution of (5.48) in the expression for  $\partial u / \partial e_1$ , or directly in (5.46), and check if there is an angle  $\alpha$  for which the new conditions are infringed. This is a problem of the class of constraint optimization, and solution methods can be found in the book of Strang [22]. We have used the code HOPDM [23] to check the new monotonicity constraint. The monotonicity with  $c_{02} = 0$  is satisfied for  $\alpha = 0$  and for  $\alpha = \pi/4$ , but not for  $\alpha = \pi/6$ .

With this result, we look for a continuous streamline approximation without imposing monotonicity on the purely upwind part for  $0 \leq \alpha \leq \pi/4$ . In basis  $b$ , this means that the stencils 1, 3, 5, and 6 are absent. The streamline condition with only two basis stencils left is

$$c_{02} = -\frac{1}{2} \sin(2\alpha)k_2 + \frac{1}{2}(\cos(2\alpha) + 1)k_4 - \frac{1}{4} \sin(2\alpha)(\cos \alpha + \sin \alpha). \quad (5.49)$$

Combined with continuity at  $\alpha = 0$  and at  $\alpha = \pi/4$ , a solution is

$$\begin{aligned} k_{x2} &= \frac{1}{2}(\cos(2\alpha) - 1), & k_{y2} &= -\frac{1}{2}, & k_{x4} &= 0, & k_{y4} &= \frac{1}{2} \cos(2\alpha), \\ k_2 &= -\frac{1}{2} \sin \alpha (1 + \sin(2\alpha)), & k_4 &= \frac{1}{2} \sin \alpha \cos(2\alpha), \end{aligned} \quad (5.50)$$

see also Sidilkover [8] and Koren [14].

We note that the freedom due to the basis of stencils can also be used to find a least non-monotone solution. When the monotonicity coefficients of the discretization, e.g. (5.46), cannot be satisfied, then choose the coefficients  $k$  such that the offending monotonicity coefficients are minimized in some norm. This may reduce the need for limiting or for artificial viscosity.

#### 5.4. Directional second order discretizations of stream-wise second derivatives in two dimensions on a $3 \times 3$ grid.

The concept of directional discretizations applies also to higher derivatives, e.g.  $\partial^2 u / \partial e_1^2$ , the stream-wise second derivative. With the coordinate transformation of (5.3) we have

$$\frac{\partial^2 u}{\partial e_1^2} = \cos^2 \alpha \frac{\partial^2 u}{\partial x^2} + 2 \cos \alpha \sin \alpha \frac{\partial^2 u}{\partial x \partial y} + \sin^2 \alpha \frac{\partial^2 u}{\partial y^2}. \quad (5.51)$$

In the previous sections we have focused on  $\partial u / \partial e_1$  and the grid-based representation  $u_x$  and  $u_y$ , but now we look for  $u_{xx}$ ,  $u_{xy}$  and  $u_{yy}$ , (5.51). The procedure to obtain directional discretizations is the same: optimize the error in the approximation to the derivative by reducing unwanted terms in the combination of the three derivatives.

The starting point is the subspace of consistent approximations of  $\partial^2 u / \partial e_1^2$  on a  $3 \times 3$  grid,

$$\begin{aligned} \Delta x^2 u_{xx} &= \Delta x^2 u_{xx,f} + \Delta x^2 u_{xx,b}(k_{xx}) = \frac{1}{4}(u_{-1,1} + 2u_{-1,0} + u_{-1,-1} \\ &\quad - 2u_{0,1} - 4u_{0,0} - 2u_{0,-1} + u_{1,1} + 2u_{1,0} + u_{1,-1}) + k_{xx}b, \\ \Delta y^2 u_{yy} &= \Delta y^2 u_{yy,f} + \Delta y^2 u_{yy,b}(k_{yy}) = \frac{1}{4}(u_{-1,1} - 2u_{-1,0} + u_{-1,-1} \\ &\quad + 2u_{0,1} + 4u_{0,0} + 2u_{0,-1} + u_{1,1} - 2u_{1,0} + u_{1,-1}) + k_{yy}b, \\ \Delta x \Delta y u_{xy} &= \Delta x \Delta y u_{xy,f} + \Delta x \Delta y u_{xy,b}(k_{xy}) \\ &= \frac{1}{4}(u_{1,1} - u_{-1,1} - u_{1,-1} + u_{-1,-1}) + k_{xy}b, \end{aligned} \quad (5.52)$$

where  $b$  is the basis stencil,

$$b = u_{-1,1} - 2u_{-1,0} + u_{-1,-1} - 2u_{0,1} + 4u_{0,0} - 2u_{0,-1} + u_{1,1} - 2u_{1,0} + u_{1,-1}, \quad (5.53)$$

see Fig. 5.18.

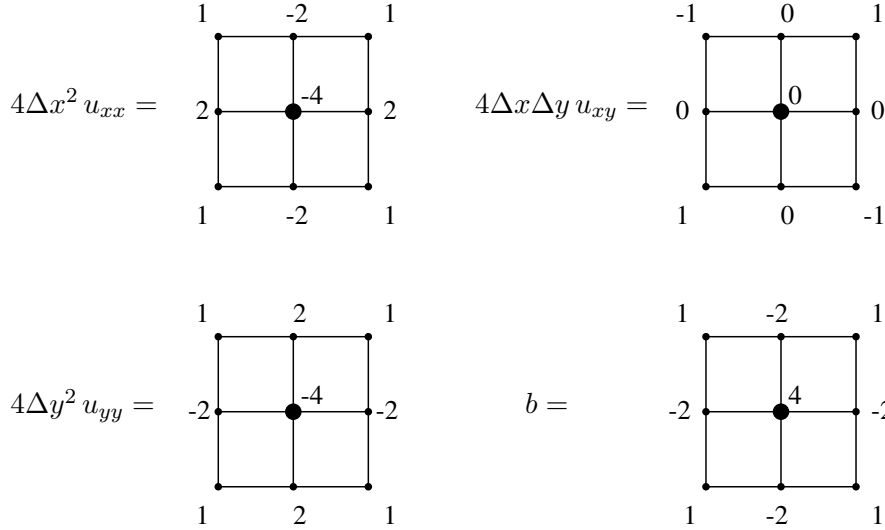


Figure 5.18. The stencils for  $u_{xx}$ ,  $u_{xy}$ , and  $u_{yy}$  of (5.52) with the stencil of the degree of freedom, approximating  $\Delta x^2 \Delta y^2 \partial^4 u / \partial x^2 \partial y^2$ .

The transformation for the second derivative normal to the advection direction is  $\partial^2 u / \partial e_2^2 = \cos^2 \alpha \partial^2 u / \partial y^2 - 2 \cos \alpha \sin \alpha \partial^2 u / \partial x \partial y + \sin^2 \alpha \partial^2 u / \partial x^2$ , and the approximation of  $\partial^2 u / \partial e_2^2$  uses also the grid-based derivatives of (5.52). We will use the notation  $k_{xx1}$ ,  $k_{xy1}$ , and  $k_{yy1}$  for  $\partial^2 u / \partial e_1^2$  and  $k_{xx2}$ ,  $k_{xy2}$ , and  $k_{yy2}$  for  $\partial^2 u / \partial e_2^2$ . The approximation of  $\partial^2 u / \partial e_1^2$  depends on the parameter  $k_1 = k_{xx1} \cos^2 \alpha + 2k_{xy1} \sin \alpha \cos \alpha + k_{yy1} \sin^2 \alpha$ , and  $\partial^2 u / \partial e_2^2$  on  $k_2 = k_{yy2} \cos^2 \alpha - 2k_{xy2} \sin \alpha \cos \alpha + k_{xx2} \sin^2 \alpha$ .

The basis stencil approximates the fourth mixed derivative  $\Delta x^2 \Delta y^2 \partial^4 u / \partial x^2 \partial y^2$  which we encountered before. The fixed stencils are chosen for obtaining simple directional errors. We will consider the principal region,  $0 \leq \alpha \leq \pi/4$ , where  $\cos \alpha \geq \sin \alpha \geq 0$ , and  $a_x / \Delta x \geq a_y / \Delta y \geq a_z / \Delta z \geq \dots \geq 0$ . For other flow angles we will use a permutation of the discretization.

The continuity of the discretization of  $\partial^2 u / \partial e_1^2$  leads at  $\alpha = \pi/4$  to the condition  $k_{xx1}(\pi/4) = k_{yy1}(\pi/4)$ , while  $k_{xy1}$  imposes no extra conditions thanks to the symmetry of the stencil. Similar conditions hold for  $\partial^2 u / \partial e_2^2$ .

The one-dimensional grid-aligned discretization is obtained both for  $\partial^2 u / \partial e_1^2$  and  $\partial^2 u / \partial e_2^2$  with  $k_{xx} = k_{yy} = -1/4$  and  $k_{xy} = 0$  or  $k = -1/4$ . For the diagonal discretization this is obtained with  $k_{xx1} = k_{yy1} = -1/4$  and  $k_{xy1} = 1/4$ , and with  $k_{xx2} = k_{yy2} = k_{xy2} = -1/4$  respectively, or  $k = 1/4(\sin(2\alpha) - 1)$ . The stencils of  $u_{xy}$  used in the diagonal approximation are shown in Fig. 5.19. The stencils for the approximations of  $u_{xx}$  and  $u_{yy}$  of the diagonal approximation are the one-dimensional grid-aligned derivatives. The diagonal approximation is continuous.

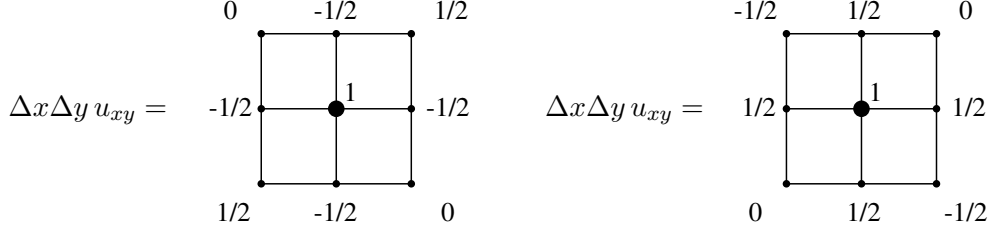


Figure 5.19. The stencils of the approximation of  $\partial^2 u / \partial x \partial y$  used in the diagonal discretizations of  $\partial^2 u / \partial e_1^2$ , left, and  $\partial^2 u / \partial e_2^2$ , right.

The diagonal discretization eliminates again the cross-derivatives when the flow is along the  $x$ -axis or along the diagonal, and reduces the approximation to a pure one-dimensional second derivative for  $\alpha = 0$  or  $\alpha = \pi/4$ .

The directional error  $\epsilon$  in the approximation of the second stream-wise derivative  $\partial^2 u / \partial e_1^2$  is obtained with a Taylor series expansion expressed in the local basis,

$$\epsilon = h^2 \left\{ \left( c_{40} \frac{\partial^2}{\partial e_1^2} + c_{31} \frac{\partial^2}{\partial e_1 \partial e_2} + c_{22} \frac{\partial^2}{\partial e_2^2} \right) \frac{\partial^2 u}{\partial e_1^2} + c_{13} \frac{\partial^4 u}{\partial e_1 \partial e_2^3} + c_{04} \frac{\partial^4 u}{\partial e_2^4} \right\} + O(h^4), \quad (5.54)$$

where  $c_{mn}$  is the coefficient of  $\partial^4 u / \partial e_1^m \partial e_2^n$ , excluding the factor  $h^4$ . The coefficients  $c_{mn}$  take the form

$$\begin{aligned} c_{40} &= \frac{1}{4} k_1 \sin^2(2\alpha) + \frac{1}{12} (1 + \sin^2(2\alpha)), \\ c_{31} &= \sin(2\alpha) \cos(2\alpha) (k_1 + \frac{1}{4}), \\ c_{22} &= k_1 (1 - \frac{3}{2} \sin^2(2\alpha)) + \frac{1}{4} (1 - \sin^2(2\alpha)), \\ c_{13} &= -\sin(2\alpha) \cos(2\alpha) (k_1 + \frac{1}{12}), \\ c_{04} &= \frac{1}{4} k_1 \sin^2(2\alpha). \end{aligned} \quad (5.55)$$

For  $\partial^2 u / \partial e_2^2$  the coefficients are  $c_{40} = 1/4 k_2 \sin^2(2\alpha)$ ,  $c_{31} = \sin(2\alpha) \cos(2\alpha) (k_2 + 1/12)$ ,  $c_{22} = k_2 (1 - 3/2 \sin^2(2\alpha)) + 1/4 \cos^2(2\alpha)$ ,  $c_{13} = -\sin(2\alpha) \cos(2\alpha) (k_2 + 1/4)$ , and  $c_{04} = 1/4 k_2 \sin^2(2\alpha) + 1/12 (1 + \sin^2(2\alpha))$ .

When solving  $\partial^2 u / \partial e_1^2 = 0$ , the coefficients  $c_{40}$ ,  $c_{31}$ , and  $c_{22}$  are irrelevant in the error, (5.54). However, the terms  $c_{13}$  and  $c_{04}$  cannot be set to zero simultaneously. For the advective derivative  $\partial u / \partial e_1$  a streamline approximation represents a condition on one normal derivative in the error term. For a second derivative there are two conditions. The fixed stencils of (5.52) result in  $c_{04} = 0$ , but  $c_{13} \neq 0$ . Let us call this an *incomplete streamline* approximation.

The sum of  $c_{13} \partial^4 u / \partial e_1 \partial e_2^3 + c_{04} \partial^4 u / \partial e_2^4$  can be eliminated when  $k_1$  is made data-dependent, i.e. a form of limiting. The estimation of  $\partial^4 u / \partial e_1 \partial e_2^3$  and  $\partial^4 u / \partial e_2^4$  requires nevertheless a larger stencil.

The Laplacian is an elliptic operator not related to an advection direction, and is invariant under rotation,  $\partial^2 u / \partial e_1^2 + \partial^2 u / \partial e_2^2 = \partial^2 u / \partial x^2 + \partial^2 u / \partial y^2$ . The stencils of the Laplacian which are based on the diagonal approximations of  $\partial^2 u / \partial e_1^2 + \partial^2 u / \partial e_2^2$  are shown in Fig. 5.20 for the case that the local basis  $B$  is along the  $x$ -axis and for the local basis  $B$  along the diagonal.

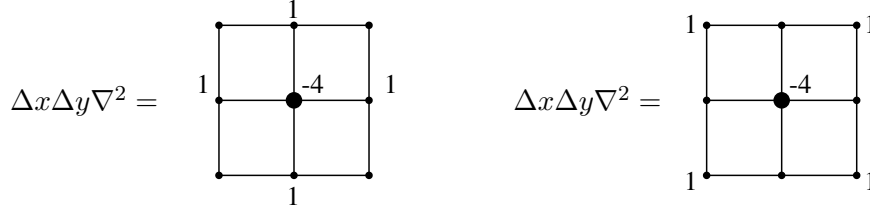


Figure 5.20. The stencils for the approximation of  $\partial^2 u / \partial e_1^2 + \partial^2 u / \partial e_2^2$  for the case that the local basis  $B$  is along the  $x$ -axis and for the local basis  $B$  along the diagonal.

It is possible to optimize the Laplacian since the errors are given by

$$\begin{aligned} c_{40} = c_{04} &= \frac{1}{4} k_3 \sin^2(2\alpha) + \frac{1}{12} (1 + \sin^2(2\alpha)), \\ c_{31} = -c_{13} &= \sin(2\alpha) \cos(2\alpha) (k_3 + \frac{1}{3}), \\ c_{22} &= k_3 (1 - \frac{3}{2} \sin^2(2\alpha)) + \frac{1}{2} \cos^2(2\alpha), \end{aligned} \quad (5.56)$$

where  $k_3$  is the degree of freedom in the approximation of the Laplacian. These errors are in basis  $B$  since we add the directional second derivatives, (5.55) and below. For  $\alpha = 0$  we get the grid-based errors. Taking  $k_3 = -1/3$  and  $\Delta x = \Delta y = h$  leads to the stencil

$$\begin{aligned} h^2 \left( \frac{\partial^2 u}{\partial e_1^2} + \frac{\partial^2 u}{\partial e_2^2} \right) &= \frac{1}{6} (u_{-1,1} + 4u_{-1,0} + u_{-1,-1} + 4u_{0,1} - 20u_{0,0} + 4u_{0,-1} \\ &\quad + u_{1,1} + 4u_{1,0} + u_{1,-1}), \end{aligned} \quad (5.57)$$

which is shown in Fig. 5.21.

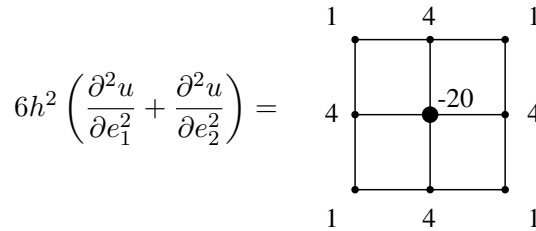


Figure 5.21. The stencil for the approximation of the Laplacian with an error of  $O(h^4)$ .

This is the approximation of Dahlquist and Bjork [9]. The error  $\epsilon$  of this approximation, substituting  $k_3 = -1/3$  in (5.56) and following a reasoning like (5.17), is of  $O(h^4)$ . The individual stencils are averages of one-dimensional second derivatives, Fig. 5.22.

When we interpret the  $y$ -axis as time, and take a new variable  $X = ax$ , we obtain the subsonic wave equation  $u_{tt} + a^2 u_{XX} = 0$  with

$$\begin{aligned} \Delta X^2 u_{XX} &= \frac{1}{12} (u_{i+1}^{n+1} - 2u_i^{n+1} + u_{i-1}^{n+1} + 10u_{i+1}^n - 20u_i^n + 10u_{i-1}^n \\ &\quad + u_{i+1}^{n-1} - 2u_i^{n-1} + u_{i-1}^{n-1}), \end{aligned}$$

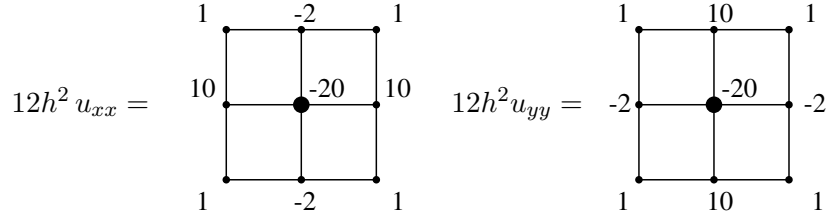


Figure 5.22. The derivatives  $u_{xx}$  and  $u_{yy}$  which add up to the stencil of Fig. 5.20.

$$\begin{aligned} \Delta t^2 u_{tt} = \frac{1}{12} & (u_{i+1}^{n+1} - 2u_{i+1}^n + u_{i+1}^{n-1} + 10u_i^{n+1} - 20u_i^n + 10u_i^{n-1} \\ & + u_{i-1}^{n+1} - 2u_{i-1}^n + u_{i-1}^{n-1}). \end{aligned} \quad (5.58)$$

This is a fourth order approximation in  $\Delta t$  and in  $\Delta X$

The analysis for the supersonic case involves  $\partial^2 u / \partial e_1^2 - \partial^2 u / \partial e_2^2$ , and the analysis is similar. This derivative is not rotationally independent, and we take  $\alpha = 0$  to find that  $k_3 = 0$  leads to

$$h^2 \left( \frac{\partial^2 u}{\partial e_1^2} - \frac{\partial^2 u}{\partial e_2^2} \right) = u_{-1,0} - u_{0,1} - u_{0,-1} + u_{1,0}. \quad (5.59)$$

The stencil of (5.59) has fourth order accuracy at convergence, and is shown in Fig. 5.23. The individual stencils for  $u_{xx}$  and  $u_{yy}$  are the ones shown in Fig. 5.18.

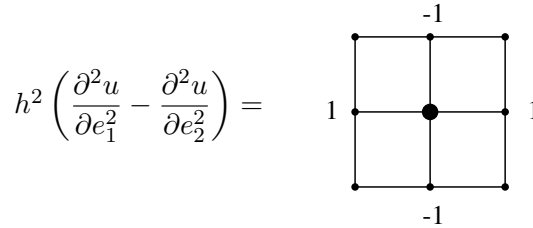


Figure 5.23. The stencil for the approximation of  $\partial^2 u / \partial e_1^2 - \partial^2 u / \partial e_2^2$  with an error of  $O(h^4)$ .

A comparison is made for three discretization of  $\partial^2 u / \partial e_1^2$ , the one-dimensional grid-aligned discretization,  $k_{xx1} = k_{yy1} = -1/4$  and  $k_{xy1} = 0$ , the diagonal discretization,  $k_{xx1} = k_{yy1} = -1/4$  and  $k_{xy1} = 1/4$ , and the incomplete streamline discretization of (5.52) with  $k_1 = 0$ . The coefficients are shown in Fig. 5.24, and the average values in Table 5.4.

Table 5.5. The average values  $I_{mn}$  of the error terms of the second stream-wise derivative  $\partial^2 u / \partial e_1^2$ : one-dimensional grid-aligned, diagonal, and the incomplete streamline stencil.

discretization	$I_{40}$	$I_{31}$	$I_{22}$	$I_{13}$	$I_{04}$
one-dimensional	0.094	0.0	0.0625	0.053	0.0313
diagonal	0.120	0.053	0.0625	0.016	0.0047
incomplete streamline	0.125	0.080	0.125	0.027	0.0

The second stream-wise directional discretizations have less error than the one-dimensional grid-aligned approximations. They can be used as directional artificial dissipation since they can be applied separately with different coefficients in the stream-wise and

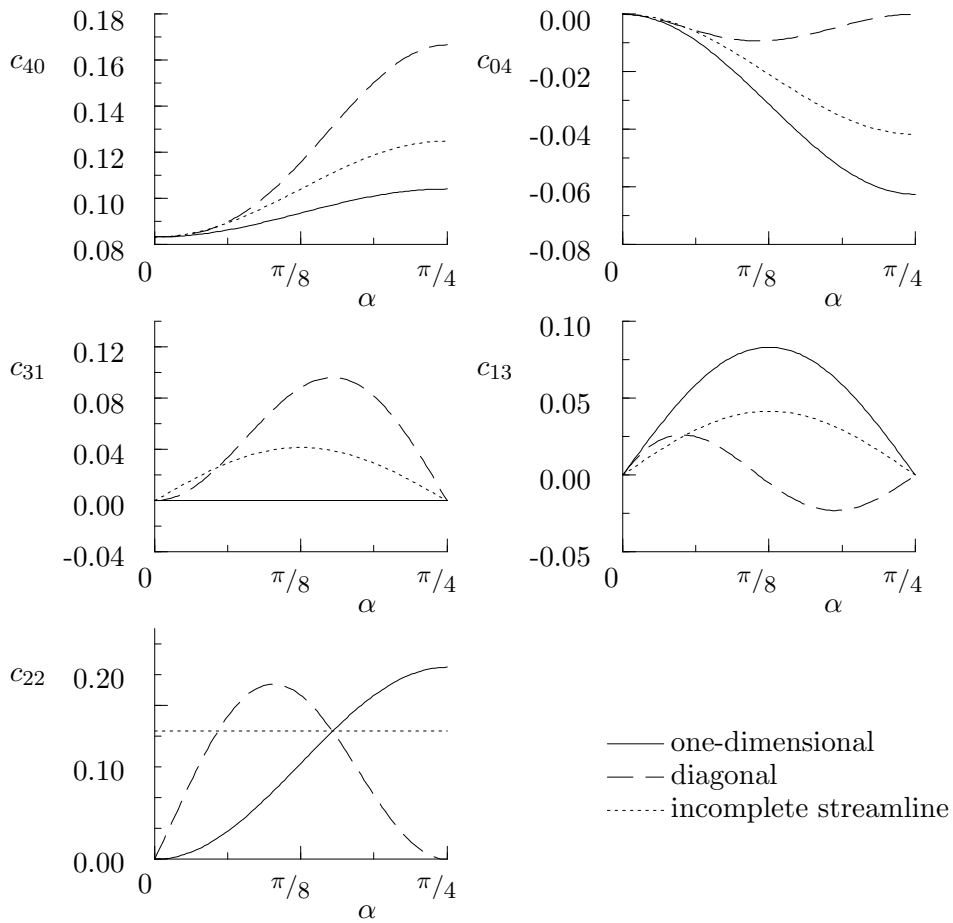


Figure 5.24. The coefficients of the error terms of the second stream-wise derivative: one-dimensional grid-aligned, diagonal, and the incomplete streamline approximation.

in the normal direction. When both coefficients are the same, the resulting Laplacian is optimal with  $k = -1/6$ , but not optimal with the diagonal approximation.

Upwind or upwind biased second derivatives can be derived in the same way on a larger stencil, but are beyond the scope of this paper.

### 5.5. Combining various approximations.

We have encountered in the previous sections approximations to derivatives with an increased accuracy and stability. The approximation for the Laplacian gains two orders of accuracy, while the advection derivative  $\partial u / \partial e_1$  gained one or two orders for the steady advection equation on the  $3 \times 3$  grid. We now turn our attention to the linear advection-diffusion equation with a source term,

$$\frac{\partial u}{\partial t} + a_x \frac{\partial u}{\partial x} + a_y \frac{\partial u}{\partial y} + \nu \nabla^2 u = s(x, y). \quad (5.60)$$

We will start by looking at the one-dimensional advection equation with a source term at steady state,

$$a_x \frac{\partial u}{\partial x} - s(x) = 0. \quad (5.61)$$

Suppose that we use an approximation of  $a_x \partial u / \partial x$  which has an error  $\epsilon$  of the form

$$\epsilon = h^j c_j \frac{\partial^j}{\partial x^j} \left( a_x \frac{\partial u}{\partial x} \right) + O(h^k), \quad \text{with } k > j, \quad (5.62)$$

with  $c_j$  some constant or function, which is typical of the approximations of the previous sections. The term between brackets in (5.62) is not of  $O(h^j)$  due to the presence of the source term in (5.61). This is easily cured by including a correction term  $-s(x)$  in the approximation. The correction term should use the same spatial approximation as the advection term, and it is convenient to discretize together  $\partial / \partial x (a_x u - hs)$ . This is the remedy of Sidilkover [8], who corrected the flux approximation to  $f_{i+1/2} = (a_x u - hs)_{i+1/2}$ . The new discretization of (5.61) has an error

$$\epsilon = h^j c_j \frac{\partial^j}{\partial x^j} \left( a_x \frac{\partial u}{\partial x} - hs \right) + O(h^k), \quad (5.63)$$

where the term between brackets is now of  $O(h^j)$ , which leads to the desired error reduction.

This procedure works also in higher dimensions. The effect of the source on stability and convergence remains to be analyzed. For systems a decomposition in waves is necessary.

The Laplacian and the diffusion term can be treated as a source term when discretizing an advection equation.

For the unsteady solution, (5.60), we seek the approximation in one more dimension, and take the time variable along the new axis.

The non-linear problem uses the discretizations described in previous sections.

### 5.6. Directional fourth order discretizations of the first derivative in two dimensions on a $5 \times 5$ grid.

The analysis is similar to the one given in §5.2. On this grid, the space of consistent approximations has a basis of ten different stencils. We use the upper triangle property to denote the basis stencils. The upper triangle nodes are  $(2, -1)$ ,  $(1, 0)$ ,  $(2, 0)$ ,  $(0, 1)$ ,  $(1, 1)$ ,  $(2, 0)$ ,  $(-1, 2)$ ,  $(0, 2)$ ,  $(1, 2)$ , and  $(2, 2)$  respectively, and for basis stencil  $b^i$  the weight of all these nodes is zero, except for upper triangle node  $i$  which has a weight of one. This basis can be found on the website [24]. The continuity constraints are similar to the ones of §5.2. There is no monotonic approximation.

We use a streamline fixed stencil,  $\partial^5 u / \partial e_2^5 = 0$  or  $c_{05} = 0$ , see Fig. 5.25. Similar to the fixed stencil (5.27), also  $c_{06} = 0$ , and at steady state the solution of the advection equation is of  $O(h^6)$ .

The basis  $\tilde{B}$  with antisymmetric and symmetric stencils is  $\tilde{B} = \{^a b^1, \dots, ^a b^5, ^a b^7, ^s b^1, \dots, ^s b^4\}$ . The antisymmetric stencils are important for the lowest order of the error of  $\partial u / \partial e_1$ , while the symmetric stencils appear one order higher in the error, and remain important for the Fourier analysis. This basis is not very convenient to work with, even when we apply the orthogonalization procedure. It is more practical to transform  $\tilde{B}$  to the regular fully orthogonal basis  $B$  of which the antisymmetric stencils are shown in Fig. 5.26.

With this basis it is easy to construct regular discretizations for which the stencil of  $u_y$  is the stencil of  $u_x$  mirrored in the  $x = y$  diagonal. The basis stencils 4, 5, and 6 have this property with respect to stencils 1, 2, and 3 respectively. A regular approximation has

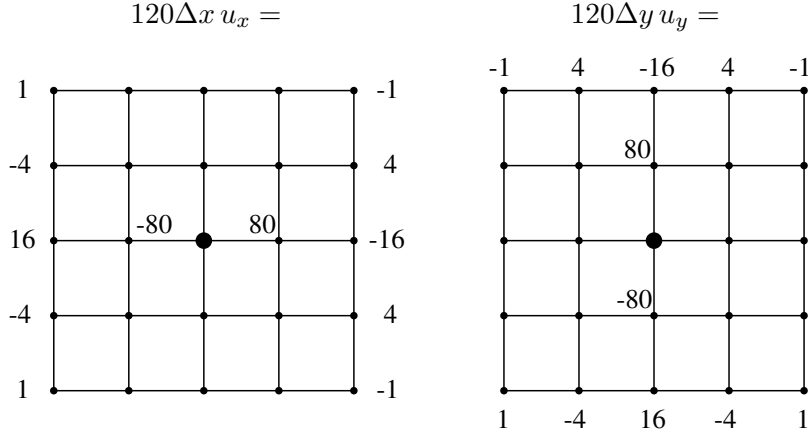


Figure 5.25. The fixed stencils for the directional fourth order approximations of  $u_x$  and  $u_y$  in two dimensions with the streamline property,  $\partial^5 u / \partial e_2^5 = 0$  or  $c_{05} = 0$ , but also  $c_{06} = 0$ .

$K_{x4} = K_{y1}$  and  $K_{y4} = K_{x1}$ , or  $K_4 = K_{y1} \cos \alpha + K_{x1} \sin \alpha$ , and similar for the combinations  $K_5$  and  $K_2$ , and  $K_6$  and  $K_1$ .

A straight approximation has  $K_{x4} = K_{x5} = K_{x6} = K_{y1} = K_{y2} = K_{y3} = 0$ , and a regular straight approximation only depends on  $K_{x1}$ ,  $K_{x2}$ , and  $K_{x3}$ .

The continuity conditions with this basis are trivial.

With the fixed stencils of Fig. 5.25 and basis  $B$  for the one-dimensional grid-aligned discretization, the  $K$ 's are zero, except  $K_{x1} = K_{y4} = 1/120$ . The diagonal approximation of (2.9) uses the same vector  $K_x$ , while  $K_y = 1/7(1/24, -2/3, -1/6, -1/10, -2/3, -1/6, 0, 0, 0, 0)^T$ .

The error terms  $c_{05}$  and  $c_{14}$ , expressed in basis  $B$ , are

$$c_{05} = \sin(2\alpha) \left\{ - (2K_1 + K_2) \cos^3 \alpha - 7K_3 \sin^2 \alpha \cos \alpha \right. \\ \left. + (2K_4 + K_5) \sin^3 \alpha + 7K_6 \cos^2 \alpha \sin \alpha \right\},$$

$$c_{14} = -\frac{1}{120}(\cos(4\alpha) + 3) \\ + (2K_1 + K_2) \cos^3 \alpha (\cos^2 \alpha - 4 \sin^2 \alpha) - 14K_3 \cos \alpha \sin^2 \alpha (2 \sin^2 \alpha - 3 \cos^2 \alpha) \\ + (2K_4 + K_5) \sin^3 \alpha (\sin^2 \alpha - 4 \cos^2 \alpha) - 14K_6 \sin \alpha \cos^2 \alpha (2 \cos^2 \alpha - 3 \sin^2 \alpha). \quad (5.64)$$

The coefficients of the error terms of  $O(h^5)$  depend on the symmetric stencils, and are proportional to the parameters  $K_7$ – $K_{10}$ .

We can obtain  $c_{05} = 0$  by solving (5.64) e.g. for  $K_1$ ,

$$K_1 = -\frac{1}{2}K_2 + \frac{7}{2}K_6 \tan \alpha - \frac{7}{2}K_3 \tan^2 \alpha + \tan^3 \alpha (K_4 + \frac{1}{2}K_5). \quad (5.65)$$

The substitution of this solution in  $c_{14}$  gives

$$c_{14} = -\frac{1}{120}(\cos(4\alpha) + 3) - 6(2K_4 + K_5) \sin^3 \alpha + 7 \sin(2\alpha)(2K_3 \sin \alpha - K_6 \cos \alpha), \quad (5.66)$$

which can only be optimized. The analysis is similar to the one of §5.2 and will not be repeated here.

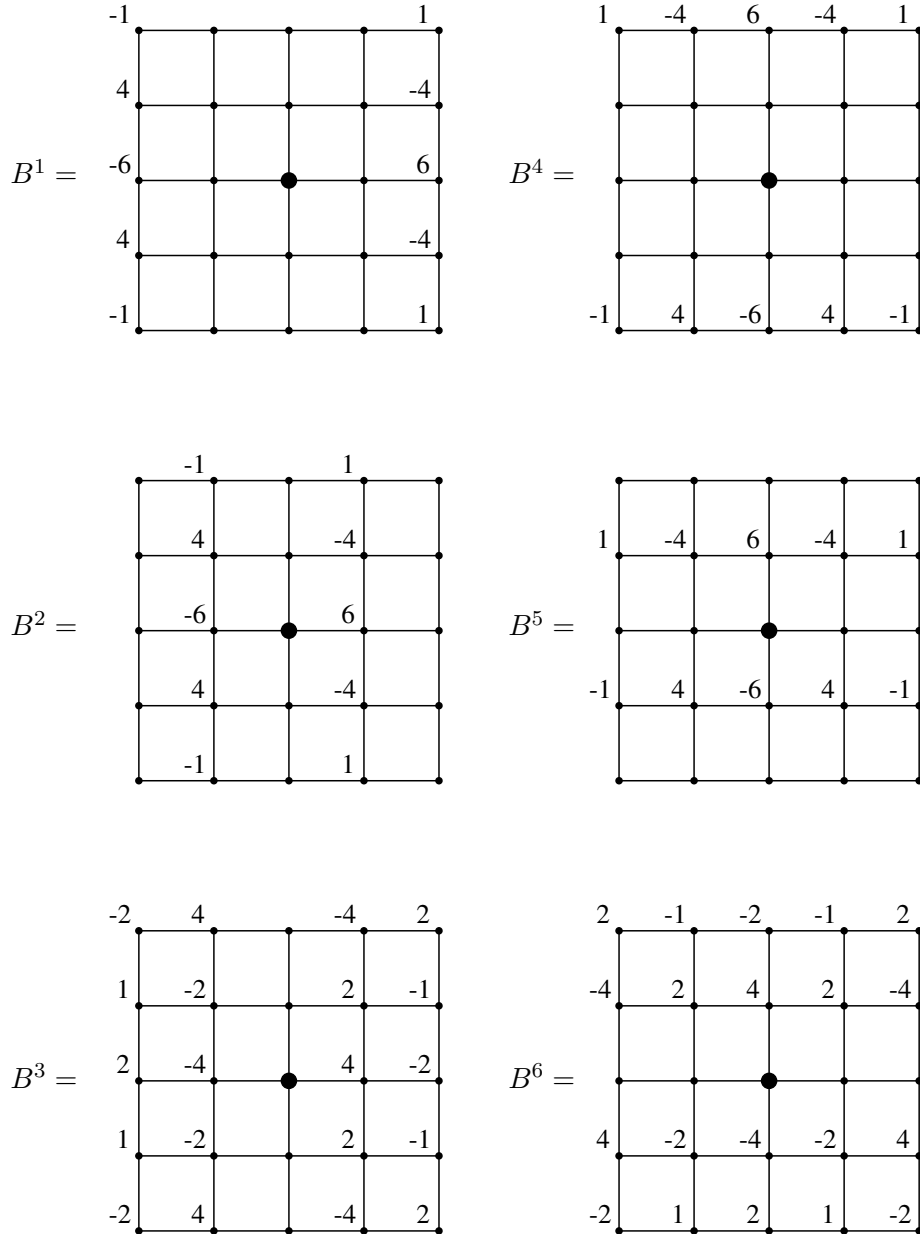


Figure 5.26. The regular antisymmetric fully orthogonal basis stencils for the fourth order approximations.

Streamline stencils which are independent of the flow angle have to satisfy (5.65) for all angles  $\alpha$ . This constraint translates to

$$\begin{aligned}
 K_{x4} &= \frac{1}{2}(-K_{x5} + 7K_{y3}), & K_{y4} &= -\frac{1}{2}K_{y5}, & K_{x1} &= -\frac{1}{2}K_{x2}, \\
 K_{y1} &= \frac{1}{2}(7K_{x6} - K_{y2}), & \text{and } K_{y6} &= K_{x3}, & & 
 \end{aligned}
 \tag{5.67}$$

which is not subject to the continuity constraints.

We will follow the steps of §5.2 in the stability analysis of the approximation which consists of the fixed stencil of Fig. 5.25 with basis  $B$  and with periodic boundary conditions.

The parameters  $K_1 \dots K_6$  contribute to the imaginary part, and  $K_7 \dots K_{10}$  to the real part of  $\Omega_{l,m}$ . The imaginary part of the eigenvalues of the space operator are

$$\begin{aligned} \Omega_{l,m} = -I \frac{a}{h} & \left( \frac{1}{15} [ \cos \alpha \sin \phi_x (20 - \cos \phi_x (2(\cos \phi_y - 1)^2 + 5)) \right. \\ & + \sin \alpha \sin \phi_y (20 - \cos \phi_y (2(\cos \phi_x - 1)^2 + 5))] \\ & + 8 \sin \phi_x (\cos \phi_y - 1) \left\{ \right. \\ & \quad (2K_1 \cos \phi_x + K_2)(\cos \phi_y - 1) + K_3(\cos \phi_x - 1)(4 \cos \phi_y + 3) \left. \right\} \\ & + 8 \sin \phi_y (\cos \phi_x - 1) \left\{ \right. \\ & \quad (2K_4 \cos \phi_y + K_5)(\cos \phi_x - 1) + K_6(\cos \phi_y - 1)(4 \cos \phi_x + 3) \left. \right\} \Big). \end{aligned} \quad (5.68)$$

The one-dimensional grid-aligned discretization has the eigenvalues

$$\Omega_{l,m} = -\frac{a}{3h} I \{ \cos \alpha \sin \phi_x (\cos \phi_x - 4) + \sin \alpha \sin \phi_y (\cos \phi_y - 4) \}. \quad (5.69)$$

The maximum eigenvalues are found at  $\phi_x = \phi_y = \phi_m$  with  $\cos \phi_m = 1 - 1/2\sqrt{6}$ , which gives  $\Omega = a/h I (\cos \alpha + \sin \alpha) M$  where  $M = [1/4 + 2\sqrt{2/3}]^{1/2} \approx 1.37$ .

For the diagonal approximation of (2.9), the eigenvalues are

$$\begin{aligned} \Omega_{l,m} = -\frac{a}{3h} I & \left\{ (\cos \alpha - \sin \alpha) \sin \phi_x (\cos \phi_x - 4) \right. \\ & \left. + \sin \alpha \sin(\phi_x + \phi_y) (\cos(\phi_x + \phi_y) - 4) \right\}, \end{aligned} \quad (5.70)$$

which are purely imaginary. The eigenvalues follow the pattern of the second order diagonal discretization, one term dependent on  $\cos \alpha - \sin \alpha$  multiplying a function of  $\phi_x$ , and another term which is dependent on  $\sin \alpha$  multiplying the same function which depends now on  $\phi_x + \phi_y$ . The maximum eigenvalue is the optimal one,  $\Omega = a/h I M \cos \alpha$ .

The fixed stencil has a maximum value of the eigenvalues which is some 5–12% larger than those of the one-dimensional grid-aligned discretization.

The general streamline approximation with flow-angle independent stencils of (5.67) is complicated to optimize. We observed in §5.2 that the optimal time step was for regular straight stencils. Combined with the streamline condition for fixed stencils, we arrive at an additional condition,  $2K_{x1} + K_{x2} = 0$ , and we are left with two parameters,  $K_{x2}$  and  $K_{x3}$ . The choice of  $K_{x2} = -1/24$  and  $K_{x3} = -1/16$  gives an approximation which is close to optimal. This approximation is shown in Fig. 5.27.

Among the discretizations on the  $5 \times 5$  grid, the approximation derived in [7] using the FVD method with the N-distribution is given by the stencils of Fig. 5.28. Like the other discretizations discussed in this section, it is a central discretization.

The eigenvalues for this approximation are

$$\begin{aligned} \Omega = & \cos \alpha [6 \sin \phi_x - 3 \sin \phi_y + 4 \cos \phi_x \sin \phi_y + 2 \cos \phi_y \sin \phi_x (1 - \cos \phi_x)] \\ & + \sin \alpha [6 \sin \phi_y - 3 \sin \phi_x + 4 \cos \phi_y \sin \phi_x + 2 \cos \phi_x \sin \phi_y (1 - \cos \phi_y)]. \end{aligned} \quad (5.71)$$

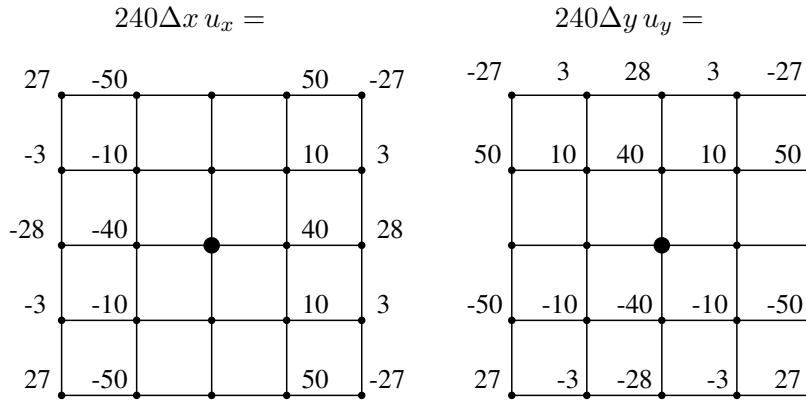


Figure 5.27. The fixed stencils for the directional fourth order approximations of  $u_x$  and  $u_y$  in two dimensions with the streamline property  $c_{05} = 0$ , and also  $c_{06} = 0$ , and with optimized time step.

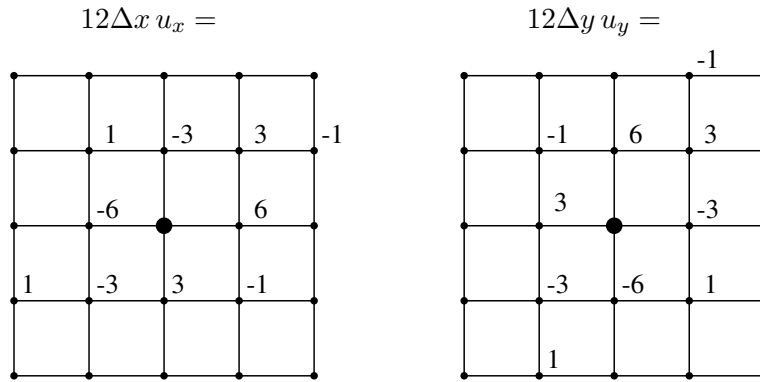


Figure 5.28. The stencils for the FVD directional fourth order central approximations of  $u_x$  and  $u_y$  in two dimensions of [7].

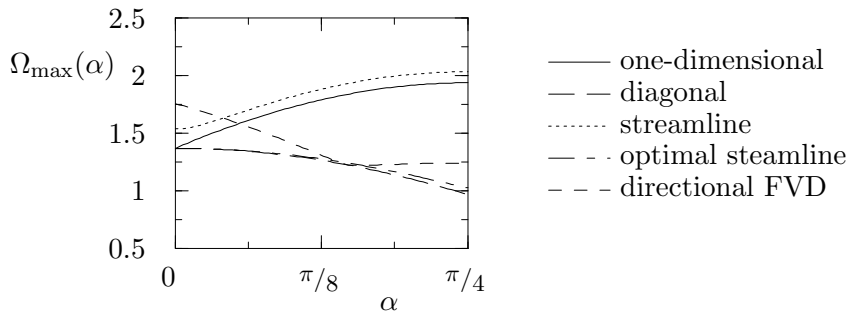


Figure 5.29. The maximum eigenvalue of  $\Omega$ , excluding the scaling factor  $a/h$ , as a function of the flow angle  $\alpha$  for the approximations: one-dimensional grid-aligned (5.69), diagonal (5.70), the streamline approximation of Fig. 5.25, the optimized streamline approximation of Fig. 5.27, and the directional FVD approximation of Fig. 5.28.

The maximum eigenvalue of  $\Omega$ , excluding the scaling factor  $a/h$ , as a function of the flow angle  $\alpha$  is given in Fig. 5.29 for the above approximations.

The stability of the optimal streamline approximation is 5% worse than the optimal

diagonal approximation at  $\alpha = \pi/4$ . A flow-angle dependent optimal streamline approximation, or dropping the streamline condition, is therefore hardly warranted. The systematic construction of approximations which exhibit the optimal  $\Omega$ , i.e. having the lowest maximum eigenvalue, also in the high frequency range, is a task which is outlined in §5.2, and which we will leave for later.

A comparison of the error components is made for the above discretizations. The six different coefficients are shown in Fig. 5.30, and the average values in Table 5.6.

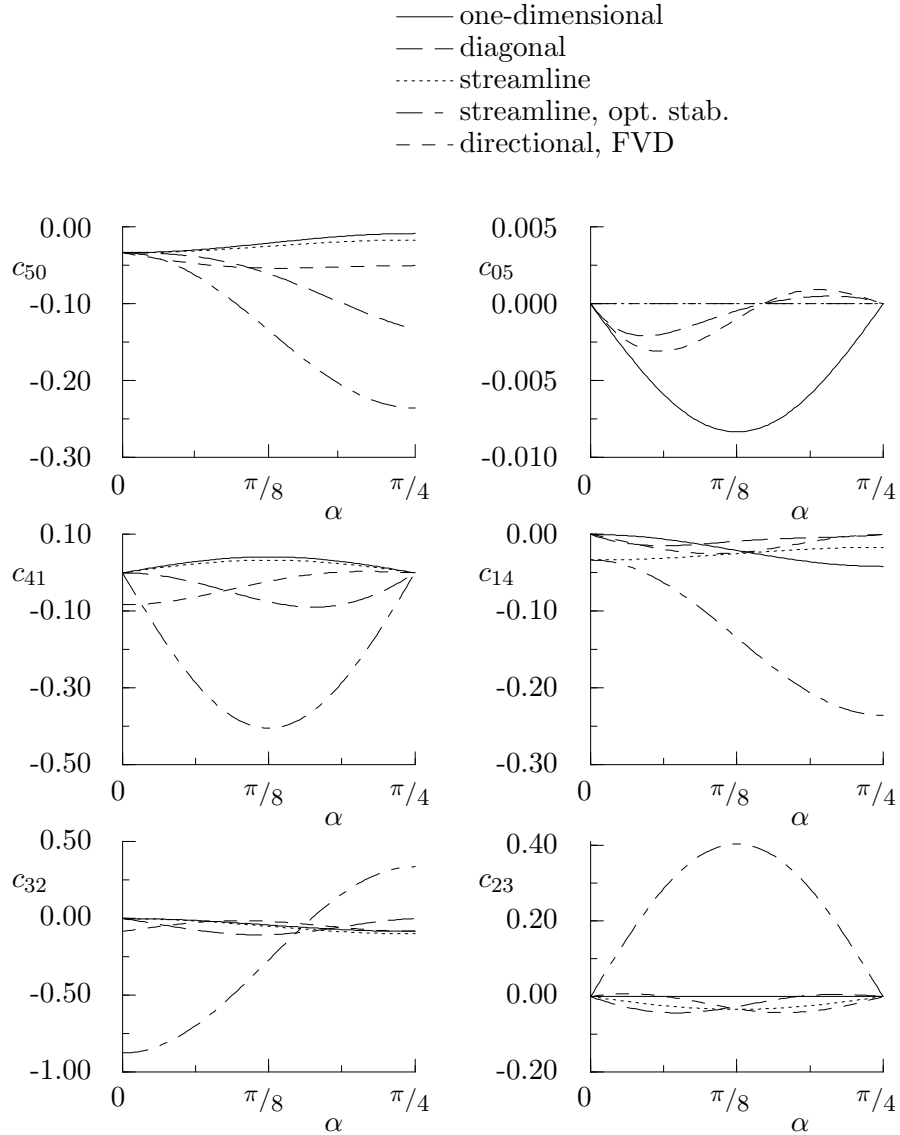


Figure 5.30. The coefficients of the error terms for the approximations of Fig. 5.29.

The reduction in the error of  $I_{05}$  for the diagonal discretization compared to the one-dimensional grid-aligned discretization is 6.16. For the FVD version this is about 1.6. For  $I_{14}$ , this is 2.64 and 1.72 respectively. The error reduction increases with the order of the discretization.

Table 5.6. The average values  $I_{mn}$  for the approximations of Fig. 5.29.

discretization	$I_{50}$	$I_{41}$	$I_{32}$	$I_{23}$	$I_{14}$	$I_{05}$
one-dimensional	0.021	0.027	0.042	0.0	0.021	0.00531
diagonal	0.070	0.048	0.060	0.020	0.008	0.00086
streamline	0.025	0.021	0.050	0.021	0.025	0.0
optimal streamline	0.134	0.257	0.425	0.257	0.134	0.0
directional, FVD	0.049	0.032	0.045	0.021	0.014	0.00138

### 5.7. Directional second and third order upwind discretizations of the first derivative in two dimensions on a $5 \times 5$ grid.

The third order accurate approximation on the  $5 \times 5$  grid has a basis of 15 stencils [24], which can be rewritten in 6 antisymmetric stencils with an error of  $O(h^4)$ , and 9 symmetric stencils with an error of  $O(h^3)$ . It is possible to choose the mix of stencils such that a fourth order approximation results, but this is not the purpose at present, just like second order approximations were not the aim in §5.3. We will consider upwind discretizations with one-dimensional fixed stencils, and start by restricting the domain to the 16 point stencil on  $[-2, 1]^2$ . The basis has now 6 stencils, of which an orthogonalized version  $B$  is given in Fig. 5.31.

In this orthogonalized basis, only stencils  $B^1$ ,  $B^2$ , and  $B^3$  are of  $O(h^3)$ . The continuity conditions for  $\alpha = 0$  are  $K_{xi} = 0$  for  $i = 1 \dots 6$ . A streamline approximation in this basis satisfies

$$2K_{x1} - 5K_{y2} = 0, \quad K_{x2} = K_{y3} = \frac{1}{120}, \quad \text{and} \quad 2K_{y1} - 5K_{x3} = 0, \quad (5.72)$$

but does not comply with the continuity conditions.

Like in §5.3, the extra upwind nodes  $[-2, 2]$ ,  $[-1, 2]$ , and  $[0, 2]$  can be included in an upwind stencil on the principal region, leading to three extra basis stencils. These three stencils have weights 1, -4, 6, -4, 1 on  $i = -2, 1, 0$  respectively. In this basis of nine stencils, the continuity conditions are for  $\alpha = 0$

$$K_{x1} = 0, \quad K_{x2} = 0, \quad K_{x3} + K_{x5} = 0, \quad K_{x4} - K_{x6} = 0, \quad (5.73)$$

and for  $\alpha = \pi/4$

$$\begin{aligned} K_{x1} = K_{y2}, \quad K_{x2} = K_{y1}, \quad K_{x3} = K_{y3}, \quad K_{x4} = K_{y4}, \quad K_{x5} = K_{y6}, \quad K_{x6} = K_{y5}, \\ K_{xi} = K_{yi} = 0 \text{ for } i = 7 \dots 9. \end{aligned} \quad (5.74)$$

The streamline condition translates into

$$\begin{aligned} -10K_{x1} + K_{y7} + K_{y8} + K_{y9} + \frac{1}{12} = 0, \quad K_{y2} = \frac{1}{120}, \\ K_{x7} + K_{x8} + K_{x9} = 0, \quad K_{x2} = K_{y3} = \frac{1}{120}. \end{aligned} \quad (5.75)$$

The continuity and streamline conditions can be solved together, involving flow-angle dependent coefficients. The degrees of freedom can be used to strive for isotropy of the directional error and of the Fourier representation with respect to the flow angle. The optimization in the Fourier domain includes also an optimal time step and an optimization

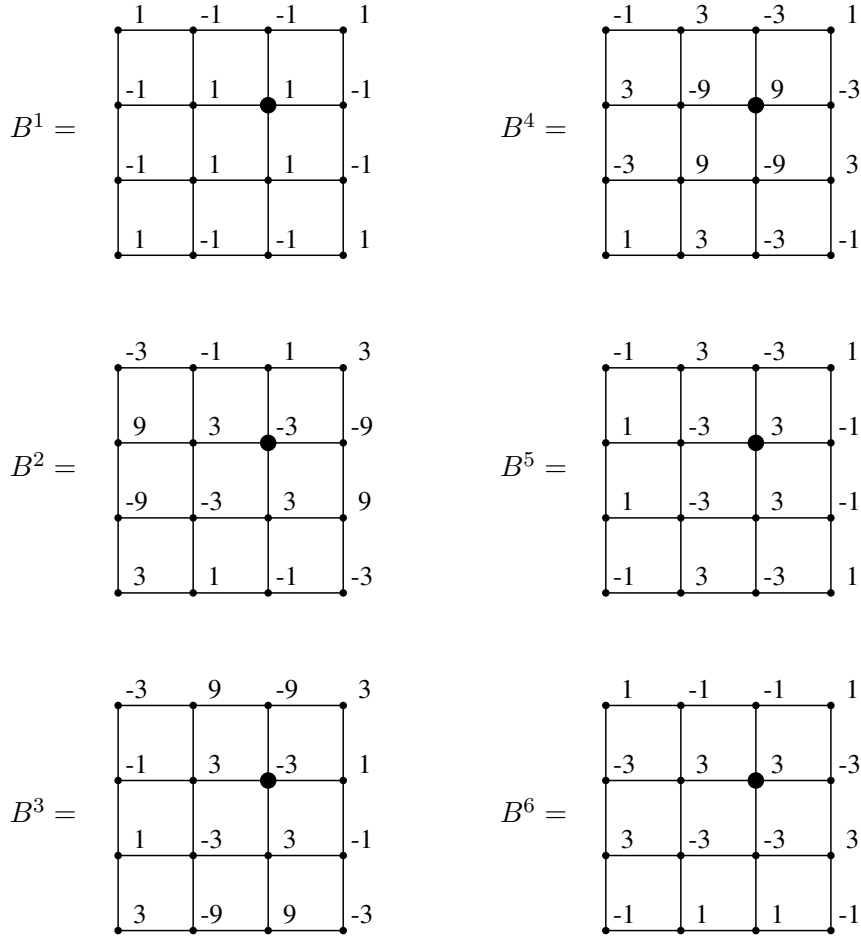


Figure 5.31. The basis stencils used in the approximation for the third order upwind approximation.

of the smoothing properties for a multi-grid application. This is, together with boundary stencils, beyond the scope of this paper.

The diagonal discretizations use twelve basis stencils for  $u_y$  and ten for  $u_x$ . The latter depends also on eight of the coefficients  $k_y$ , similar to (5.44). The upwind-biased subset of approximations is found on the region  $i \leq 1$  and  $i + j \leq 1$ . On this domain, we find the FD continuous diagonal approximation of §2.5, (2.8). A FV continuous approximation can be derived in the spirit of (5.11), (5.12).

The second order accurate discretizations have a basis of 19 stencils. When we consider the monotonicity of the approximation like in §5.3, we obtain equations similar to (5.46). Using again the code HOPDM [23] we verify that there is no second order monotonic approximation on the  $5 \times 5$  grid.

The upwind basis on the  $[-2, 0]^2$  region consists of three stencils ; including the nodes  $[-2, 1]$ ,  $[-2, 2]$ , and  $[-1, 1]$  leads to a basis of six stencils. On this extended base, we can apply the optimizations described for the third order upwind biased discretizations.

The central approximation of §5.2 needs streamline upwind stencils at the boundary with the property  $c_{03} = 0$ . For a node on the left boundary we consider the sector  $0 \leq i \leq 2$ ,  $-2 \leq j \leq 2$  where nine stencils are available. These stencils are not sufficient to satisfy the condition  $c_{04} = 0$ , and we need to enlarge the domain to  $0 \leq i \leq 3$ . There are many

streamline solutions for the node  $(0, j)$  on this domain. We retain the stencils given by

$$\begin{aligned}
 12\Delta x u_x &= -3u_{0,j+1} + 4u_{1,j+1} - u_{2,j+1} - 12u_{0,j} + 16u_{1,j} - 4u_{2,j} \\
 &\quad - 3u_{0,j-1} + 4u_{1,j-1} - u_{2,j-1}, \\
 24\Delta y u_y &= 7u_{0,j+1} + 11u_{1,j+1} - 7u_{2,j+1} + u_{3,j+1} \\
 &\quad - 7u_{0,j-1} - 11u_{1,j-1} + 7u_{2,j-1} - u_{3,j-1},
 \end{aligned} \tag{5.76}$$

which apply to the left boundary of the domain, and which are shown in Fig. 5.32.

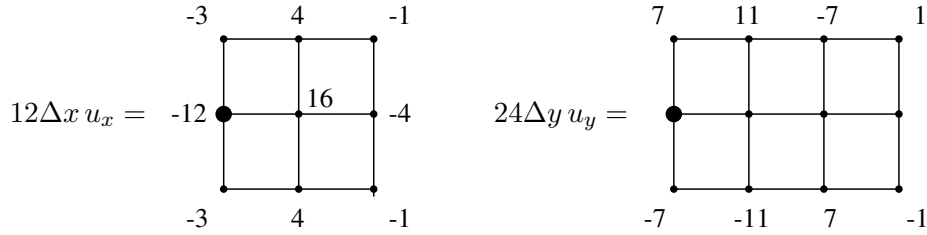


Figure 5.32. The boundary stencils for the derivatives  $u_x$  and  $u_y$  of (5.76) with the streamline property and  $c_{04} = 0$ .

The streamline stencils with  $c_{04} = 0$  for the corner are the mirror image of each other, as can be seen from Fig. 5.33. They are again weighted averages of upwind differences.

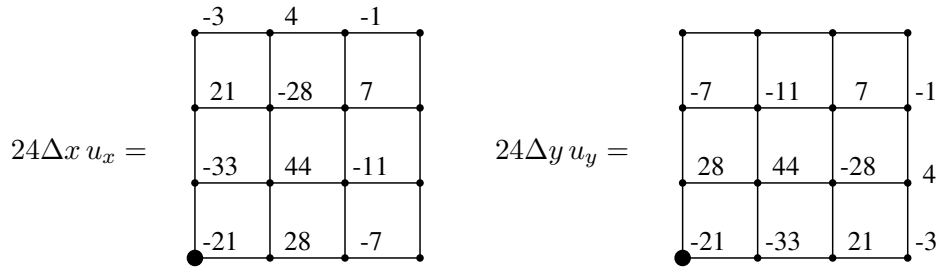


Figure 5.33. The corner stencils of  $u_x$  and  $u_y$  used in the approximation for the second order streamline derivative, with  $c_{04} = 0$ .

The above approximations are chosen for compactness and symmetry properties. An additional constraint which is not taken into account is the time step restriction for the overall approximation, and this may lead to yet different stencils.

The translation to FV interface fluxes is straightforward.

Among the second order upwind discretizations are the one-dimensional grid-aligned approximation and the diagonal approximation of (2.7). Their stencils is on the quadrant  $i \leq 0, j \leq 0$ . Another example is the second order almost upwind discretization found in [7]. This approximation is derived on a regular grid consisting of triangles by the FVD method. The discretization is given by

$$\begin{aligned}
 \Delta x u_x &= 2u_{0,0} - 2u_{-1,0} - \frac{1}{2}u_{0,1} - \frac{1}{2}u_{-1,-1} + \frac{1}{2}u_{-2,-1} + \frac{1}{2}u_{-1,1}, \\
 \Delta y u_y &= \frac{3}{2}u_{-1,0} - \frac{3}{2}u_{-1,-1} - \frac{1}{2}u_{0,-1} + \frac{1}{2}u_{0,1} + \frac{1}{2}u_{-1,-2} - \frac{1}{2}u_{-1,1},
 \end{aligned} \tag{5.77}$$

and the stencils are given in Fig. 5.34.

This discretization includes the node  $(0,1)$ , and the approximation is not strictly upwind. It is not a pure one-dimensional discretization when the flow is along the  $x$ -axis or along the diagonal. The approximation is discontinuous for  $\alpha = 0$ .

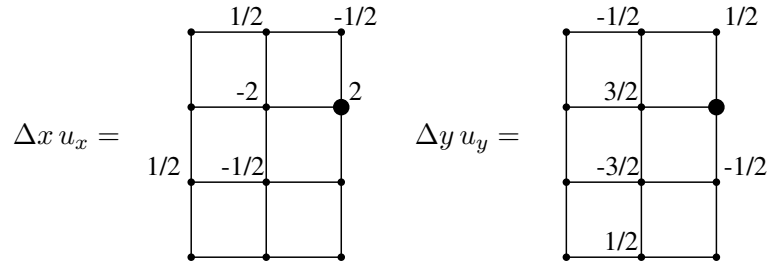


Figure 5.34. The stencils for the FVD directional upwind approximations of  $u_x$  and  $u_y$  in two dimensions of [7], (5.77).

The four coefficients  $c_{nm}$  for the one-dimensional grid-aligned discretization, the diagonal discretization of (2.7), and the FVD discretization above are shown in Fig. 5.35, and the average values in Table 5.7. The corresponding coefficients for the central approximations are given in Table 5.4.

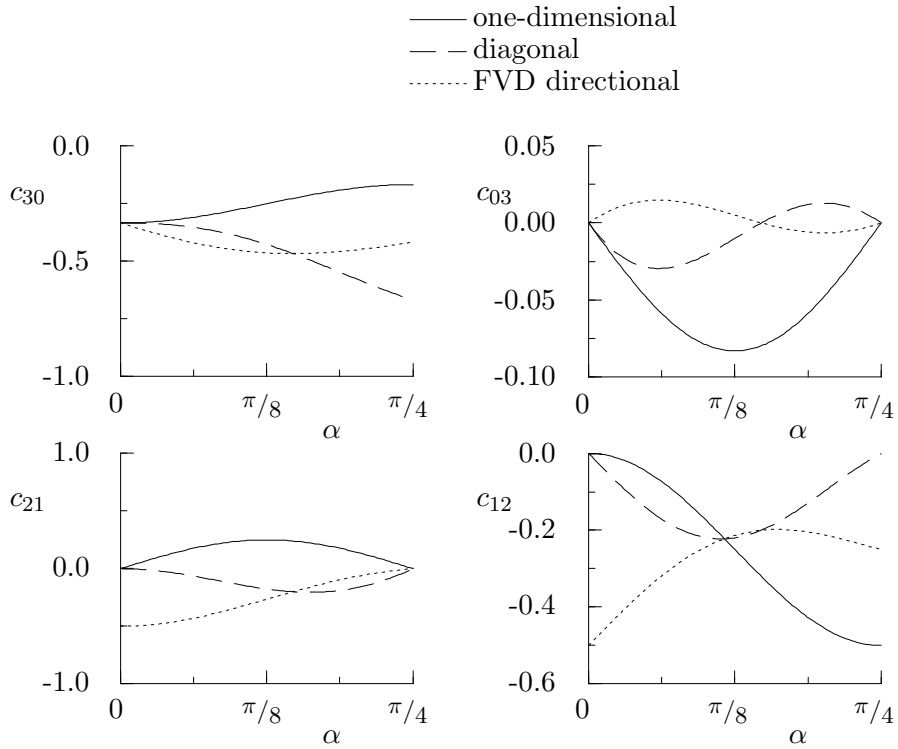


Figure 5.35. The coefficients of the error terms for the one-dimensional grid-aligned discretization, the diagonal discretization of (2.7), and the FVD discretization, (5.77).

The reduction in the error for the diagonal discretization compared to the one-dimensional grid-aligned discretization is 3.65, which is the same as for the second order central directional discretization. The FVD directional discretization reduces the term  $c_{03}$  by twice that amount, 7.29, but now the next term  $c_{12}$  may become important.

Table 5.7. The average values  $I_{mn}$  for the one-dimensional grid-aligned discretization, the diagonal discretization of (2.7), and the FVD discretization, (5.77).

discretization	$I_{30}$	$I_{21}$	$I_{12}$	$I_{03}$
one-dimensional	0.250	0.159	0.250	0.0531
diagonal	0.455	0.114	0.136	0.0146
FVD directional	0.432	0.261	0.273	0.0073

**5.8. The scheme of Lax and Wendroff.**

This numerical scheme is based on a Taylor series development in time for the unknown at the point of computation  $P$ , see [25],

$$u^{n+1} = u^n + \Delta t u_t + \frac{1}{2} \Delta t^2 u_{tt} + \dots \tag{5.78}$$

Applied to an  $N$ -dimensional linear advection equation,

$$u_t + \vec{a} \cdot \vec{\nabla} u = 0 \quad \text{or} \quad u_t = -a u_{e_1}, \tag{5.79}$$

the partial derivatives with respect on time in (5.78) can be rewritten in space derivatives. When the Taylor series is truncated after the second term, the resulting scheme is

$$u^{n+1} = u^n - a \Delta t u_{e_1} + \frac{1}{2} (a \Delta t)^2 u_{e_1 e_1}. \tag{5.80}$$

Many variants of the Lax-Wendroff scheme have since been derived, including non-linear versions, or interpretations as a multi-level scheme. For an overview, also on related schemes like the Beam and Warming scheme and the McCormack scheme, see [26]. We will restrict the discussion to the linear case in a one-step scheme.

For the first derivative in (5.80) in two dimensions, we use the stream-wise fixed stencil and basis  $B = \{B^1, B^2, B^3\}$  with coefficients  $K_1, K_2, K_3$  of §5.2, and for the second derivative the incomplete streamline fixed stencil and the basis stencil  $B^4$  with coefficient  $K_4$  of §5.4. Remark that  $B^3 = B^4$ . With this combination of derivatives there is no increase in the order of accuracy at steady state.

The coefficients  $c_{mn}$  in the error of  $\partial u / \partial e_1$  of the Lax-Wendroff scheme can be found in Fig. 5.15, and the average error values  $I_{mn}$  in Table 5.4.

For the stability of the Lax-Wendroff scheme, the amplification  $G$  as a function of  $\nu = a \Delta t / h$  depends on the coefficients  $K$ ,

$$\begin{aligned} G(\nu) = 1 - \nu & \left( \frac{1}{3} I [ \cos \alpha \sin \phi_x (\cos \phi_y + 2) + \sin \alpha \sin \phi_y (\cos \phi_x + 2) ] \right. \\ & + 4K_1 I \sin \phi_x (\cos \phi_y - 1) + 4K_2 I \sin \phi_y (\cos \phi_x - 1) \\ & - 4(K_3 + \frac{1}{2} \nu K_4) (\cos \phi_x - 1) (\cos \phi_y - 1) \\ & \left. - \frac{1}{2} \nu (\cos(2\alpha) (\cos \phi_x - \cos \phi_y) - \sin(2\alpha) \sin \phi_x \sin \phi_y + \cos \phi_x \cos \phi_y - 1) \right), \end{aligned} \tag{5.81}$$

where the first part is just (5.35).

An analytic optimization of (5.81) involves many variables. Computing  $G$ , given  $K$ , for a range of  $\alpha$ ,  $\phi_x$ , and  $\phi_y$ , gives a first impression of the maximum value of  $\nu$  for a

Table 5.8. The maximum allowable value of  $\nu$  for different combinations of a first derivative of §5.2, and a second derivative of §5.4 in the Lax-Wendroff scheme.

$\frac{\partial^2 u}{\partial e_1^2}$ \backslash $\frac{\partial u}{\partial e_1}$	one-dim.	diagonal	streamline	opt. time step
one-dimensional	0.503	0.943	0.958	0.943
diagonal	x	1.0	0.820	x

x: the scheme is not stable.

stable approximation. For the various combinations of first and second derivatives in the Lax-Wendroff approximation, the maximum value of  $\nu$  is given in Table 5.8.

Approximations involving as second derivative the incomplete streamline stencil are unstable. Awaiting a full parametric optimization of (5.81), we note that with directional discretizations the Lax-Wendroff scheme almost doubles the allowable time step compared to the one-dimensional grid-aligned scheme, while improving accuracy. The optimal combinations is a diagonal stencil for both the first and the second derivative. These stencils are flow-angle dependent, and a good compromise with fixed stencils is the streamline approximation for the first derivative and the one-dimensional approximation for the second derivative. It is remarkable that this combination has a larger  $\nu$  than the combination diagonal and one-dimensional.

In order to obtain a streamline approximation which increases the order of accuracy at steady state, rewrite (5.80) as

$$u^{n+1} = u^n - a\Delta t \frac{\partial}{\partial e_1} \left( u - \frac{1}{2} a\Delta t \frac{\partial u}{\partial e_1} \right), \quad (5.82)$$

and approximate the term between brackets with the streamline approximation of (5.27). This means that  $u_{e_1}$  is required at the nodes used in the streamline approximation. However, the explicit time integration of (5.82) is unstable, also in one dimension.

## 6. Directional discretizations of derivatives in three dimensions.

We continue the analysis in three dimensions of the directional discretizations of  $\partial u / \partial e_1$ . This discretization appears in the scalar advection equation in nonlinear or linear form,

$$\frac{\partial u}{\partial t} + \frac{\partial f}{\partial x} + \frac{\partial g}{\partial y} + \frac{\partial h}{\partial z} = 0, \quad \text{or} \quad \frac{\partial u}{\partial t} + a_x \frac{\partial u}{\partial x} + a_y \frac{\partial u}{\partial y} + a_z \frac{\partial u}{\partial z} = 0, \quad (6.1)$$

with  $a_x = \partial f / \partial u$ ,  $a_y = \partial g / \partial u$ ,  $a_z = \partial h / \partial u$ , and the velocity  $a = \sqrt{a_x^2 + a_y^2 + a_z^2}$ .

The bases contain many stencils, but properties like symmetry, orthogonality, and regularity will help to make even large bases manageable.

### 6.1. Directional first order upwind discretizations of the first derivative in three dimensions on a $2 \times 2 \times 2$ grid.

We start with the simplest discretizations, following the steps of the two-dimensional analysis. Discretizations on this grid have been analyzed in [10].

*The basis of stencils.* The conditions  $a_x \geq 0$ ,  $a_y \geq 0$ , and  $a_z \geq 0$  define an upwind region where the  $2 \times 2 \times 2$  stencil is situated. For the fixed stencils of the approximation to  $\partial u / \partial e_1$  we take the one-dimensional grid-aligned upwind discretization. The basis for consistent first order upwind approximations to the first derivative contains four stencils for each grid-based derivative, where in two dimensions we have just one basis stencil. The program GDD orders the basis stencil using the upper tetrahedron consisting of the four nodes  $(0,0,-1)$ ,  $(0,-1,0)$ ,  $(-1,0,0)$ , and  $(0,0,0)$ . At these nodes basis stencil  $b^i$  has a weight one. The stencils which represent various second derivatives are shown in Fig. 6.1.

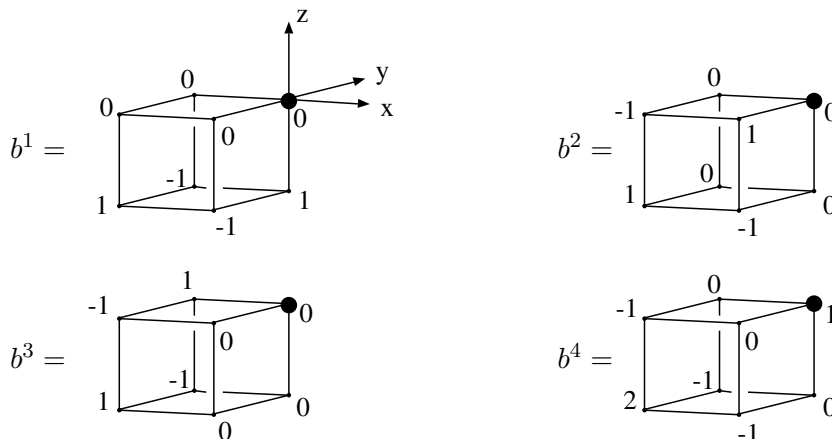


Figure 6.1. The basis of stencils for  $u_x$ ,  $u_y$ , and  $u_z$  used in the first order approximation of the first derivative  $\partial u / \partial e_1$ . The stencils represent approximations to second derivatives.

The diagonal approximation of (2.5) is obtained with the stencil coefficients  $k$  taken as  $k_x = (0, 0, 0, 0)^T$ ,  $k_y = (0, 1, 1, -1)^T$ , and  $k_z = (1, 0, 0, -1)^T$ .

The stencil  $B^4$  with  $k = (-1, -1, -1, 1)^T$  is an approximation to the third derivative  $\Delta x \Delta y \Delta z \partial^3 u / \partial x \partial y \partial z$ , see Fig. 6.2. The error of this stencil is one order higher than the truncation error, and in the following we take as basis  $B = \{b^1, b^2, b^3, B^4\}$  with coefficients  $K$ . The diagonal approximation of (2.5) is with this basis the combination  $K_x = (0, 0, 0, 0)^T$ ,  $K_y = (-1, 0, 0, -1)^T$ , and  $K_z = (0, -1, -1, -1)^T$ .

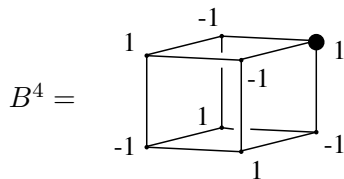


Figure 6.2. The stencil  $B^4$  which is used in basis  $B$ .

The diagonal condition restricts the basis to  $\{B^4\}$ . The fixed stencils and the basis used in [10] can be expressed in basis  $b$  or in  $B$ .

We call an approximation *regular* when a rotation of the stencil  $u_x$  along the  $(1, 1, 1)^T$  axis over  $2\pi/3$  gives  $u_y$ , and  $u_y$  leads to  $u_z$ . The permutation from the stencil of  $u_x$  to the stencil  $u_y$  can also be obtained from two successive mirror operations in the  $x = y$  plane and in the  $x = z$  plane.

In basis  $B$ , the stencils  $b^2$  and  $b^3$  are regular permutations of  $b^1$ . A regular approximation has therefore  $K_{z3} = K_{y2} = K_{x1}$ ,  $K_{x3} = K_{z2} = K_{y1}$ , and  $K_{y3} = K_{x2} = K_{z1}$ .

*The approximation in stream-wise coordinates.* The coordinate transformation of (4.4) in three dimensions relates the local basis  $B$  with the grid basis  $G$ . The transformation between two arbitrary axes systems consists of three successive rotations involving the Euler angles. We can use a less complicated transformation since we are interested in the principal region  $a_x/\Delta x \geq a_y/\Delta y \geq a_z/\Delta z \geq 0$ . For other flow angles we use a permutation of the discretization.

On this restricted domain, two successive rotations transfer the grid  $x$ -axis to the  $e_1$ -axis of the local basis  $B$ . The first is in the grid basis  $G$  around the  $z$ -axis with angle  $\alpha$ , resulting in the axis system  $A'(x', y', z')$  with  $z' = z$ . This is followed by a rotation around the  $y'$ -axis with angle  $\beta$ , as shown in Fig. 6.3. The axis system is  $A''(x'', y'', z'')$ , with  $y'' = y'$ . Another rotation with a yet unspecified angle  $\gamma$  around the  $x'' = e_1$ -axis positions the  $e_2$  and  $e_3$  axes, giving the directional axis system  $B$ .

This choice of rotations differs from the Euler angles in the choice of the third rotation axis. Also, we define the second rotation positive to have  $\alpha, \beta > 0$  for the flow with  $a_x \geq 0$ ,  $a_y \geq 0$ , and  $a_z \geq 0$ .

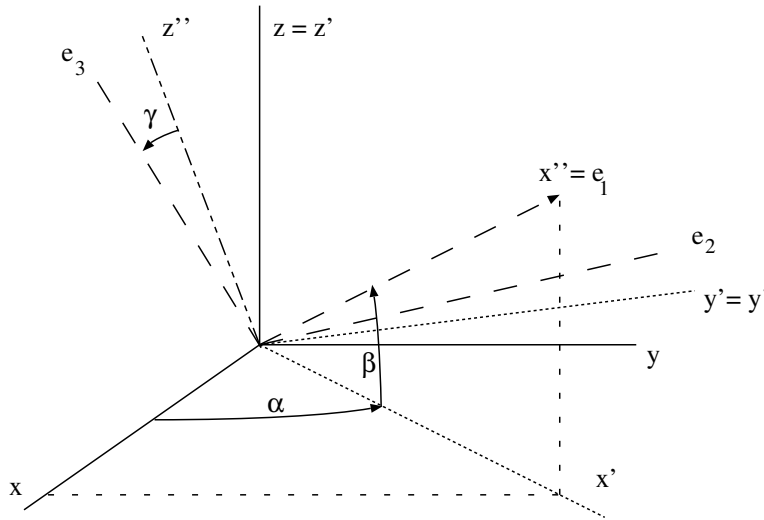


Figure 6.3. The three rotations linking the axes of the grid basis  $G = \{x, y, z\}$  with the axes of the local basis  $B = \{e_1, e_2, e_3\}$ .

The rotations are given by their matrices,  $\vec{x} = M_\alpha \vec{x}'$ ,  $\vec{x}' = M_\beta \vec{x}''$ , and  $\vec{x}'' = M_\gamma \vec{e}$ , similar to (5.3),

$$M_\alpha = \begin{pmatrix} \cos \alpha & -\sin \alpha & 0 \\ \sin \alpha & \cos \alpha & 0 \\ 0 & 0 & 1 \end{pmatrix}, \quad M_\beta = \begin{pmatrix} \cos \beta & 0 & -\sin \beta \\ 0 & 1 & 0 \\ \sin \beta & 0 & \cos \beta \end{pmatrix}, \quad M_\gamma = \begin{pmatrix} 1 & 0 & 0 \\ 0 & \cos \gamma & -\sin \gamma \\ 0 & \sin \gamma & \cos \gamma \end{pmatrix}, \quad (6.2)$$

and the transformation  $\vec{x} = M\vec{e} = M_\alpha M_\beta M_\gamma \vec{e}$  of (4.4) is

$$M = \begin{pmatrix} \cos \alpha \cos \beta & -\sin \alpha \cos \gamma + \cos \alpha \sin \beta \sin \gamma & -\sin \alpha \sin \gamma - \cos \alpha \sin \beta \cos \gamma \\ \sin \alpha \cos \beta & \cos \alpha \cos \gamma + \sin \alpha \sin \beta \sin \gamma & \cos \alpha \sin \gamma - \sin \alpha \sin \beta \cos \gamma \\ \sin \beta & -\cos \beta \sin \gamma & \cos \beta \cos \gamma \end{pmatrix}, \quad (6.3)$$

which is used in (4.5). The inverse of  $M$ ,  $M^{-1} = M^T$ , is used in  $\vec{e} = M^{-1}\vec{x}$ , and in the expression for the derivative along  $e_1$ ,

$$\frac{\partial u}{\partial e_1} = \cos \alpha \cos \beta \frac{\partial u}{\partial x} + \sin \alpha \cos \beta \frac{\partial u}{\partial y} + \sin \beta \frac{\partial u}{\partial z}, \quad (6.4)$$

which only involves the angles  $\alpha$  and  $\beta$ . The coefficients  $k_{xi}$ ,  $k_{yi}$ , and  $k_{zi}$  appear therefore in (6.4) as

$$k_i = k_{xi} \cos \alpha \cos \beta + k_{yi} \sin \alpha \cos \beta + k_{zi} \sin \beta. \quad (6.5)$$

In basis  $B$  with coefficients  $K$ , we arrive at

$$\begin{aligned} \frac{\partial u}{\partial e_1} = \frac{1}{h} \{ & (K_4 + \cos \alpha \cos \beta + \sin \alpha \cos \beta + \sin \beta)u_{0,0,0} \\ & + (K_3 - K_4 - \cos \alpha \cos \beta)u_{-1,0,0} + (K_2 - K_4 - \sin \alpha \cos \beta)u_{0,-1,0} \\ & + (K_1 - K_4 - \sin \beta)u_{0,0,-1} - (K_2 + K_3 - K_4)u_{-1,-1,0} \\ & - (K_1 + K_3 - K_4)u_{-1,0,-1} - (K_1 + K_2 - K_4)u_{0,-1,-1} \\ & + (K_1 + K_2 + K_3 - K_4)u_{-1,-1,-1} \}. \end{aligned} \quad (6.6)$$

*Monotonicity of the approximation.* On the principal region  $a_x/\Delta x \geq a_y/\Delta y \geq a_z/\Delta z \geq 0$ , the velocity components are  $a_x = a \cos \alpha \cos \beta$ ,  $a_y = a \sin \alpha \cos \beta$ , and  $a_z = a \sin \beta$ . The Euler backward scheme for (6.1) with (6.6) expresses  $u^{n+1}$  as an average of the nodes of the stencil. The monotonicity condition states that this should be a convex average, which leads to eight conditions on the  $K$ 's similar to (5.6),

$$\begin{aligned} K_3 - K_4 - \cos \alpha \cos \beta &\leq 0, & K_2 - K_4 - \sin \alpha \cos \beta &\leq 0, & K_1 - K_4 - \sin \beta &\leq 0, \\ K_1 + K_2 + K_3 - K_4 &\leq 0, & K_4 + \cos \alpha \cos \beta + \sin \alpha \cos \beta + \sin \beta &\leq \frac{h}{a\Delta t}, \\ K_2 + K_3 - K_4 &\geq 0, & K_1 + K_3 - K_4 &\geq 0, & K_1 + K_2 - K_4 &\geq 0. \end{aligned} \quad (6.7)$$

The monotonicity conditions are satisfied by the one-dimensional grid-aligned approximation with a time step restriction  $\Delta t \leq h/[a(\cos \alpha \cos \beta + \sin \alpha \cos \beta + \sin \beta)] = h/(a_x + a_y + a_z)$ . The diagonal discretization is also monotone and has a less restrictive time step of  $\Delta t \leq h/(a \cos \alpha \cos \beta) = h/a_x$ , see also [10].

The combination of optimal time step and monotonicity is obtained with the coefficients

$$K_1 = -\sin \alpha \cos \beta, \quad K_2 = K_3 = -\sin \beta, \quad \text{and} \quad K_4 = -\sin \alpha \cos \beta - \sin \beta. \quad (6.8)$$

*Finite Difference and Finite Volume formulations.* The FV formulation in three dimension uses fluxes through the sides of the dual volume surrounding the node. The fluxes can be written similar to (5.8)–(5.9) using the approximation of (6.6).

*Continuity of the approximation.* On the principal region  $a_x/\Delta x \geq a_y/\Delta y \geq a_z/\Delta z \geq 0$ , the continuity in a FD context in basis  $B$  of the approximation of  $\partial u/\partial e_1$  with respect to changing flow directions imposes the following conditions on the  $K$ 's:

1. Flow in the  $z = 0$  plane,  $\beta = 0$ , where  $\partial u/\partial e_1 = \cos \alpha \partial u/\partial x + \sin \alpha \partial u/\partial y$ . The stencil should have mirror symmetry with respect to the  $z = 0$  plane, and on this small stencil this implies that the weights of the nodes outside of the  $z = 0$  plane should be zero. This means that  $K_1(\alpha, 0) = K_4(\alpha, 0)$  and  $K_2(\alpha, 0) = K_3(\alpha, 0) = 0$ .
2. Flow in the  $x = y$  plane,  $\alpha = \pi/4$  and  $\partial u/\partial e_1 = 1/2\sqrt{2} \cos \beta (\partial u/\partial x + \partial u/\partial y) + \sin \beta \partial u/\partial z$ . The stencil should have mirror symmetry with respect to the plane  $x = y$  and  $K_2(\pi/4, \beta) = K_3(\pi/4, \beta)$ . The stencils  $b^1$  and  $B^4$  have this symmetry.
3. Flow in the  $y = z$  plane,  $\beta_\alpha = \arctan(\sin(\alpha))$  with  $\partial u/\partial e_1 = (1 + \sin^2 \alpha)^{-1/2} [\cos \alpha \partial u/\partial x + \sin \alpha (\partial u/\partial y + \partial u/\partial z)]$ . The stencil should have mirror symmetry with respect to the plane  $y = z$ . This requires  $K_1(\alpha, \beta_\alpha) = K_2(\alpha, \beta_\alpha)$ .

Combinations of these conditions occur at intersections of the delimiting planes. For the vector  $\vec{e}_1$  along the  $x$ -axis,  $\alpha = \beta = 0$ , and conditions 1 and 3 apply. When  $\vec{e}_1$  is along the diagonal in the  $x$ - $y$  plane,  $\alpha = \pi/4$ ,  $\beta = 0$ . Conditions 1 and 2 apply. Finally, when  $\vec{e}_1$  is along the body diagonal in  $x$ - $y$ - $z$  space,  $\alpha = \pi/4$ ,  $\beta = \arctan(1/2\sqrt{2})$ , and conditions 2 and 3 apply.

For a FV application as explained in §5.1, the fluxes  $f$ ,  $g$ , and  $h$  should be continuously dependent on the unknowns at the nodes when the stencil changes position on the grid. The individual stencils  $u_x$ ,  $u_y$  and  $u_z$  will have to satisfy additional mirror conditions:

1. The derivatives  $u_x$  and  $u_y$  should each have mirror symmetry with respect to the  $z = 0$  plane, and the conditions on  $K$  now apply to  $K_x$  and  $K_y$  individually,  $K_{x1}(\alpha, 0) = K_{x4}(\alpha, 0)$ ,  $K_{y1}(\alpha, 0) = K_{y4}(\alpha, 0)$ , and also  $K_{x2}(\alpha, 0) = K_{x3}(\alpha, 0) = K_{y2}(\alpha, 0) = K_{y3}(\alpha, 0) = 0$ .
2. The derivatives  $u_x$  and  $u_y$  should be their mirror image with respect to the  $x = y$  plane and  $u_z$  should have mirror symmetry with respect to that plane. This translates into  $K_{x1}(\pi/4, \beta) = K_{y1}(\pi/4, \beta)$ ,  $K_{x2}(\pi/4, \beta) = K_{y3}(\pi/4, \beta)$ ,  $K_{x3}(\pi/4, \beta) = K_{y2}(\pi/4, \beta)$ ,  $K_{x4}(\pi/4, \beta) = K_{y4}(\pi/4, \beta)$ , and  $K_{z2}(\pi/4, \beta) = K_{z3}(\pi/4, \beta)$ .
3. The derivatives  $u_y$  and  $u_z$  should be their mirror image with respect to the  $y = z$  plane and  $u_x$  should have mirror symmetry with respect to that plane. The FV conditions are  $K_{y1}(\alpha, \beta_\alpha) = K_{z2}(\alpha, \beta_\alpha)$ ,  $K_{y2}(\alpha, \beta_\alpha) = K_{z1}(\alpha, \beta_\alpha)$ ,  $K_{y3}(\alpha, \beta_\alpha) = K_{z3}(\alpha, \beta_\alpha)$ ,  $K_{y4}(\alpha, \beta_\alpha) = K_{z4}(\alpha, \beta_\alpha)$ , and finally  $K_{x1}(\alpha, \beta_\alpha) = K_{x2}(\alpha, \beta_\alpha)$ .

The remaining constraints are the combinations of 1 and 3, 1 and 2, and 2 and 3 as before.

In the FD formulation, the diagonal directional discretizations of §2 depend continuously on the grid unknowns for all flow angles. However, these discretizations are not continuous in a FV formulation. Condition 2 is violated since  $K_{x1} \neq K_{y1}$  and  $K_{x4} \neq K_{y4}$ , and also condition 3 is infringed with  $K_{y3} \neq K_{z3}$ . The monotone solution with the diagonal time step in the FV formulation needs  $K$ 's which depend on the flow angles.

Solutions of (6.8) which are FV continuous are similar to (5.11) and (5.12). The approximation which is diagonal for  $\alpha = \beta = 0$  is

$$\begin{aligned}
K_{x1} &= \frac{1}{4}(\cos(2\alpha) - 1)(\cos(2\beta) + 1), & K_{y1} &= \frac{1}{2}\left(\frac{1}{2}\sin(2\alpha) - 1\right)(\cos(2\beta) + 1), \\
K_{z1} &= -\frac{1}{2}\sin\alpha\sin(2\beta), \\
K_{x2} &= K_{x3} = \frac{1}{2}(\cos(2\alpha) - 1)(1 - \cos(2\beta)), \\
K_{y2} &= K_{y3} = \frac{1}{2}\left(\frac{1}{2}\sin(2\alpha) - 1\right)(1 - \cos(2\beta)), \\
K_{z2} &= K_{z3} = \sin\alpha\sin(2\beta) - 1, \\
K_{x4} &= \frac{1}{4}(\cos(2\alpha) - 1)(3 - \cos(2\beta)), & K_{y4} &= \frac{1}{2}\left(\frac{1}{2}\sin(2\alpha) - 1\right)(3 - \cos(2\beta)), \\
K_{z4} &= \frac{1}{2}\sin\alpha\sin(2\beta) - 1.
\end{aligned} \tag{6.9}$$

The approximation which is one-dimensional grid-aligned for  $\alpha = \beta = 0$  has  $K_x = K_y = K_z$ , which leads to

$$\begin{aligned}
K_{x1} &= K_{y1} = K_{z1} = \frac{-\sin\alpha\cos\beta}{\cos\alpha\cos\beta + \sin\alpha\cos\beta + \sin\beta}, \\
K_{x2} &= K_{y2} = K_{z2} = K_{x3} = K_{y3} = K_{z3} = \frac{-\sin\beta}{\cos\alpha\cos\beta + \sin\alpha\cos\beta + \sin\beta}, \\
K_{x4} &= K_{y4} = K_{z4} = K_{x1} + K_{x2}.
\end{aligned} \tag{6.10}$$

At the  $x - y$  diagonal in the  $z = 0$  plane,  $k_1 = k_4 = -1/2$  and  $k_2 = k_3 = 0$ , while at the body diagonal  $x = y = z$ , we have  $k_1 = k_2 = k_3 = -1/3$  and  $k_4 = -2/3$ .

*Computing the flow angles.* We determine the angles  $\alpha$  and  $\beta$  in a fashion similar to Fig. 5.6 and (5.13).

Consider the tetrahedron which is formed by the node  $p_0$  at the origin, the node  $p_1$  on the  $x$  axis, the node  $p_2$  on the diagonal  $x = y$  in the  $z = 0$  plane, and by the node  $p_3$  on the body diagonal  $x = y = z$ , see Fig. 6.4. On an irregular grid, this tetrahedron will have an angle  $p_0p_1p_2$  or  $p_1p_2p_3$  or  $p_0p_2p_3$  which is not straight.

Define the vectors  $\vec{p}_1 = \overrightarrow{p_0p_1}$ ,  $\vec{p}_2 = \overrightarrow{p_0p_2}$  and  $\vec{p}_3 = \overrightarrow{p_0p_3}$ , and write  $\vec{a} = a\vec{e}_1$ ,

$$\vec{e}_1 = a_1\vec{p}_1 + a_2\vec{p}_2 + a_3\vec{p}_3, \tag{6.11}$$

with

$$a_1 = \frac{1}{V_T}\vec{e}_1 \cdot (\vec{p}_2 \times \vec{p}_3), \quad a_2 = \frac{1}{V_T}\vec{e}_1 \cdot (\vec{p}_3 \times \vec{p}_1), \quad \text{and} \quad a_3 = \frac{1}{V_T}\vec{e}_1 \cdot (\vec{p}_1 \times \vec{p}_2), \tag{6.12}$$

where the volume of the tetrahedron is  $V_T = \vec{p}_1 \cdot (\vec{p}_2 \times \vec{p}_3)$ . The vector  $\vec{p}_4 = \overrightarrow{p_0p_4}$  is the projection of the vector  $\vec{e}_1$  in the plane  $p_0p_1p_2$ . The projection is parallel to the vector  $\vec{p}_{23} = \overrightarrow{p_2p_3}$ . This projection ensures that  $\alpha = \pi/4$  when  $\vec{e}_1$  is in the plane  $p_0p_2p_3$ . We use the vectors  $\vec{p}_1$ ,  $\vec{p}_4$ , and  $\vec{p}_2$  in the method of (5.13) to find

$$\tan\alpha = \frac{(a_2 + a_3)\vec{p}_1 \cdot \vec{p}_2}{a_1\vec{p}_1 \cdot \vec{p}_2 + (a_2 + a_3)\vec{p}_2 \cdot \vec{p}_2}. \tag{6.13}$$

The projection of the vector  $\vec{e}_1$  in the plane  $p_0p_1p_3$  gives the vector  $\vec{p}_5 = \overrightarrow{p_0p_5}$ , where the projection is again parallel to the vector  $\vec{p}_{23} = \overrightarrow{p_2p_3}$ . The vectors  $\vec{p}_4$ ,  $\vec{e}_1$ , and  $\vec{p}_5$  enable us to find

$$\tan\beta = \frac{\frac{a_3}{a_2^* + a_3}\vec{p}_4 \cdot \vec{p}_5}{\frac{a_3}{a_2^* + a_3}\vec{p}_4 \cdot \vec{p}_5 + \vec{p}_5 \cdot \vec{p}_5} \sin\alpha, \tag{6.14}$$

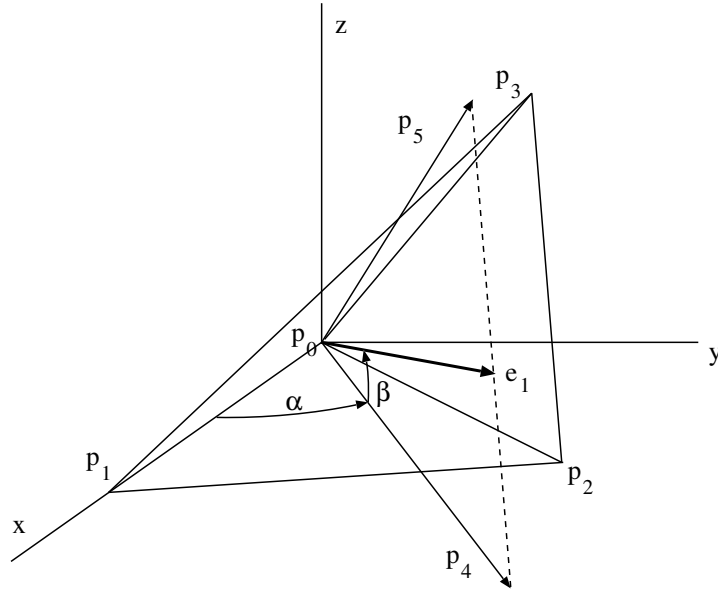


Figure 6.4. The projections used in the determination of the angles  $\alpha$  and  $\beta$ .

where  $a_2^* = a_2 + \epsilon \cos \alpha |\vec{p}_1| |\vec{p}_3|$ . We use a factor  $\epsilon$  to compute  $a_2^*$ , since for  $\alpha \downarrow 0$  both  $a_2$  and  $a_3 \rightarrow 0$ . A numerical code which computes  $\tan \beta$  is then in trouble.

The computation of the angles this way is complicated. A three-dimensional transformation to a uniform  $(\xi, \eta, \zeta)$  grid avoids this problem, and the angles are  $\alpha = \arctan(\eta/\xi)$  and  $\beta = \arctan(\zeta/\sqrt{\xi^2 + \eta^2})$ . Like in two dimensions, the angle evaluation is easy, but the accuracy in a FV context on a fairly smooth grid is only partly restored.

*Optimizing the directional error.* The error of the first order approximation of  $\partial u / \partial e_1$  is composed of six derivatives  $\partial^2 u / \partial e_1^l \partial e_2^m \partial e_3^n$  with coefficients  $c_{lmn}$ ,  $l + m + n = 2$ . These coefficients are elaborate functions of the three rotation angles  $\alpha$ ,  $\beta$ , and  $\gamma$ , but  $c_{200}$  is independent of  $\gamma$ .

Like in two dimensions, we consider the highest derivatives normal to the direction  $\vec{e}_1$ . In three dimensions, these derivatives are in the  $e_2$ - $e_3$  plane normal to the  $e_1$  axis. In this plane, a vector  $\vec{r}$  normal to  $e_1$  is indicated in Fig. 6.5.

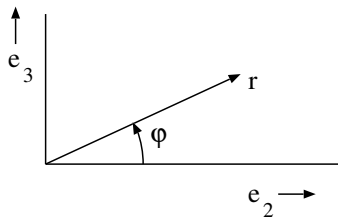


Figure 6.5. The  $e_2$ - $e_3$  plane with vector  $\vec{r}$  normal to  $\vec{e}_1$ .

We can express the derivative along  $r$  in the derivatives with respect to  $e_2$  and  $e_3$ . The transformation  $e_2 = r \cos \phi$  and  $e_3 = r \sin \phi$  leads to

$$\frac{\partial u}{\partial r} = \cos \phi \frac{\partial u}{\partial e_2} + \sin \phi \frac{\partial u}{\partial e_3}. \quad (6.15)$$

The second derivative in the  $r$  direction is

$$\frac{\partial^2 u}{\partial r^2} = \cos^2 \phi \frac{\partial^2 u}{\partial e_2^2} + 2 \cos \phi \sin \phi \frac{\partial^2 u}{\partial e_2 \partial e_3} + \sin^2 \phi \frac{\partial^2 u}{\partial e_3^2}. \quad (6.16)$$

We take therefore as a measure of the overall error for given angles  $\alpha$ ,  $\beta$ , and  $\gamma$  the combinations

$$\begin{aligned} c_{r2} &= c_{200}, \\ c_{r1} &= \cos \phi c_{110} + \sin \phi c_{101}, \\ c_{r0} &= \cos^2 \phi c_{020} + 2 \cos \phi \sin \phi c_{011} + \sin^2 \phi c_{002}. \end{aligned} \quad (6.17)$$

The streamline error reduction  $c_{r0} = 0$  for any angle  $\phi$  is obtained with  $c_{020} = c_{002} = c_{011} = 0$ , and this requires

$$\begin{aligned} K_1 &= -\frac{1}{2}(\sin \alpha + \cos \alpha) \cos \beta, & K_2 &= -\frac{1}{2}(\cos \alpha \cos \beta + \sin \beta), \\ K_3 &= -\frac{1}{2}(\sin \alpha \cos \beta + \sin \beta). \end{aligned} \quad (6.18)$$

Each of the coefficients  $c_{0ij}$ ,  $i+j=2$ , depend on the angle  $\gamma$ , but the solution to  $c_{r0} = 0$  is only dependent on the angles  $\alpha$  and  $\beta$ . There are contributions from three basis stencils, since the error of the fourth stencil is one order higher than the truncation error. Like in two dimensions, the update for  $c_{r0} = 0$  is not monotone and the coefficients are not continuous.

We wish to write the coefficients  $c_r$  of (6.17) as functions of the angles  $\alpha$  and  $\beta$ . Let us start by choosing the angle  $\gamma$ , e.g.  $\gamma = 0$ . For a certain combination of the angles  $\alpha$  and  $\beta$ , the coefficients  $c_r$  then only depend on  $\phi$ . We take for  $c_r$  the largest absolute value present on the domain  $\phi \in [0, 2\pi]$ . This means that we can compute  $c_r(\alpha, \beta)$  for any value of  $\gamma$ .

When the angle  $\beta = 0$ , the coefficients  $c_r$  depend only on  $\alpha$ . This corresponds to the two-dimensional case, Fig. 5.7. Since  $c_r$  is computed with an absolute value, we can make a comparison when we take the absolute value of the curves of Fig. 5.7. Varying  $\gamma$ , we find that  $c_{r0}(\alpha, 0)$  is the two-dimensional coefficient  $c_{02}$  for  $\gamma = 0$  modulo  $\pi/2$ .

Taking  $\gamma = 0$ , the transformation of (6.3) simplifies to

$$M = \begin{pmatrix} \cos \alpha \cos \beta & -\sin \alpha & -\cos \alpha \sin \beta \\ \sin \alpha \cos \beta & \cos \alpha & \sin \alpha \sin \beta \\ \sin \beta & 0 & \cos \beta \end{pmatrix}. \quad (6.19)$$

The transformation depends now on two angles. The coefficients in (6.5) are therefore  $k = k(\alpha, \beta)$ .

The measure of the error of the discretizations involves averages of the coefficients  $c_r$  over the angles  $\alpha$  and  $\beta$ . The averages  $I$  are over the part of a sphere limited by the  $x$  axis, the  $x$ - $y$  diagonal, and the  $x$ - $y$ - $z$  diagonal, for which  $0 \leq \alpha \leq \pi/4$ , and  $0 \leq \beta \leq \arctan(\sin \alpha)$ . This corresponds to having  $a_x/\Delta x \geq a_y/\Delta y \geq a_z/\Delta z \geq 0$ . Figure 6.6 shows the area, while the delimiting axes are indicates at the corners of the deformed triangle.

The surface of this area is

$$S = \int_0^{\pi/4} \left\{ \int_0^{\arctan(\sin \alpha)} \cos \beta \, d\beta \right\} d\alpha = \frac{\pi}{12}, \quad (6.20)$$

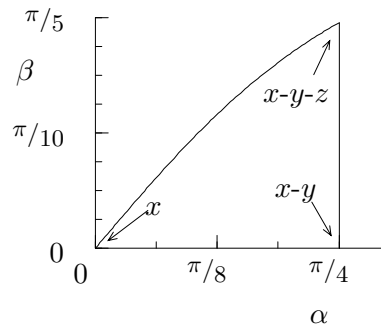


Figure 6.6. The area of integration in the  $\alpha$ - $\beta$  plane. The position of the  $x$  axis, the  $x$ - $y$  diagonal, and the  $x$ - $y$ - $z$  diagonal are indicated.

and the average over the surface is

$$I_r = \frac{1}{S} \int_0^{\pi/4} \left\{ \int_0^{\arctan(\sin \alpha)} c_r \cos \beta \, d\beta \right\} d\alpha. \quad (6.21)$$

The coefficient  $c_{r0}$  is shown for the one-dimensional grid-aligned approximation and for the diagonal directional approximation in Fig. 6.7.

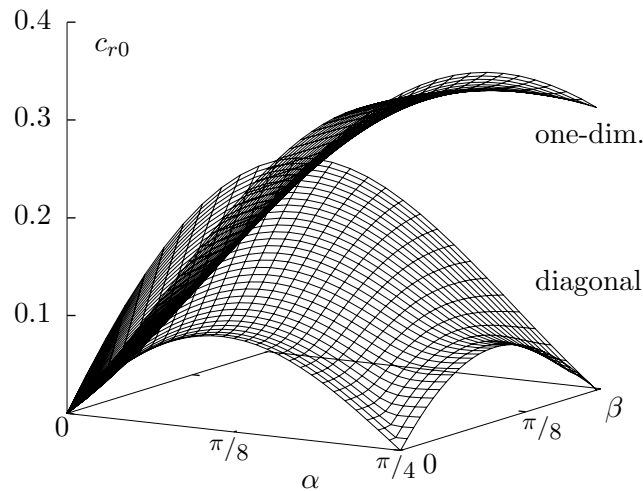


Figure 6.7. The coefficient  $c_{r0}$  for the one-dimensional grid-aligned approximation and for the diagonal approximation.

For the diagonal discretization, the coefficient  $c_{r0}$  is zero at the  $x$  axis, the  $x$ - $y$  diagonal, and the  $x$ - $y$ - $z$  diagonal, the corners indicated in Fig. 6.6.

The average values  $I_{r2}$ ,  $I_{r1}$ , and  $I_{r0}$  are listed in Table 6.1 for the one-dimensional grid-aligned approximation, the diagonal approximation, and the streamline directional approximation with  $c_{r0} = 0$ .

*The Fourier components.* For the analysis in the Fourier domain we use components of the form

$$U_{i,j,k}^n = U_0 \rho^n e^{I(i\phi_x + j\phi_y + k\phi_z)}, \quad (6.22)$$

Table 6.1. The average values  $I$  for the one-dimensional upwind discretization, the directional central discretization of (2.5), and the streamline approximation.

discretization	$I_{r2}$	$I_{r1}$	$I_{r0}$
one-dimensional	0.375	0.152	0.268
diagonal	0.640	0.092	0.111
streamline, $c_{r0} = 0$	0.750	0.401	0.0

similar to §5.1. The amplification factor for the discretization of (6.6) in an Euler backward scheme is

$$\begin{aligned}
 G &= 1 - \nu \left\{ \cos \alpha \cos \beta (1 - e^{-I\phi_x}) + \cos \beta \sin \alpha (1 - e^{-I\phi_y}) + \sin \beta (1 - e^{-I\phi_z}) \right. \\
 &\quad + K_1 e^{-I\phi_z} (e^{-I\phi_x} - 1)(e^{-I\phi_y} - 1) + K_2 e^{-I\phi_y} (e^{-I\phi_x} - 1)(e^{-I\phi_z} - 1) \\
 &\quad \left. + K_3 e^{-I\phi_x} (e^{-I\phi_y} - 1)(e^{-I\phi_z} - 1) + K_4 (1 - e^{-I\phi_x})(1 - e^{-I\phi_y})(1 - e^{-I\phi_z}) \right\}, \\
 g_r &= 1 - \nu \left\{ \cos \alpha \cos \beta (1 - \cos \phi_x) + \cos \beta \sin \alpha (1 - \cos \phi_y) + \sin \beta (1 - \cos \phi_z) \right. \\
 &\quad + K_1 (\cos \phi_z - \cos(\phi_x + \phi_z) - \cos(\phi_y + \phi_z) + \cos(\phi_x + \phi_y + \phi_z)) \\
 &\quad + K_2 (\cos \phi_y - \cos(\phi_x + \phi_y) - \cos(\phi_y + \phi_z) + \cos(\phi_x + \phi_y + \phi_z)) \\
 &\quad + K_3 (\cos \phi_x - \cos(\phi_x + \phi_y) - \cos(\phi_x + \phi_z) + \cos(\phi_x + \phi_y + \phi_z)) \\
 &\quad - K_4 (\cos \phi_x + \cos \phi_y + \cos \phi_z - \cos(\phi_x + \phi_y) - \cos(\phi_x + \phi_z) - \cos(\phi_y + \phi_z) \\
 &\quad \left. + \cos(\phi_x + \phi_y + \phi_z) - 1) \right\}, \\
 g_i &= -\nu \left\{ \cos \alpha \cos \beta \sin \phi_x + \cos \beta \sin \alpha \sin \phi_y + \sin \beta \sin \phi_z \right. \\
 &\quad + K_1 (-\sin \phi_z + \sin(\phi_x + \phi_z) + \sin(\phi_y + \phi_z) - \sin(\phi_x + \phi_y + \phi_z)) \\
 &\quad + K_2 (-\sin \phi_y + \sin(\phi_x + \phi_y) + \sin(\phi_y + \phi_z) - \sin(\phi_x + \phi_y + \phi_z)) \\
 &\quad + K_3 (-\sin \phi_x + \sin(\phi_x + \phi_y) + \sin(\phi_x + \phi_z) - \sin(\phi_x + \phi_y + \phi_z)) \\
 &\quad + K_4 (\sin \phi_x + \sin \phi_y + \sin \phi_z - \sin(\phi_x + \phi_y) - \sin(\phi_x + \phi_z) - \sin(\phi_y + \phi_z) \\
 &\quad \left. + \sin(\phi_x + \phi_y + \phi_z)) \right\}, \tag{6.23}
 \end{aligned}$$

where  $\nu = a\Delta t/h$ . For arbitrary  $K$  and for  $\phi_x = \pi$ ,  $\phi_y = 0$ ,  $\phi_z = 0$ , stability imposes that  $\Delta t \leq h/(a \cos \alpha \cos \beta) = h/a_x$ . This is the optimal step for stability which we find for the diagonal approximation. The one-dimensional grid-aligned approximation has a time step based on stability which is  $\Delta t \leq h/[a(\cos \alpha \cos \beta + \sin \alpha \cos \beta + \sin \beta)] = h/(a_x + a_y + a_z)$ .

### 6.2. Directional second order discretizations of the first derivative in three dimensions on a $3 \times 3 \times 3$ grid.

We continue the analysis on the  $[-1, 1]^3$  stencil with 27 nodes. This is the second smallest stencil in three dimensions, but the small increase in size causes a huge increase in degrees of freedom.

*The basis of stencils.* On a  $3 \times 3 \times 3$  grid around the origin, the basis for a consistent second order approximation to the first derivative  $\partial u / \partial e_1$  consists of 17 stencils [24]. The terms represent various third derivatives. The stencils generated by the program GDD have one node with a weight of one in the upper tetrahedron.

The basis  $\tilde{B}$  with ten antisymmetric and seven symmetric stencils is  $\tilde{B} = \{a^1, \dots, a^8, a^{10}, a^{12}, s^1, \dots, s^7\}$ . This basis is not very convenient to work with, even when we apply the orthogonalization procedure. It is more practical to transform  $\tilde{B}$  to the regular fully orthogonal basis  $B$ , of which some of the stencils are shown in Fig. 6.8. This basis is the result of pursuing simple expressions for the directional error and for the amplification.

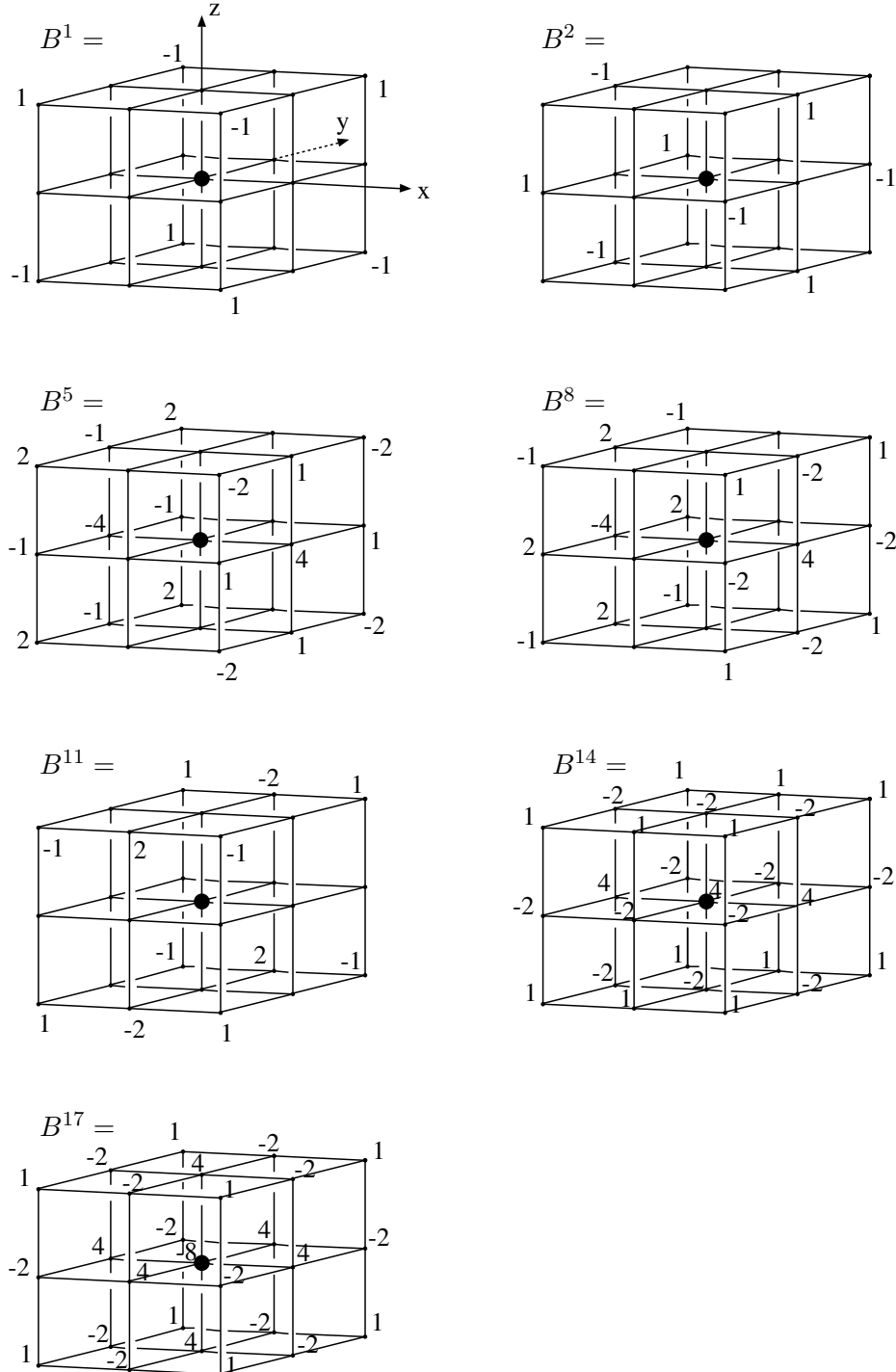


Figure 6.8. Some of the basis stencils for the second order approximations on the  $[-1, 1]^3$  stencil. The remaining stencils are obtained by rotations of these stencils.

With the corner nodes  $\pm 1$ , stencil  $B^1$  is an approximation to the mixed third derivative  $8\Delta x\Delta y\Delta z \partial^3 u / \partial x\partial y\partial z$ . Stencil  $B^2$  is an approximation to the mixed third derivative  $2\Delta x\Delta z^2 \partial^3 u / \partial x\partial z^2 - 2\Delta x\Delta y^2 \partial^3 u / \partial x\partial y^2$ . A rotation along the  $(1, 1, 1)^T$  axis over  $2\pi/3$  gives stencil  $B^3$ , which in turn leads to stencil  $B^4$ . Stencil  $B^5$  is an approximation to the mixed third derivative  $-6\Delta x\Delta z^2 \partial^3 u / \partial x\partial z^2 - 6\Delta x\Delta y^2 \partial^3 u / \partial x\partial y^2$ , and leads to  $B^6$  and  $B^7$ . Stencil  $B^8$  is an approximation to the fifth derivative  $2\Delta x\Delta y^2\Delta z^2 \partial^5 u / \partial x\partial y^2\partial z^2$ , and produces with the regular rotation  $B^9$ , which in turn gives  $B^{10}$ .

Considering the symmetric stencils,  $B^{11}$  is an approximation to the fourth derivative  $4\Delta x^2\Delta y\Delta z \partial^4 u / \partial x^2\partial y\partial z$  and leads to  $B^{12}$  and to  $B^{13}$ , while stencils  $B^{16}$  and  $B^{15}$  follow from  $B^{14}$ , an approximation to the fourth derivative  $3\Delta y^2\Delta z^2 \partial^4 u / \partial y^2\partial z^2$ . Finally,  $B^{17}$  is an approximation to the sixth derivative  $\Delta x^2\Delta y^2\Delta z^2 \partial^6 u / \partial x^2\partial y^2\partial z^2$ . With this basis it is easy to construct regular discretizations. The first seven stencils are the most important since they are the first to show up in the truncation error.

The basis  $b$  of 17 third derivatives is transformed to basis  $B$ , where seven stencils are approximations of third derivatives. The remaining 10 stencils are approximations of fourth derivatives up to a sixth derivative. In two dimensions, the highest derivative in the new basis is a fourth derivative.

Concerning the antisymmetric part, a regular approximation has  $K_{x1} = K_{y1} = K_{z1}$ ,  $K_{z4} = K_{y3} = K_{x2}$ ,  $K_{x4} = K_{z3} = K_{y2}$ , and  $K_{y4} = K_{x3} = K_{z2}$ . Similar relations hold for the combinations  $K_5$ ,  $K_6$ , and  $K_7$ , and  $K_8$ ,  $K_9$ , and  $K_{10}$ . This means that  $K_1 = K_{x1}(\cos \alpha \cos \beta + \sin \alpha \cos \beta + \sin \beta)$ ,  $K_3 = K_{z2} \cos \alpha \cos \beta + K_{x2} \sin \alpha \cos \beta + K_{y2} \sin \beta$ , and  $K_4 = K_{y2} \cos \alpha \cos \beta + K_{z2} \sin \alpha \cos \beta + K_{x2} \sin \beta$ , and so on.

For a straight approximation we have  $K_{yi} = K_{zi} = 0$  for  $i = 2, 5, 8$ ,  $K_{zi} = K_{xi} = 0$  for  $i = 3, 6, 9$ ,  $K_{xi} = K_{yi} = 0$  for  $i = 4, 7, 10$ , and  $K_{xi} = K_{yi} = K_{zi} = 0$ , for  $i = 1, 11, 12, 13$ .

A regular approximation now depends on seven parameters, ignoring stencils 8–10, while in two dimensions there were two parameters.

*Monotonicity of the approximation.* The update is not monotone.

*Continuity of the approximation.* We consider discretizations on the principal region  $a_x/\Delta x \geq a_y/\Delta y \geq a_z/\Delta z \geq 0$ . For other flow angles we use a permutation of the discretization. For the angle-dependent approximations, the continuity of the approximation with respect to changing flow directions imposes the following conditions on the  $K$ 's which are related to the antisymmetric/symmetric basis  $B$ . The notation  $K$  stands for  $K(\alpha, \beta)$ :

1. Flow in the  $z = 0$  plane,  $\beta = 0$ , and  $K_1 = K_4 = K_7 = K_{10} = K_{11} = K_{12} = 0$ .
2. Flow in the  $x = y$  plane,  $\alpha = \pi/4$ , and  $K_2 + K_3 = 0$ ,  $K_4 = 0$ ,  $K_5 - K_6 = 0$ ,  $K_8 - K_9 = 0$ ,  $K_{11} - K_{12} = 0$ , and  $K_{14} - K_{15} = 0$ .
3. Flow in the  $y = z$  plane,  $\beta_\alpha = \arctan(\sin(\alpha))$ , and  $K_2 = 0$ ,  $K_3 + K_4 = 0$ ,  $K_6 - K_7 = 0$ ,  $K_9 - K_{10} = 0$ ,  $K_{12} - K_{13} = 0$ , and  $K_{15} - K_{16} = 0$ .

Combinations of these conditions occur at intersections of the delimiting planes, as explained before. For a FV application, the individual stencils  $u_x$ ,  $u_y$ , and  $u_z$  will have to satisfy additional mirror conditions:

1. The derivatives  $u_x$  and  $u_y$  should each have mirror symmetry with respect to the  $z = 0$  plane, and the above conditions on  $K$  now apply to  $K_x$ .

2. The derivatives  $u_x$  and  $u_y$  should be their mirror image with respect to the  $x = y$  plane, and  $u_z$  should have mirror symmetry with respect to that plane. The relations  $K_{xi} = K_{yj}$ ,  $K_{xj} = K_{yi}$ , and  $K_{zi} = K_{zj}$  hold for  $i = 5, j = 6$ , for  $i = 8, j = 9$ , for  $i = 11, j = 12$ , and for  $i = 14, j = 15$ . With the opposite sign we have  $K_{x2} = -K_{y3}$ ,  $K_{x3} = -K_{y2}$ , and  $K_{z2} = -K_{z3}$ . Finally,  $K_{xi} = K_{yi}$  for  $i = 1, 7, 10, 13, 16, 17$ ,  $K_{x4} = -K_{y4}$ , and  $K_{z4} = 0$ .
3. The derivatives  $u_y$  and  $u_z$  should be their mirror image with respect to the  $y = z$  plane, and  $u_x$  should have mirror symmetry with respect to that plane. The relations  $K_{yi} = K_{zj}$ ,  $K_{yj} = K_{zi}$ , and  $K_{xi} = K_{xj}$  hold for  $i = 6, j = 7$ , for  $i = 9, j = 10$ , for  $i = 12, j = 13$ , and for  $i = 15, j = 16$ . With the opposite sign we have  $K_{y3} = -K_{z4}$ ,  $K_{y4} = -K_{z3}$ , and  $K_{x3} = -K_{x4}$ . Finally,  $K_{yi} = K_{zi}$  for  $i = 1, 5, 8, 11, 14, 17$ , and  $K_{y2} = -K_{z2}$ , and  $K_{x2} = 0$ .

The remaining constraints are the combinations of 1 and 3, 1 and 2, and 2 and 3.

The diagonal discretization of (2.6) is not continuous in the FV formulation. With (6.9) or (6.10) we obtain a continuous version taking an average of the velocities  $\vec{a}$  and  $-\vec{a}$ .

*Optimizing the directional error.* The error of the second order approximation of  $\partial u / \partial e_1$  is composed of ten third derivatives  $\partial^3 u / \partial e_1^l \partial e_2^m \partial e_3^n$  with coefficients  $c_{lmn}$ ,  $l + m + n = 3$ . The highest derivative normal to the direction  $e_1$  is

$$\frac{\partial^3 u}{\partial r^3} = \cos^3 \phi \frac{\partial^3 u}{\partial e_3^3} + 3 \cos^2 \phi \sin \phi \frac{\partial^3 u}{\partial e_2^2 \partial e_3} + 3 \cos \phi \sin^2 \phi \frac{\partial^3 u}{\partial e_2 \partial e_3^2} + \sin^3 \phi \frac{\partial^3 u}{\partial e_2^3}. \quad (6.24)$$

We take therefore as a measure of the overall error the derivatives with normal components in the combinations

$$\begin{aligned} c_{r3} &= c_{300}, \\ c_{r2} &= \cos \phi c_{210} + \sin \phi c_{201}, \\ c_{r1} &= \cos^2 \phi c_{120} + 2 \cos \phi \sin \phi c_{111} + \sin^2 \phi c_{102}, \\ c_{r0} &= \cos^3 \phi c_{030} + 3 \cos^2 \phi \sin \phi c_{021} + 3 \cos \phi \sin^2 \phi c_{012} + \sin^3 \phi c_{003}. \end{aligned} \quad (6.25)$$

These coefficients are easiest computed taking a streamline fixed stencil, similar to §5.2, Fig. 5.10, and (5.27). Such a stencil is shown in Fig. 6.9 for the approximation of  $u_x$ . The derivatives  $u_y$  and  $u_z$  are the regular permutations of  $u_x$ .

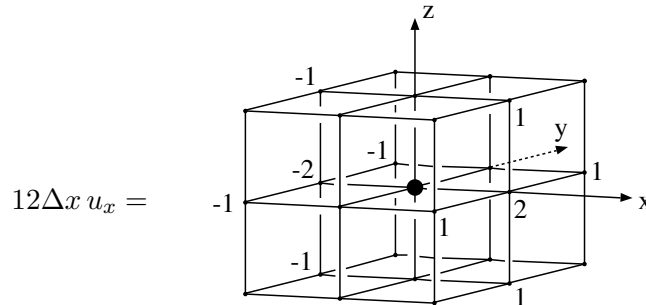


Figure 6.9. An approximation for  $u_x$  which, when combined with the regular approximations for  $u_y$  and  $u_z$ , leads to a streamline approximation of  $\partial u / \partial e_1$ .

The streamline error reduction  $c_{r0} = 0$  for any angle  $\phi$  is obtained with  $c_{030} = c_{021} = c_{012} = c_{003} = 0$ , leading to

$$\begin{aligned} & \cos \alpha \cos \beta [3K_5(2 \cos^2 \alpha \cos^2 \beta - 1) - 4K_1 \sin \alpha \cos \beta \sin \beta] \\ & + 3K_6 \sin \alpha \cos \beta (2 \sin^2 \alpha \cos^2 \beta - 1) + 3K_7 \sin \beta (2 \sin^2 \beta - 1) = 0, \\ & K_2 \cos \alpha \cos \beta - 3K_6 \sin \alpha \cos \beta + 3K_7 \sin \beta = 0, \\ & 3K_5 \cos \alpha \cos \beta + K_3 \sin \alpha \cos \beta - 3K_7 \sin \beta = 0, \\ & 3K_5 \cos \alpha \cos \beta - 3K_6 \sin \alpha \cos \beta - K_4 \sin \beta = 0. \end{aligned} \quad (6.26)$$

Each of the coefficients  $c_{0ij}$ ,  $i + j = 3$ , depend on the angle  $\gamma$ , but the solution to  $c_{r0} = 0$  is only dependent on the angles  $\alpha$  and  $\beta$ .

Streamline stencils which are independent of the flow angle have to satisfy (6.26) for all angles  $\alpha, \beta$ . When we restrict the approximation to regular straight derivatives with the low order basis stencils  $B^1$ – $B^7$ , the solution is the stencil of Fig. 6.9. Like in two dimensions, no degrees of freedom remain. Nevertheless, in three dimensions the stencils  $B^8$ ,  $B^9$ ,  $B^{10}$ , and  $B^{17}$  can be used while retaining a fourth order solution for the advection equation at steady state. For a regular straight streamline approximation, we have two degrees of freedom more than in two dimensions, (5.38). In both cases, the final degree of freedom introduces skewness.

We eliminate the angle  $\gamma$  from the coefficients of (6.25) by comparing  $c_{r0}$  for  $\beta = 0$  with the two-dimensional coefficient  $c_{03}$  of Fig. 5.15. The solution is, as before,  $\gamma = 0$  modulo  $\pi/2$ .

The streamline stencil can also be used for a two-dimensional time dependent approximation, like (5.32). For the unsteady problem we use the  $z$ -axis as the time variable. With an advection speed  $\vec{a} = (a, b, 1)^T$  and  $\vec{\nabla}u = (\partial/\partial x, \partial/\partial y, \partial/\partial t)^T$ , the steady approximation  $a\vec{e}_1 \cdot \vec{\nabla}u = 0$  now represents  $u_t + au_x + bu_y = 0$ . The angle  $\alpha$  is between 0 and  $\pi$ , and the angle  $\beta$  is between 0 and  $\pi/2$ . We have

$$\begin{aligned} \Delta x u_x &= \frac{1}{12} \left( u_{i+1,j}^{n+1} + u_{i+1,j+1}^n + 2u_{i+1,j}^n + u_{i+1,j-1}^n + u_{i+1,j}^{n-1} \right. \\ & \quad \left. - u_{i-1,j}^{n+1} - u_{i-1,j+1}^n - 2u_{i-1,j}^n - u_{i-1,j-1}^n - u_{i-1,j}^{n-1} \right), \\ \Delta y u_x &= \frac{1}{12} \left( u_{i,j+1}^{n+1} + u_{i+1,j+1}^n + 2u_{i,j+1}^n + u_{i-1,j+1}^n + u_{i,j+1}^{n-1} \right. \\ & \quad \left. - u_{i-1,j}^{n+1} - u_{i-1,j+1}^n - 2u_{i,j-1}^n - u_{i-1,j-1}^n - u_{i-1,j}^{n-1} \right), \\ \Delta t u_t &= \frac{1}{12} \left( u_{i+1,j}^{n+1} + u_{i,j+1}^{n+1} + 2u_{i,j}^{n+1} + u_{i-1,j}^{n+1} + u_{i,j-1}^{n+1} \right. \\ & \quad \left. - u_{i-1,j}^{n-1} - u_{i-1,j+1}^{n-1} - 2u_{i-1,j}^{n-1} - u_{i-1,j-1}^{n-1} - u_{i-1,j}^{n-1} \right). \end{aligned} \quad (6.27)$$

The error of this scheme follows from the truncated Taylor series expansion in  $x$ ,  $y$ , and  $t$ ,

$$\begin{aligned} \vec{e}_1 \cdot \vec{\nabla}u &= \frac{\partial u}{\partial t} + a \frac{\partial u}{\partial x} + b \frac{\partial u}{\partial y} + \frac{1}{6} \left( \Delta x^2 \frac{\partial^2}{\partial x^2} + \Delta y^2 \frac{\partial^2}{\partial y^2} + \Delta t^2 \frac{\partial^2}{\partial t^2} \right) \left( \frac{\partial u}{\partial t} + a \frac{\partial u}{\partial x} + b \frac{\partial u}{\partial y} \right) \\ & \quad + O(\Delta x^4, \Delta y^4, \Delta x^2 \Delta t^2, \Delta y^2 \Delta t^2, \Delta t^4). \end{aligned} \quad (6.28)$$

The term  $u_t + au_x + bu_y$  between brackets is at least of  $O(\Delta x^2, \Delta y^2, \Delta t^2)$ , and we obtain an approximation which is fourth order in time and space when the time step  $\Delta t$  is proportional to  $\Delta x$  and  $\Delta y$ .

*The Fourier components.* We compute the eigenvalues of the space operator with periodic boundary conditions using basis  $B$  with the fixed stencil of Fig. 6.9, and obtain

$$\begin{aligned}
\Omega_{l,m,n} = & -4\frac{a}{h} \left\{ I \left[ \frac{1}{12} \left( \begin{aligned} & \cos \alpha \cos \beta \sin \phi_x (\cos \phi_y + \cos \phi_z + 1) \\ & + \sin \alpha \cos \beta \sin \phi_y (\cos \phi_x + \cos \phi_z + 1) \\ & + \sin \beta \sin \phi_z (\cos \phi_x + \cos \phi_y + 1) \end{aligned} \right) \right. \right. \\
& - 2K_1 \sin \phi_x \sin \phi_y \sin \phi_z \\
& + K_2 \sin \phi_x (\cos \phi_z - \cos \phi_y) \\
& + K_3 \sin \phi_y (\cos \phi_x - \cos \phi_z) \\
& + K_4 \sin \phi_z (\cos \phi_y - \cos \phi_x) \\
& + K_5 \sin \phi_x (\cos \phi_y + \cos \phi_z - 4 \cos \phi_y \cos \phi_z + 2) \\
& + K_6 \sin \phi_y (\cos \phi_z + \cos \phi_x - 4 \cos \phi_z \cos \phi_x + 2) \\
& + K_7 \sin \phi_z (\cos \phi_x + \cos \phi_y - 4 \cos \phi_x \cos \phi_y + 2) \\
& + 2K_8 \sin \phi_x (\cos \phi_y - 1)(\cos \phi_z - 1) \\
& + 2K_9 \sin \phi_y (\cos \phi_z - 1)(\cos \phi_x - 1) \\
& + 2K_{10} \sin \phi_z (\cos \phi_x - 1)(\cos \phi_y - 1) \left. \right] \\
& - 2K_{11} (\cos \phi_x - 1) \sin \phi_y \sin \phi_z \\
& - 2K_{12} (\cos \phi_y - 1) \sin \phi_z \sin \phi_x \\
& - 2K_{13} (\cos \phi_z - 1) \sin \phi_x \sin \phi_y \\
& + K_{14} (2 \cos \phi_x + 1)(\cos \phi_y - 1)(\cos \phi_z - 1) \\
& + K_{15} (2 \cos \phi_y + 1)(\cos \phi_z - 1)(\cos \phi_x - 1) \\
& + K_{16} (2 \cos \phi_z + 1)(\cos \phi_x - 1)(\cos \phi_y - 1) \\
& \left. + 2K_{17} (\cos \phi_x - 1)(\cos \phi_y - 1)(\cos \phi_z - 1) \right\}. \quad (6.29)
\end{aligned}$$

For two-dimensional flow  $\beta = 0$ ,  $\phi_z = 0$ , the stencils such as e.g.  $B^1$  collapse, and the eigenvalues of (5.35) are recovered.

The eigenvalues are not particularly useful in printed form. This is especially the case in three dimensions, where the basis of stencils tends to be large. Using a program capable of symbolic manipulations, starting with the GDD basis [24], basis  $B$  is easily reconstructed, and the analysis can be performed on a computer.

We discuss briefly the eigenvalues of the space operator for some approximations. The one-dimensional grid-aligned approximation has  $K_{xi} = K_{yi} = K_{zi} = 0$ , except  $K_{x8} = K_{y9} = K_{z10} = 1/18$ , and  $K_{x5} = K_{y6} = K_{z7} = 1/36$ . The purely imaginary eigenvalues are

$$\Omega_{l,m,n} = -\frac{a}{h} I (\cos \alpha \cos \beta \sin \phi_x + \sin \alpha \cos \beta \sin \phi_y + \sin \beta \sin \phi_z). \quad (6.30)$$

The largest eigenvalues are obtained for  $\sin \phi_x = \sin \phi_y = \sin \phi_z = 1$ ,  $\phi_x = \phi_y = \phi_z = \pi/2$  with the value  $-a/h I (\cos \alpha \cos \beta + \sin \alpha \cos \beta + \sin \beta)$ . The time step restriction in a Runge-Kutta scheme is therefore proportional to  $h/[a (\cos \alpha \cos \beta + \sin \alpha \cos \beta + \sin \beta)] = h/(a_x + a_y + a_z)$ .

For the diagonal approximation of (2.6),  $K_{xi}$  is the same as for the one-dimensional grid-aligned approximation,  $-K_{y2} = K_{y3} = 1/8$ ,  $K_{y5} = -1/24$ ,  $K_{y6} = -1/72$ ,  $K_{y8} = -1/12$ ,

and  $K_{y9} = -1/36$ . The values for  $K_z$  are  $K_{z1} = K_{z2} = -K_{z3} = 1/8$ ,  $-K_{z5} = -K_{z6} = K_{z8} = K_{z9} = 1/24$ ,  $K_{z7} = -1/18$ , and  $K_{z10} = 1/72$ . The purely imaginary eigenvalues are

$$\Omega_{l,m,n} = -\frac{a}{h}I \left( \cos \beta \left[ (\cos \alpha - \sin \alpha) \sin \phi_x + \sin \alpha \sin(\phi_x + \phi_y) \right] + \sin \beta \left[ \sin(\phi_x + \phi_y + \phi_z) - \sin(\phi_x + \phi_y) \right] \right). \quad (6.31)$$

The largest eigenvalue is  $-a/hI \cos \alpha \cos \beta$ , and it leads to a time step restriction  $\Delta t \sim h/(a \cos \alpha \cos \beta) = h/a_x$ , which is the optimal time step.

The regular straight streamline approximation with flow-angle independent stencils is given in Fig. 6.9. When we include the fifth derivative stencils  $B^8$ ,  $B^9$ , and  $B^{10}$ , one free parameter  $K_{x8}$  remains, and the amplification is

$$\Omega_{l,m,n} = -\frac{a}{h}I \left\{ \frac{1}{3} \left[ \cos \alpha \cos \beta \sin \phi_x (\cos \phi_y + \cos \phi_z + 1) + \sin \alpha \cos \beta \sin \phi_y (\cos \phi_z + \cos \phi_x + 1) + \sin \beta \sin \phi_z (\cos \phi_x + \cos \phi_y + 1) \right] + 8K_{x8} \left[ \cos \alpha \cos \beta \sin \phi_x (1 - \cos \phi_y)(1 - \cos \phi_z) + \sin \alpha \cos \beta \sin \phi_y (1 - \cos \phi_z)(1 - \cos \phi_x) + \sin \beta \sin \phi_z (1 - \cos \phi_x)(1 - \cos \phi_y) \right] \right\}. \quad (6.32)$$

The eigenvalues for the fixed stencil of Fig. 6.9 are those with  $K_{x8} = 0$ , and vary between 1 and 1.04. Like in two dimensions, the time step is not optimal.

The stability can be marginally improved for  $\beta > 0$  with the degree of freedom represented by  $K_{x8}$ , and the optimal value for  $K_{x8}$  is around  $-1/48$ . The discretization for  $u_x$  is shown in Fig. 6.10.

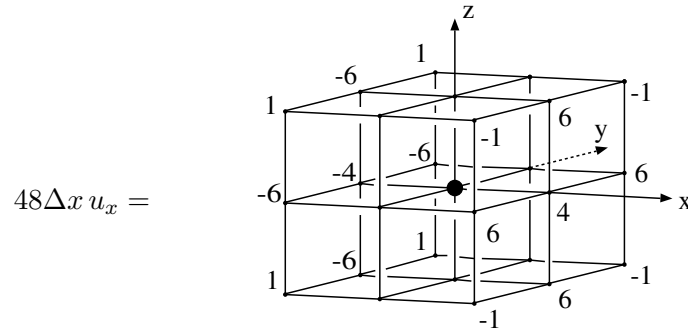


Figure 6.10. An approximation for  $u_x$  to be combined with regular permutations for  $u_y$  and  $u_z$  for a fixed streamline approximation with optimal stability.

A better stability of the steam line approximation needs flow-angle dependent stencils. This is a more complicated problem than in two dimensions, if only due to the larger number of parameters involved. A simple guessed solution like in two dimensions does not lead to the desired result. A more complete optimization is left for later.

The straight regular approximation without the streamline condition depends on the parameters  $K_{x2}$ ,  $K_{x5}$ , and  $K_{x8}$ . The minimal value of the eigenvalues at  $\alpha = \pi/4$ ,  $\beta_\alpha = \arctan(\sin(\alpha))$  is estimated by brute force, varying the parameters. An optimum is reached for  $K_{x2} = 0$ ,  $K_{x5} = 1/72$ , and  $K_{x8} = -1/18$ , and the approximation for  $u_x$  is shown in Fig. 6.11.

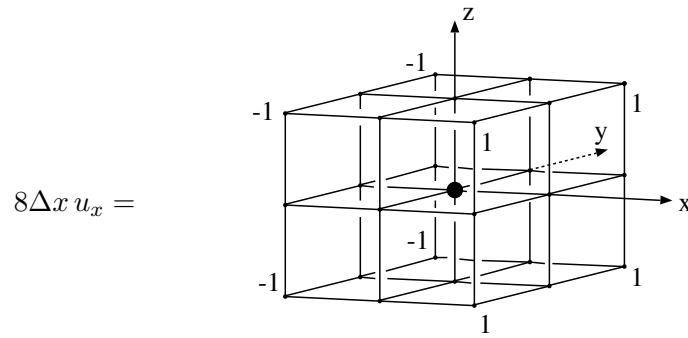


Figure 6.11. An approximation for  $u_x$  which, when combined with similar regular rotated approximations for  $u_y$  and  $u_z$ , has the optimal stability for approximation of  $\partial u / \partial e_1$ .

The eigenvalues which are associated with this approximation with optimal time step are

$$\begin{aligned} \Omega_{l,m,n} = & \cos \alpha \cos \beta \sin \phi_x \cos \phi_y \cos \phi_z \\ & + \sin \alpha \cos \beta \cos \phi_x \sin \phi_y \cos \phi_z + \sin \beta \cos \phi_x \cos \phi_y \sin \phi_z . \end{aligned} \quad (6.33)$$

The maximum eigenvalue of  $\Omega$ , excluding the scaling factor  $a/h$ , as a function of the flow angle  $\alpha$  is given in Fig. 6.12 for the above approximations.

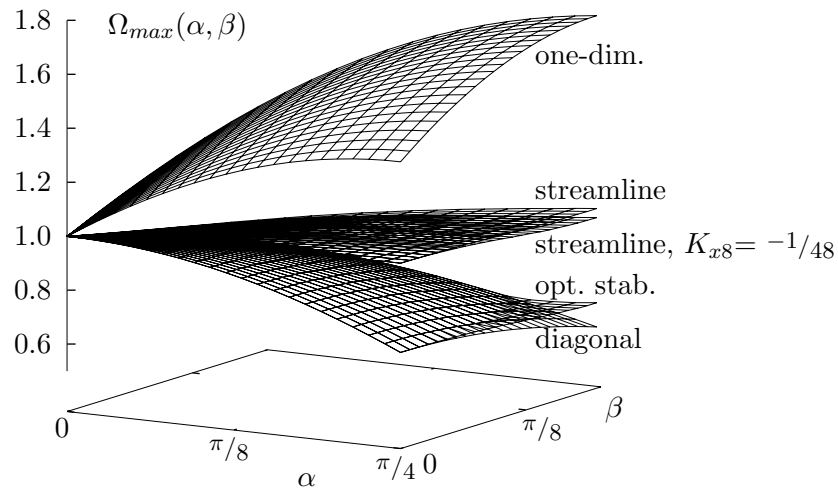


Figure 6.12. The stability expressed by  $\Omega_{max}(\alpha, \beta)$  for the one-dimensional grid-aligned approximation, the streamline approximations with  $K_{x8} = 0$  and  $K_{x8} = -1/48$ , the fixed approximation with optimal stability, Fig. 6.11, and the diagonal approximation.

The surface of  $\Omega_{max}(\alpha, \beta)$  of (6.33), based on the stencil of Fig. 6.11, follows the one for the diagonal approximation, except for higher values of  $\alpha$  and  $\beta$ . With  $\alpha_m = \pi/4$  and  $\beta_m = \arctan(\sin \alpha_m)$ , we find  $\Omega_{max}(\alpha_m, \beta_m) = 2/3$  for (6.33), and  $\Omega_{max}(\alpha_m, \beta_m) = \sqrt{3}/3$  for the diagonal approximation.

Optimizing the high frequency domain of the eigenvalues is a task we leave for later.

The coefficients  $c_r$  are a function of the angles  $\alpha$  and  $\beta$ , and  $c_{r0}$  is shown for the one-dimensional grid-aligned approximation, the diagonal approximation and the fixed stencil with optimal stability in Fig. 6.13.

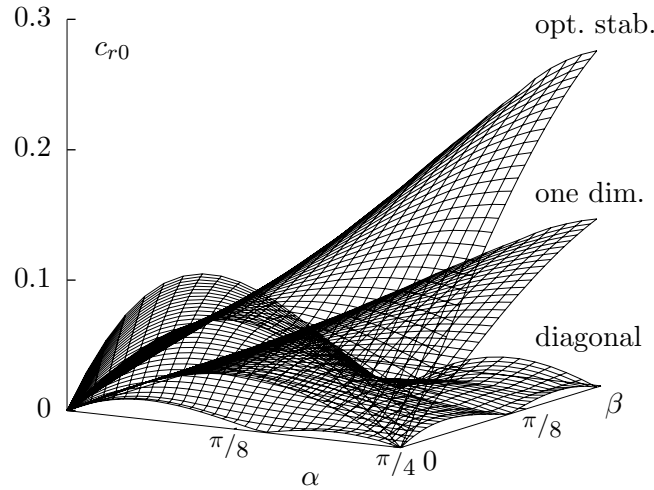


Figure 6.13. The coefficient  $c_{r0}$  for the one-dimensional grid-aligned approximation, the diagonal, and the fixed optimal stable approximation.

For the diagonal discretization, Fig. 6.13, the coefficient  $c_{r0}$  is zero at the  $x$  axis, the  $x$ - $y$  diagonal, and the  $x$ - $y$ - $z$  diagonal, the corners indicated in Fig. 6.6.

The average values for the above discretizations, together with the streamline approximation, are listed in Table 6.2.

Table 6.2. The average values  $I_{mn}$  of the error terms of the derivative  $\partial u / \partial e_1$  for the one-dimensional discretization, the diagonal discretization, the streamline approximation, and the fixed stencil with optimal stability.

	$I_{r3}$	$I_{r2}$	$I_{r1}$	$I_{r0}$
one-dimensional	0.100	0.091	0.170	0.058
diagonal	0.288	0.110	0.137	0.025
streamline	0.167	0.0	0.167	0.0
optimal stability	0.300	0.183	0.440	0.115

### 6.3. Directional second order discretizations of stream-wise second derivatives in three dimensions on a $3 \times 3 \times 3$ grid.

Using the coordinate transformation of (6.3), we have

$$\begin{aligned} \frac{\partial^2 u}{\partial e_1^2} &= \cos^2 \alpha \cos^2 \beta \frac{\partial^2 u}{\partial x^2} + \sin^2 \alpha \cos^2 \beta \frac{\partial^2 u}{\partial y^2} + \sin^2 \beta \frac{\partial^2 u}{\partial z^2} \\ &+ 2 \cos \alpha \cos^2 \beta \sin \alpha \frac{\partial^2 u}{\partial x \partial y} + 2 \cos \alpha \cos \beta \sin \beta \frac{\partial^2 u}{\partial x \partial z} + 2 \sin \alpha \cos \beta \sin \beta \frac{\partial^2 u}{\partial y \partial z}. \end{aligned} \quad (6.34)$$

The analysis of approximations like  $\partial^2 u / \partial e_2^2$  is similar and will not be treated here.

The basis consists of ten stencils, three antisymmetric and seven symmetric. We recycle the basis of §6.2 by taking stencils 8...17 from Fig. 6.8, which constitute stencils 1...10 in our new basis. In this basis, stencils 1...3 and 10 are approximations which have an error which is one or two orders beyond the truncation error.

The fixed incomplete streamline stencils which result in  $c_{r0} = 0$ , but  $c_{r1} \neq 0$ , are shown in Fig. 6.14,

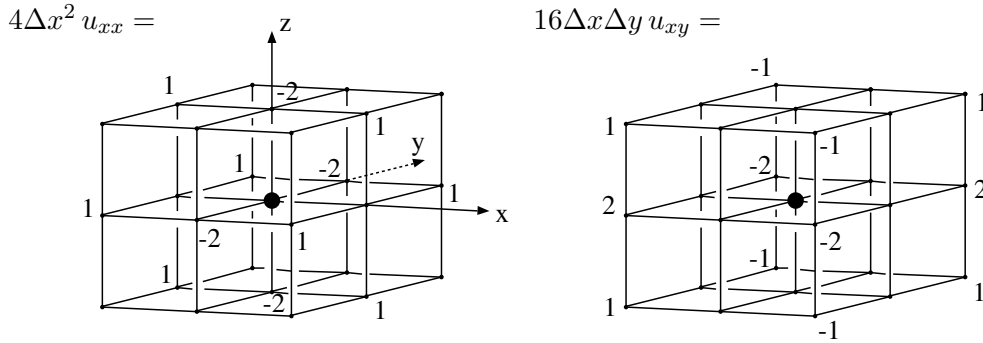


Figure 6.14. The stencils for  $u_{xx}$  and  $u_{xy}$ , which are used together with the regular permutations for the remaining grid-based second derivatives in  $\partial^2 u / \partial e_1^2$  of (6.34).

In this basis, the one-dimensional grid-aligned approximation is recovered with  $k_{yz4} = k_{xz5} = k_{xy6} = -1/16$ ,  $k_{yy7} = k_{zz7} = k_{xx8} = k_{zz8} = k_{xx9} = k_{yy9} = -1/12$  and  $k_{xx10} = k_{yy10} = k_{zz10} = 1/6$ , and the diagonal approximation needs  $k_{xz4} = k_{yz5} = k_{xz6} = k_{yz6} = -k_{xy6} = 1/16$ ,  $k_{yz7} = k_{xz8} = k_{xy9} = 1/12$ ,  $k_{zz7} = k_{yy7} = k_{zz8} = k_{xx8} = k_{xx9} = k_{yy9} = -1/12$ ,  $k_{xx10} = k_{yy10} = k_{zz10} = 1/6$ , and  $k_{xy10} = k_{xz10} = k_{yz10} = -1/48$ . The stencils for the cross derivatives of the diagonal approximation are shown in Fig. 6.15.

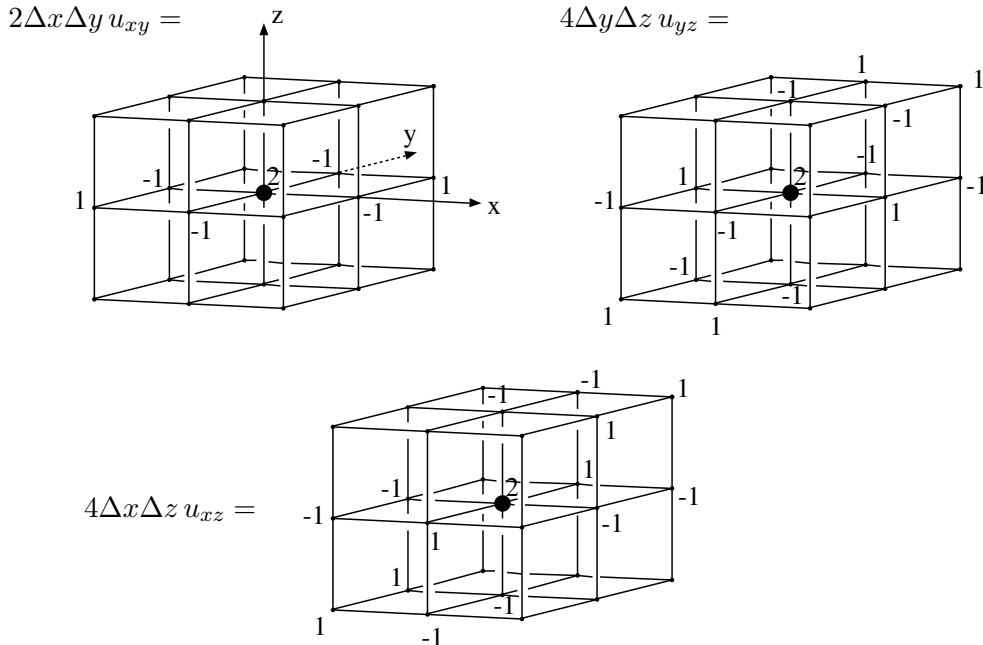


Figure 6.15. The stencils for the cross derivatives of the diagonal approximation.

Remark that the diagonal approximation is not regular since  $u_{yz}$  is not a regular permutation of  $u_{xy}$ . When we use only regular permutations of  $u_{xy}$  we have an approximation of  $\partial^2 u / \partial e_1^2$  shown in Fig. 6.16. We will call this approximation regular non-diagonal. There is no regular diagonal approximation of  $\partial^2 u / \partial e_1^2$ .

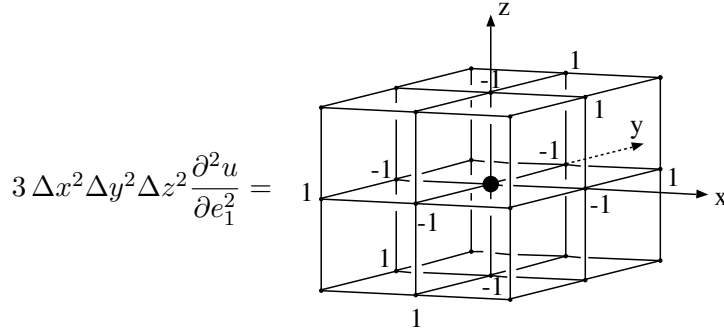


Figure 6.16. The approximation of  $\partial^2 u / \partial e_1^2$  with the regular non-diagonal approximation for the case that  $e_1$  is along the body diagonal.

These approximations are used on the principal region  $a_x / \Delta x \geq a_y / \Delta y \geq a_z / \Delta z \geq 0$ . For other flow angles we use a permutation of the discretization.

The continuity conditions for the second derivative in the  $z = 0$  plane for the FV formulation are  $K_{xx3} = K_{xx4} = K_{xx5} = K_{xy3} = K_{xy4} = K_{xy5} = K_{yy3} = K_{yy4} = K_{yy5} = 0$ , and  $K_3 = K_4 = K_5 = 0$  with FD. For the  $x = y$  plane this is  $K_{xx1} = K_{xx2} - 2K_{xy1} + 2K_{xy2} - K_{yy1} + K_{yy2}$ ,  $K_{xx4} = K_{xx5} - 2K_{xy4} + 2K_{xy5} - K_{yy4} + K_{yy5}$ ,  $K_{xx7} = K_{xx8} - 2K_{xy7} + 2K_{xy8} - K_{yy7} + K_{yy8}$ ,  $K_{xz1} = K_{xz2} - K_{yz1} + K_{yz2}$ ,  $K_{xz4} = K_{xz5} - K_{yz4} + K_{yz5}$ ,  $K_{xz7} = K_{xz8} - K_{yz7} + K_{yz8}$ ,  $K_{zz1} = K_{zz2}$ ,  $K_{zz4} = K_{zz5}$ ,  $K_{zz7} = K_{zz8}$ , and  $K_1 = K_2$ ,  $K_4 = K_5$  and  $K_7 = K_8$ . The conditions for the  $y = z$  plane are  $K_{xx2} = K_{xx3}$ ,  $K_{xx5} = K_{xx6}$ ,  $K_{xx8} = K_{xx9}$ ,  $K_{xy2} = K_{xy3} - K_{xz2} + K_{xz3}$ ,  $K_{xy5} = K_{xy6} - K_{xz5} + K_{xz6}$ ,  $K_{xy8} = K_{xy9} - K_{xz8} + K_{xz9}$ ,  $K_{yy2} = K_{yy3} - 2K_{yz2} + 2K_{yz3} - K_{zz2} + K_{zz3}$ ,  $K_{yy5} = K_{yy6} - 2K_{yz5} + 2K_{yz6} - K_{zz5} + K_{zz6}$ ,  $K_{yy8} = K_{yy9} - 2K_{yz8} + 2K_{yz9} - K_{zz8} + K_{zz9}$ , and  $K_2 = K_3$ ,  $K_5 = K_6$ ,  $K_8 = K_9$ . The approximations presented above are continuous.

Like in two dimensions, there is no streamline approximation, and limiting is needed to obtain a higher order steady solution of the approximation. The conditions for  $c_{r0} = 0$  are

$$K_4 \sin \beta = \sin \alpha \cos \beta K_6, \quad K_5 \sin \beta = \cos \alpha \cos \beta K_6, \quad K_i = 0, \quad i = 7 \dots 9. \quad (6.35)$$

The coefficients  $c_{r0}$  depend on the angle  $\gamma$ . We eliminate this dependency from the coefficients by comparing  $c_{r0}$  for  $\beta = 0$  with the two-dimensional coefficient  $c_{04}$  of Fig. 5.24. The solution is, as before,  $\gamma = 0$  modulo  $\pi/2$ .

The optimal Laplacian with symmetries imposed has one degree of freedom, stencil  $B^{10}$ , and is shown in Fig. 6.17.

This approximation lends itself to time accurate discretizations in two dimensions.

The coefficients  $c_r$  are a function of the angles  $\alpha$  and  $\beta$ , and  $c_{r0}$  is shown for the one-dimensional grid-aligned approximation, the diagonal approximation, and the regular non-diagonal approximation in Fig. 6.18.

For the diagonal discretization, Fig. 6.18, the coefficient  $c_r$  is zero at the  $x$  axis, the  $x$ - $y$  diagonal, and the  $x$ - $y$ - $z$  diagonal, the corners indicated in Fig. 6.6.

The average values for the above discretizations are listed in Table 6.3.

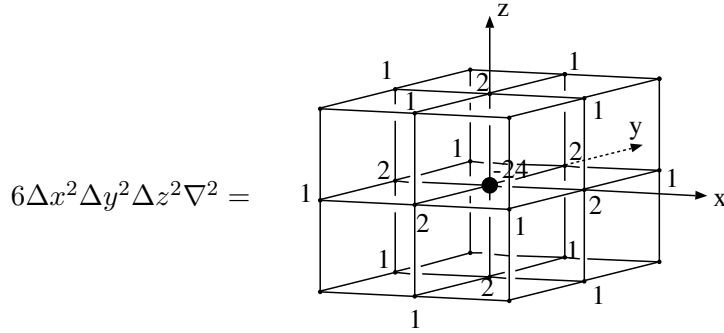


Figure 6.17. The optimal Laplacian.

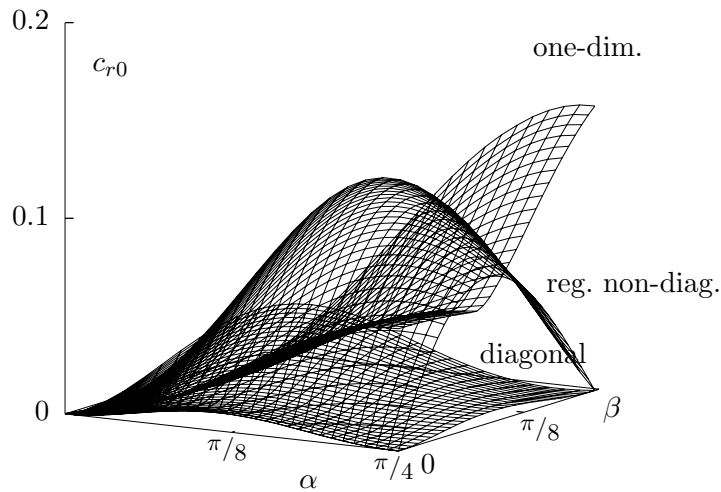


Figure 6.18. The coefficient  $c_{r0}$  for the one-dimensional grid-aligned approximation, the diagonal, and the regular non-diagonal approximation.

Table 6.3. The average values  $I_{mn}$  of the error terms of the second stream-wise derivative  $\partial^2 u / \partial e_1^2$ : one-dimensional grid-aligned, diagonal, the incomplete streamline stencil, and the regular non-diagonal stencil.

	$I_{r5}$	$I_{r4}$	$I_{r3}$	$I_{r2}$	$I_{r1}$
one-dimensional	0.100	0.024	0.108	0.084	0.053
diagonal	0.155	0.087	0.103	0.028	0.013
incomplete streamline	0.150	0.091	0.220	0.057	0.0
regular non-diagonal	0.129	0.054	0.163	0.104	0.058

#### 6.4. Boundary approximations for the second order first derivative in three dimensions.

On larger grids, we present boundary stencils for the streamline second order approximation of the first derivative, (6.26). The streamline approximations  $c_{r0} = 0$  are given for the case that the boundary node is on a single boundary plane  $i = 0$ , Fig. 6.19.

When the boundary node is on two boundary planes,  $i = 0$  and  $j = 0$ , we get the stencils of Fig. 6.20 and Fig. 6.21.

Finally, with the boundary node on the intersection of three boundary planes,  $i = 0$

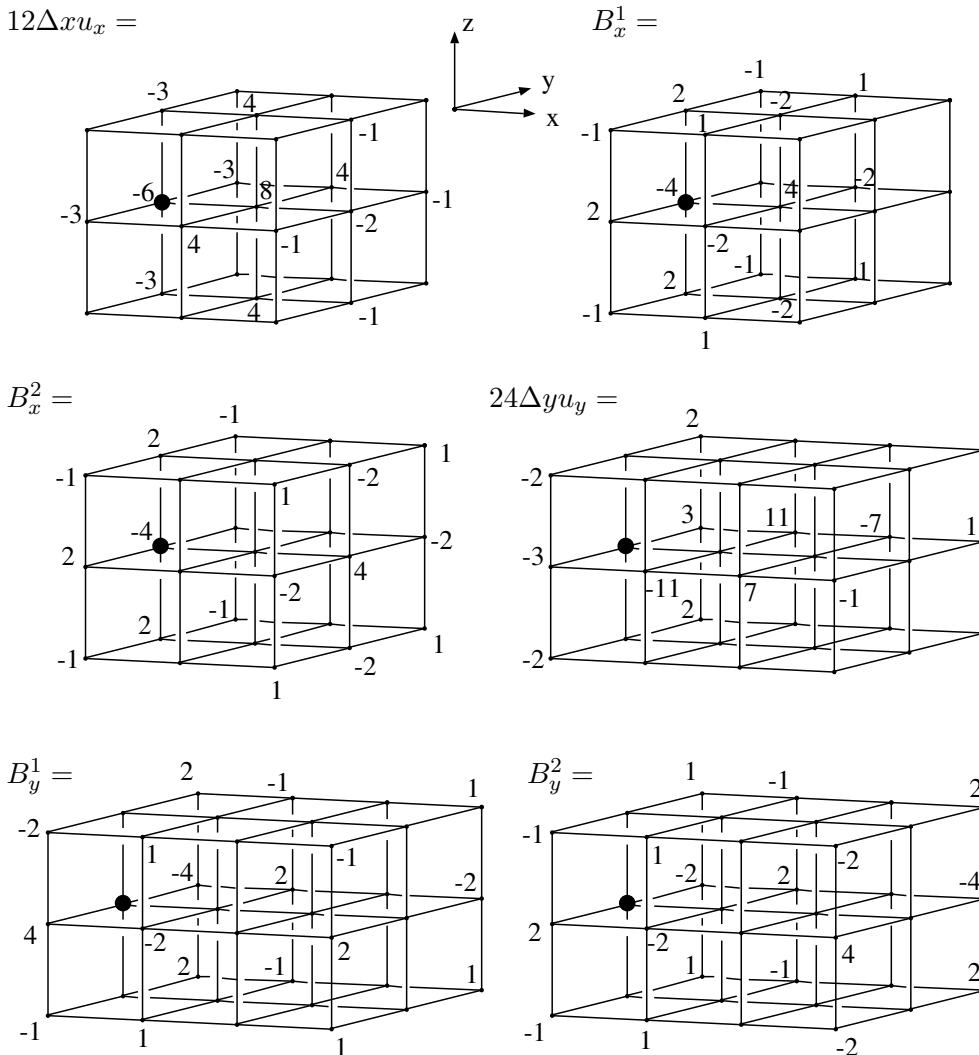


Figure 6.19. Streamline boundary approximations for the boundary at  $i = 0$  for the central approximation of §6.2. The boundary stencil  $u_x$  is shown with two basis stencils, and  $u_y$  with also two basis stencils. A rotation over  $\pi/4$  along the  $i$  grid line through the point of discretization of  $u_y$  gives  $u_z$ .

$j = 0$  and  $k = 0$ , we get the stencils of Fig. 6.22.

These boundary stencils reduce to Fig. 5.32 and Fig. 5.33 in two dimensions. No attempt has been made to use the degrees of freedom to find boundary stencils which lead to an optimally stable approximation.

**6.5. The scheme of Lax and Wendroff.**

For the first derivative in (5.80) in three dimensions we use the stream-wise fixed stencil and basis  $B$  with coefficients  $K$  of §6.2, and for the second derivative the incomplete streamline fixed stencil and the basis stencils of §6.3. The latter we will indicate by coefficients  $K'$ .

The coefficient  $c_{r0}$  in the error of  $\partial u / \partial e_1$  of the Lax-Wendroff scheme can be found in Fig. 6.13, and the average error values  $I_{mn}$  in Table 6.2.

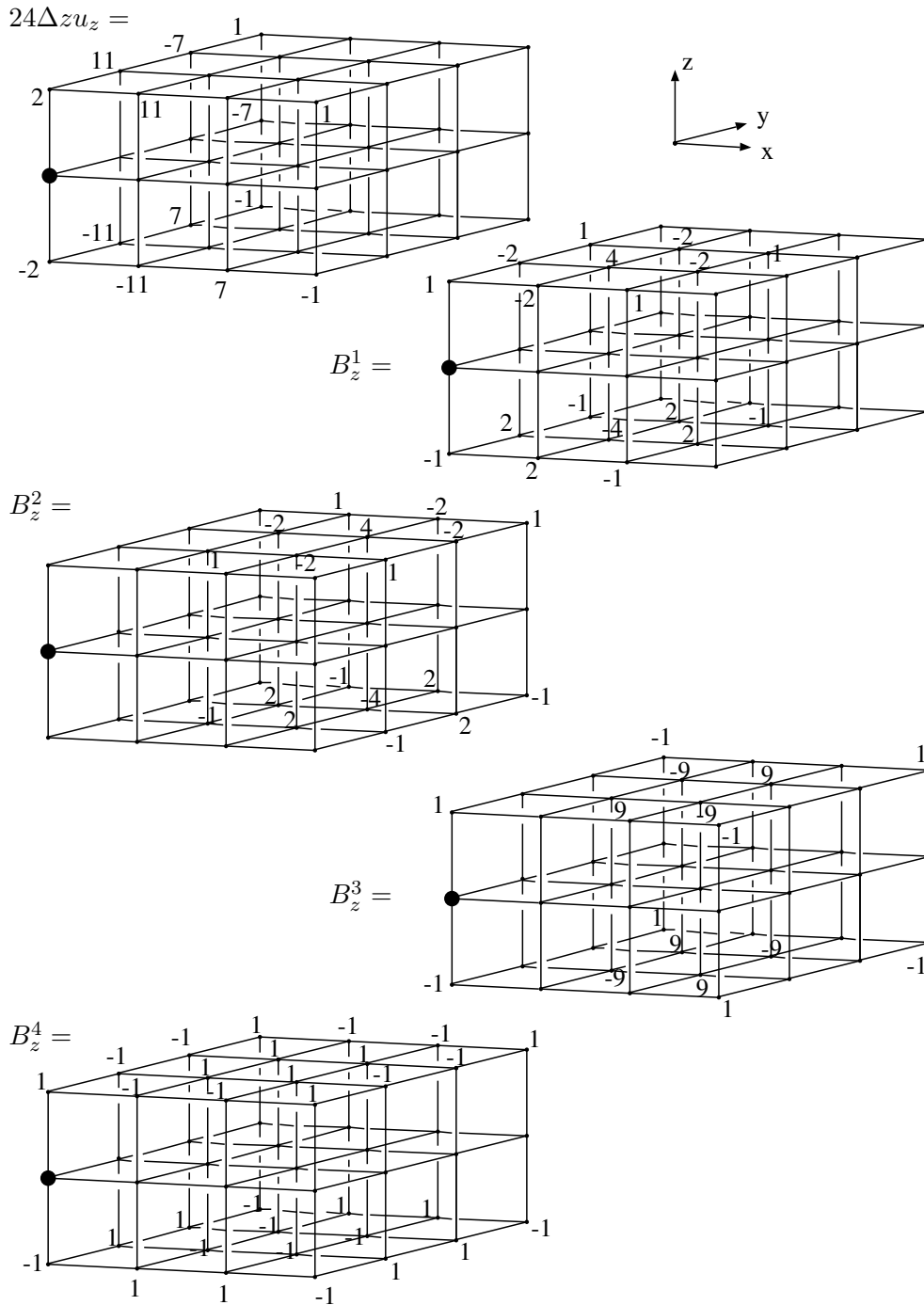


Figure 6.20. Streamline boundary approximations for the boundary at the intersection  $i = j = 0$  for the central approximation of §6.2. The boundary stencil  $u_z$  is given with four basis stencils.

The amplification  $G$  as a function of  $\nu = a\Delta t/h$  for the stability of the Lax-Wendroff scheme depends on the 27 coefficients  $K$  and  $K'$ . The amplification  $G$  is similar to  $\Omega$  of (6.29), where  $K_8$  appears with  $K'_1$  etc., cf. (5.81) and (5.35).

An analytic optimization is complicated. A first impression of the maximum value of  $\nu$  for a stable approximation is to compute  $G$ , given  $K$ , for a range of  $\alpha$ ,  $\beta$ ,  $\phi_x$ ,  $\phi_y$ , and  $\phi_z$ .

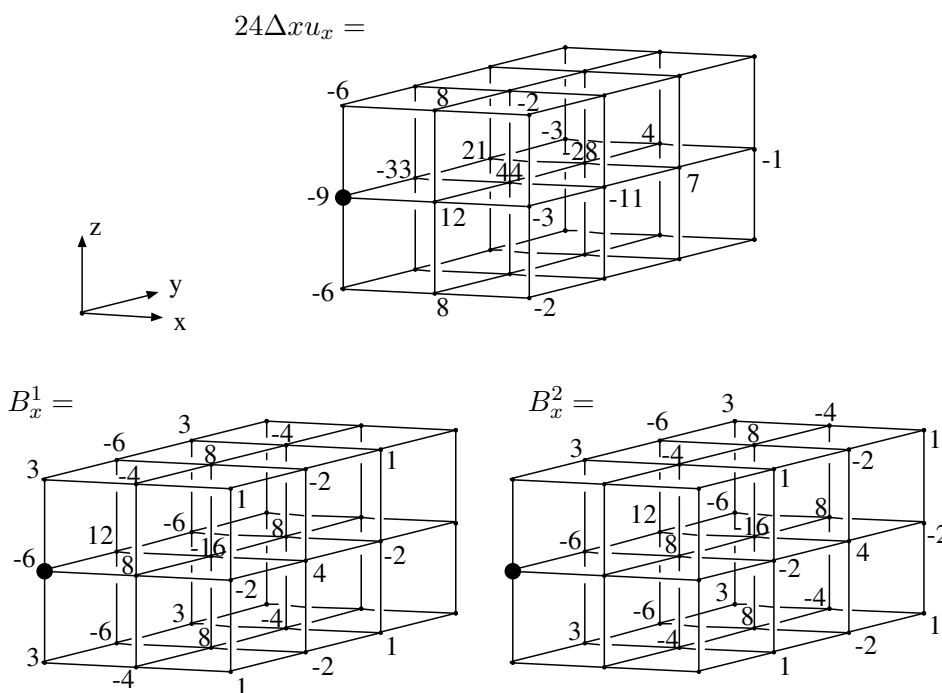


Figure 6.21. Streamline boundary approximations for the boundary at the intersection  $i = j = 0$  for the central approximation of §6.2. The boundary stencil  $u_x$  is shown with two basis stencils. A regular rotation over  $\pi/4$  gives  $u_y$ .

For some combinations of first and second derivatives in the Lax-Wendroff approximation the maximum value of  $\nu$  is given in Table 6.4.

Table 6.4. The maximum allowable value of  $\nu$  for different combinations of a first derivative of §6.2 and a second derivative of §6.3 in the Lax-Wendroff scheme.

$\partial^2 u / \partial e_1^2 \backslash \partial u / \partial e_1$	one-dim.	diagonal	streamline	opt. time step
one-dimensional	0.339	x	0.944	0.914
diagonal	x	x	0.550	x

x : the scheme is not stable.

Approximations involving the incomplete streamline stencil as second derivative are unstable, like in two dimensions. Also discretizations with the regular non-diagonal stencil are unstable. The combination of the diagonal approximation is only stable with a streamline first order approximation. Unexpectedly, the scheme involving a diagonal approximation for the first derivative is unstable. In two dimensions, this combination gave the best result. The diagonal second derivative is not regular. This may reduce stability.

A full parametric analysis of the amplification for the optimization of  $\nu$  remains to be done. Nevertheless, the streamline first order approximation with a one-dimensional second derivative in a Lax-Wendroff scheme almost triples the stability compared with the full one-dimensional scheme.

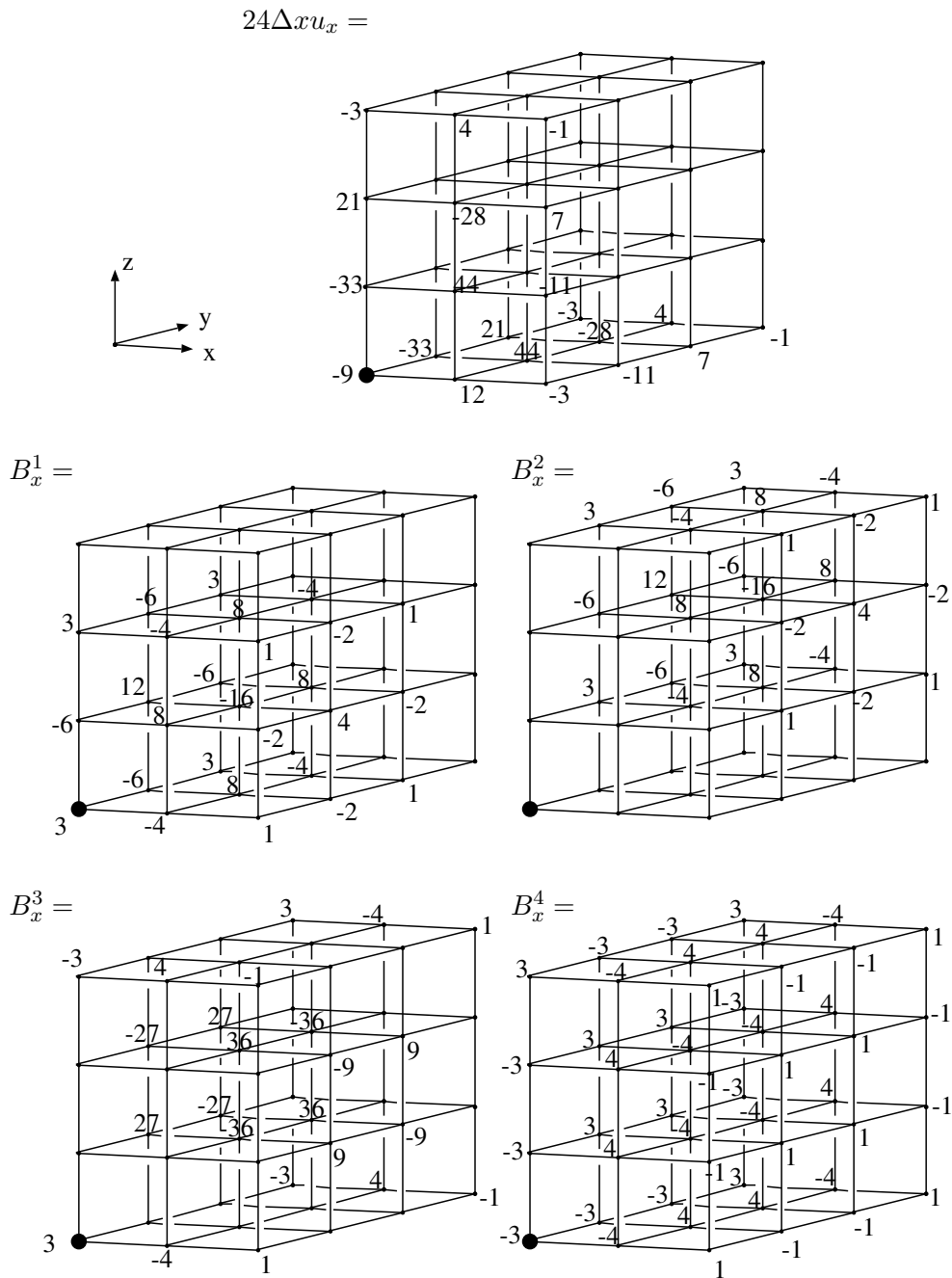


Figure 6.22. Streamline boundary approximations for the boundary at the intersection  $i = j = k = 0$  for the central approximation of §6.2. The boundary stencil  $u_z$  is presented with four basis stencils. A regular rotation over  $\pi/4$  gives  $u_y$ , and consequently  $u_x$ .

### 7. Directional discretizations on unstructured grids.

On unstructured grids, the creation of approximations by means of a basis of stencils, analysis and optimization is similar to structured grids. The bases are generated with the program GDD, which now reads an unstructured stencil.

However, the number of volumes like triangles or tetrahedra which surround a node on unstructured grids may vary. The stencil is the same everywhere on a structured grid, except for the one-sided approximations at the boundaries. Even if the structured grid is distorted, the same approximations are used for any interior node in a FD or FV solver.

On an unstructured grid, the one-dimensional FV method leads to a consistent approximation. The distribution methods based on the N scheme lose consistency on irregular grids, and in three dimensions [7].

The basis of stencils can be applied on irregular grids in a FD context. Consistency and optimization are applied to the individual nodes.

We will consider first order upwind and second order central discretizations in two and three dimensions. First order upwind approximations have been treated from different points of view elsewhere, see e.g. [6]. In the following, we will use as fixed stencils for  $u_x$ ,  $u_y$ , and  $u_z$  the approximations which result from a FV approach, presented in a FD formulation.

### 7.1. Directional first order upwind discretizations of the first derivative in two dimensions on equilateral triangles.

A simple regular unstructured grid in two dimensions is composed of equilateral triangles with  $h$  the length of the side. The point of discretization is surrounded by six triangles, and the stencil is a hexagon. The node numbers of this stencil are shown in Fig. 7.1.

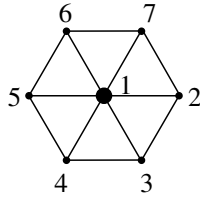


Figure 7.1. The node numbers on the hexagonal stencil.

The first order approximation on this grid is shown in Fig. 7.2.

We consider the principal region  $0 \leq \alpha \leq \pi/6$ . For other flow angles a permutation is used. On the principal region, upwind discretizations reduce the basis to the single stencil  $b$  with  $k_2 = -k_1$ ,  $k_3 = k_1$ , and  $k_4 = 0$ , see Fig. 7.3.

We replace the fixed stencils by those of the distribution N scheme, Fig. 7.4.

The first order upwind stream-wise derivative is, with the fixed stencils of Fig. 7.4, and the basis stencil  $b$  of Fig. 7.3,

$$\begin{aligned} \frac{\partial u}{\partial e_1} = \frac{1}{h} \{ & (-k + \cos \alpha + \frac{1}{\sqrt{3}} \sin \alpha) u_1 + (k - \frac{2}{\sqrt{3}} \sin \alpha) u_4 \\ & + (-k - \cos \alpha + \frac{1}{\sqrt{3}} \sin \alpha) u_5 + k u_6 \}. \end{aligned} \quad (7.1)$$

The monotonicity conditions for this approximation are

$$\begin{aligned} 1 - \frac{a\Delta t}{h} (-k + \cos \alpha + \frac{1}{\sqrt{3}} \sin \alpha) &\geq 0, & -k + \frac{2}{\sqrt{3}} \sin \alpha &\geq 0, \\ k + \cos \alpha - \frac{1}{\sqrt{3}} \sin \alpha &\geq 0, & k &\leq 0. \end{aligned} \quad (7.2)$$

For sufficiently small  $\Delta t$  and on the principal region this reduces to

$$0 \geq k \geq \frac{1}{\sqrt{3}} \sin \alpha - \cos \alpha. \quad (7.3)$$

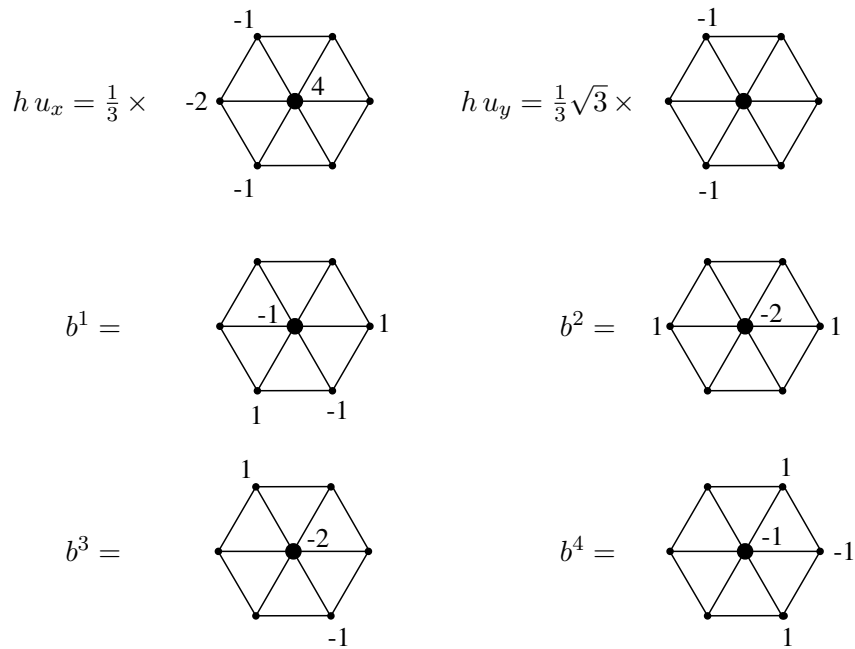


Figure 7.2. The FV derivatives  $u_x$  and  $u_y$ , together with the basis stencils for the first order discretization on a hexagonal stencil.

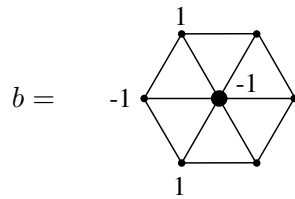


Figure 7.3. The single basis stencil  $b$  for the first order upwind discretization.

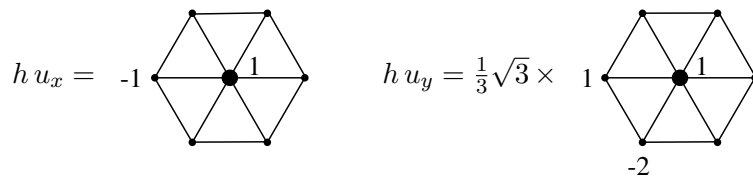


Figure 7.4. The distribution N scheme derivatives  $u_x$  and  $u_y$  for the first order discretization on a hexagonal stencil.

The fixed stencil of Fig. 7.2 has  $k = 1/3(\sqrt{3} \sin \alpha - \cos \alpha)$  and is monotone, but has a smaller allowable time step than the stencil of Fig. 7.4.

The streamline solution satisfies  $c_{02} = 0$  with

$$c_{02} = \frac{1}{4}(3 \cos^2 \alpha - \sin^2 \alpha)(k - \frac{1}{3}\sqrt{3} \sin \alpha). \tag{7.4}$$

The simple solution  $k_x = 0$  and  $k_y = 1/3\sqrt{3}$  does not satisfy the monotonicity conditions, and is not continuous at  $\alpha = \pi/6$ .

**7.2. Directional second order central discretizations of the first derivative in two dimensions on equilateral triangles.**

The basis for the central second order approximations is shown in Fig. 7.5.

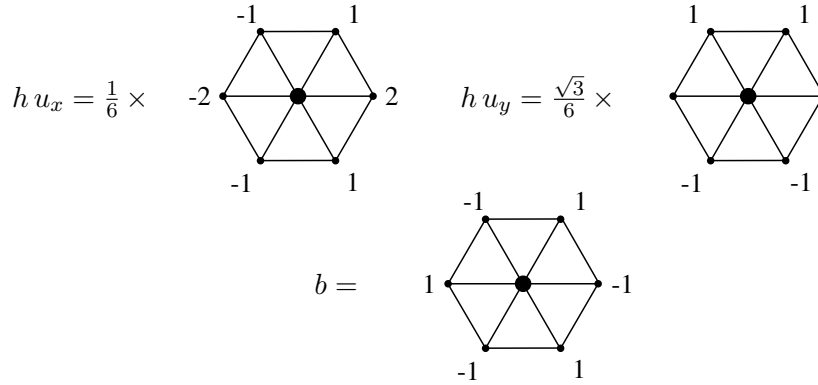


Figure 7.5. The derivatives  $u_x$  and  $u_y$ , together with the basis stencil  $b$ , for the second order central discretization on a hexagonal stencil.

The basis consist of one stencil. There are less degrees of freedom than on the structured grid since the stencil contains less nodes.

A directional analysis gives as error terms

$$\begin{aligned} c_{30} &= -\frac{1}{8} + \frac{1}{4}k \cos(3\alpha), & c_{21} &= \frac{3}{4}k \sin(2\alpha), \\ c_{12} &= \frac{1}{8} + \frac{3}{4}k \cos(3\alpha), & c_{03} &= -\frac{1}{4}k \sin(3\alpha). \end{aligned} \tag{7.5}$$

This reveals that the fixed FV derived stencil has the streamline property.

The general streamline approximation has  $k = 0$ , and the FV stencil is the only flow-angle independent streamline approximation.

**7.3. Directional second order central discretizations of the first derivative in three dimensions on an icosahedron.**

We take an icosahedron as the stencil. The point of discretization is surrounded by twenty tetrahedra. The surface consists of equilateral triangles, which edge length is about 5% longer than the distance to the center. We take the nodes on a sphere with radius  $h$ . These nodes are permutations of  $(p h, q h, 0)$  with  $p = \sqrt{(5 + \sqrt{5})/10}$  and  $q = \sqrt{(5 - \sqrt{5})/10}$ .

On this grid, we have a basis of three stencils. The fixed stencil for  $u_x$  and the basis stencil  $b^1$  is shown in Fig. 7.6. The remaining fixed derivatives  $u_y$  and  $u_z$ , and basis stencils  $b^2$  and  $b^3$  are obtained by rotations.

With this basis there are no streamline stencils possible. There are just not enough degrees of freedom, since we have a compact surrounding of the node at the origin.

The first order upwind discretization has a basis of nine stencils on this grid.

This result is a drawback for unstructured methods in three dimensions. While a subdivision of space in tetrahedra with equilateral sides is impossible, the icosahedron comes very close. In other words, an unstructured grid generator is likely to fill large amounts of the domain with nodes which are surrounded by twenty tetrahedra and twelve nodes, just like an icosahedron.

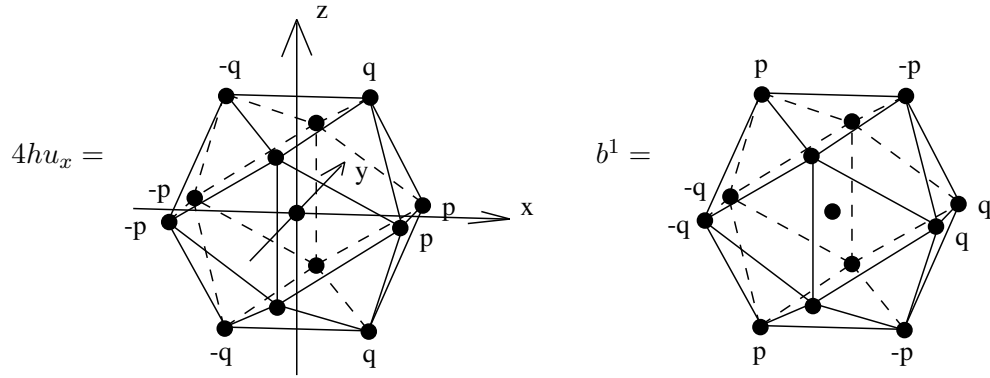


Figure 7.6. The fixed stencil  $u_x$  and the basis stencil  $b^1$  for the second order approximation. The remaining grid derivatives and basis stencils are obtained with rotations.

It is of course possible to consider a stencil which includes nodes which are further away, but then it may be easier to apply a classical fourth order method, at perhaps a lower cost.

We can still define a regular straight approximation, for which  $k_{x1} = k_{y2} = k_{z3}$ , and with the remaining  $k$ 's zero.

The stability analysis indicates that the amplification of the fixed stencil is almost optimal. The regular approximation with  $k_{x1}$  near  $1/6$  reduces  $\Omega_{max}(0, 0)$  from 1.3 to 1.2, but increases the maximum value for  $\alpha = \pi/4$ .

Optimization in the high frequency part of the eigenvalues is possible.

Unstructured second order discretizations in three dimensions are therefore facing the problems of hardly an increase in stability, an absence of stream-wise discretization, combined with the restriction to a FD discretization for consistency.

#### 7.4. Directional second order central discretizations of the first derivative in three dimensions on twenty four tetrahedra.

We will take as the stencil for this central approximation a cluster of twenty four tetrahedra. This cluster can be constructed as follows. Consider a cube, dissected into six tetrahedra ([7]), see Fig. 7.7.

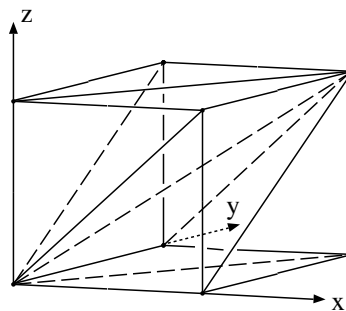


Figure 7.7. A subdivision of a cube in six tetrahedra.

The node at the origin is surrounded by eight of such cubes, and the node is part of twenty four tetrahedra. The resulting approximation is shown in Fig. 7.8.

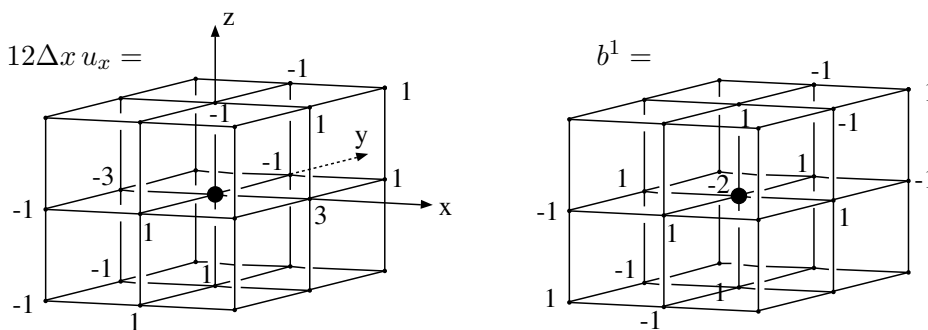


Figure 7.8. The fixed stencil  $u_x$  and the basis stencil  $b^1$  for the second order approximation. The remaining grid derivatives and basis stencils are obtained with rotations.

The basis consists of three stencils. On this grid, we cannot have straight approximations. Regular approximations require  $k_{x1} = k_{y2} = k_{z3}$ , and the remaining  $k$ 's zero.

We can obtain the fixed stencil of Fig. 7.8 with the basis of §6.2, taking there  $K_x = 1/144(6, 0, 6, 0, 8, -1, -3, -8, -1, -3, 0, 0, 0, 0, 0, 0, 0, 0)^T$ , and similar for the other derivatives. The basis stencils are symmetric, and e.g.  $b^1$  is the combination  $b^1 = 1/4(0, 0, 0, 0, 0, 0, 0, 0, 0, 1, -1, 1, -2, 1, 0, 0)^T$ .

A directional analysis reveals that the fixed stencils, obtained from a FV method, form a streamline approximation. We now have enough nodes for streamline approximations, without increasing the number of basis stencils compared to the icosahedron grid.

The question is if an unstructured grid generator will produce such configuration in a majority of the cases. Starting with a structured grid is no solution, since the ease of generating an unstructured grid is mainly the reason for unstructured solvers.

In Fig. 7.9 we have collected the stability surfaces of  $\Omega_{max}(\alpha, \beta)$  for the structured central optimal stable approximation of Fig. 6.11 and the unstructured approximations on 20 and 24 tetrahedra, the latter one computed with the structured tools of the previous section.

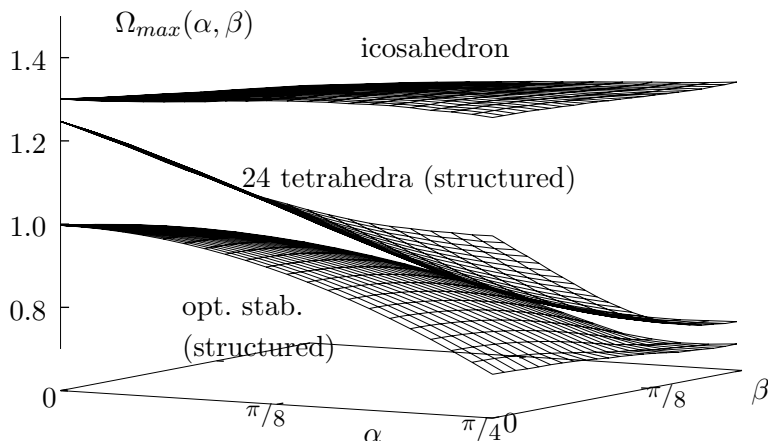


Figure 7.9. The stability expressed by  $\Omega_{max}(\alpha, \beta)$  for the unstructured approximation on 20 tetrahedra, on 24 tetrahedra (structured), and the structured approximation with optimal stability.

For given grid size  $h$ , the allowable time step is smaller on the icosahedron grid than on the structured grid. The comparison would be fairer when we consider an unstructured  $h_u$  and a structured  $h_s$  which give the same node density.

## 8. Numerical results.

We will present here the first results for some approximations. We restrict ourselves to first order and second order approximations in two dimensions, for the scalar advection equation and the Euler equations. This enables us to verify part of the analysis presented before, and to get an impression of the properties of a few approximations.

We start with a scalar linear advection problem, comparing the convergence of the first order upwind approximation in the one-dimensional grid-aligned version, and with the diagonal discretization. The behavior is known [4, 8, 10], but for completeness we include here the convergence plot for the two approximations. The test problem is a unit square domain with  $32 \times 32$  cells on a regular grid. At the inlet a profile is specified, which is advected through the domain with flow direction  $\alpha$ . The convergence in the  $L_\infty$  norm is shown in Fig. 8.1.

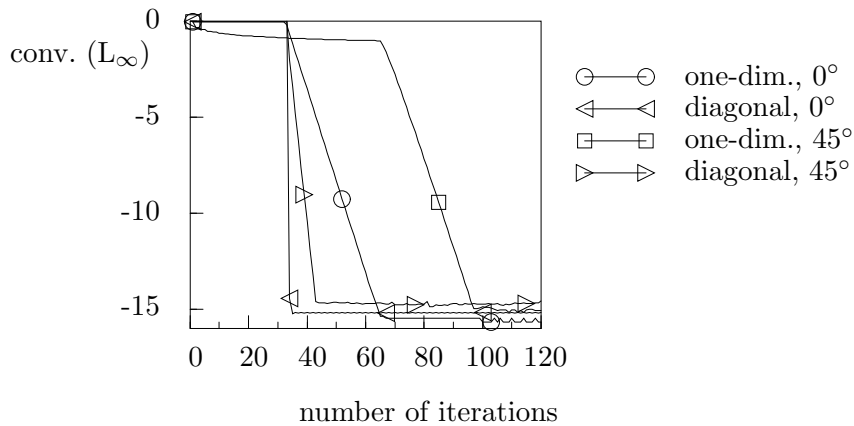


Figure 8.1. The convergence in the  $L_\infty$  norm for first order upwind approximations for the linear advection problem on a regular grid of  $32 \times 32$  cells, with local time step for flow angles  $0^\circ$  and  $45^\circ$ .

As expected, the number of iterations is virtually independent of the flow angle for the diagonal approximation.

For an assessment of the accuracy, we consider the central second order approximation in the three forms : the standard one-dimensional grid-aligned version, the diagonal approximation of (2.6), and the streamline approximation of (5.32). The latter is without the correction of §5.5.

We use the linear scalar advection problem on a unit square domain with a flow angle of  $\alpha = 30^\circ$  on a regular grid with 12-33 nodes on each axis and a smooth exponential inlet profile. The error is the difference of the numerical result and the analytical solution, and is similar for FD and the FV method, Fig. 8.2.

The slope is 2, 2.5, and 4 for the three approximations respectively in either the  $L_1$ ,  $L_2$  or in the  $L_\infty$  norm. The improved accuracy is compromised, or even lost, on a less regular

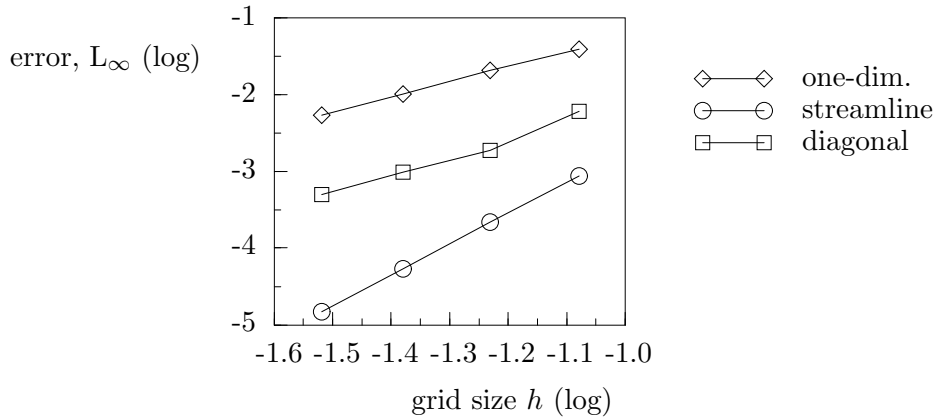


Figure 8.2. The log of the error in  $L_\infty$  norm as function of the log of the grid size  $h$  for three central second order approximations : the standard one-dimensional grid-aligned version, the diagonal approximation of (2.6), and the streamline approximation of (5.32).

grid in the FV method. On the somewhat deformed grid of Fig. 8.3, the errors are shown in Fig. 8.4.

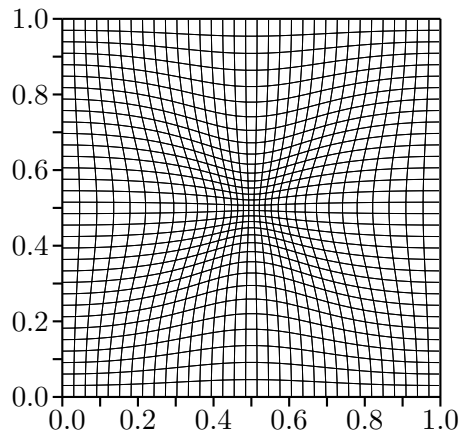


Figure 8.3. A slightly deformed grid on the unit domain.

A whiff of fourth order artificial viscosity is needed. The accuracy is reduced, and the slopes are 1.9, 2.4, and 2.6 respectively. The streamline approximation is now similar to the diagonal approximation, but the error is less than of the one-dimensional approximation. Convergence is better than for the one-dimensional grid-aligned approximation.

Only the FD method can take into account in a derivation similar to (5.32) the actual grid node positions. The alternative is a coordinate transformation, as discussed in §5.2, but this does not restore the accuracy in this case.

The behavior for systems of equations is analyzed by computing the solution of the Euler equations for subsonic flow in a channel which has a sinusoidal bump on the lower wall [27]. The grid of the channel is shown in Fig. 8.5 for the grid size  $h = 1/12$  in the uniform region.

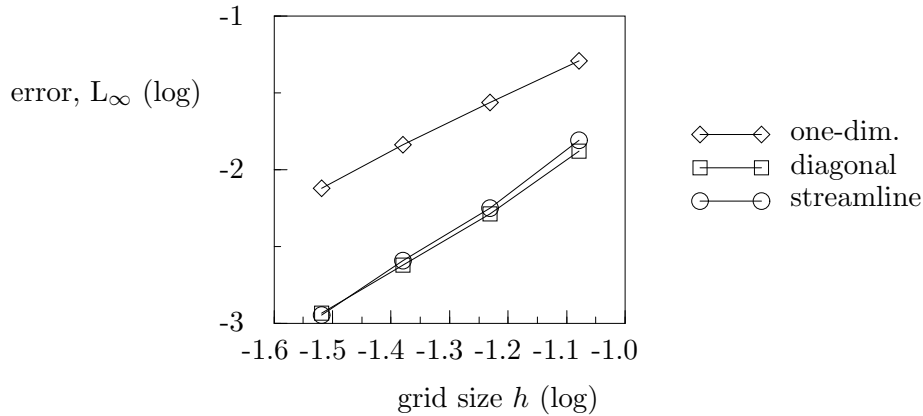


Figure 8.4. The log of the error in  $L_\infty$  norm as function of the log of the grid size  $h$  for the three central second order approximations on the grid of Fig. 8.3.

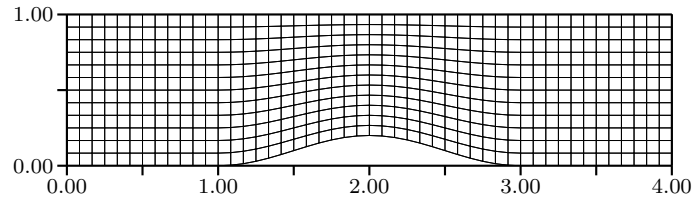


Figure 8.5. The grid of the channel with bump for the grid size  $1/12$  in the uniform region.

We compute FV solutions with the one-dimensional central second order approximation, with the streamline approximation of (5.32), and the latter with a transformation to a uniform computational grid. The streamline approximations are without the correction of §5.5.

The spurious entropy is for subsonic flow an indication of the error, but in practice the behavior of a parameter like the Mach number may be important. We apply characteristic boundary conditions with the Mach number  $M = 0.3$  imposed at the outlet, with at the inlet free-stream conditions. The entropy  $S = p/\rho^\gamma - 1$ , based on adimensional values, and the Mach number are shown in Fig. 8.6 for grid sizes between  $1/12 - 1/34$ .

The slopes of the entropy  $S$  are 1.7, 1.7, and 2.7 respectively for the three approximations. The grid transformation on this relatively smooth grid helps to recover some of the accuracy of the streamline approximation, but does not produce any improvement for the one-dimensional computation. The error of solution judged by the entropy is considerably lower for the streamline approximations than for the one-dimensional grid-aligned approximation. The reduced error for the streamline approximations is less visible in the Mach number, but still permits a coarser grid. For the same quantitative result about half the number of grid points is needed in two dimensions. The computational cost per node is only about 5% more than the one-dimensional approximation. Combined with better convergence, Fig. 8.7, the streamline approximations permit computational savings.

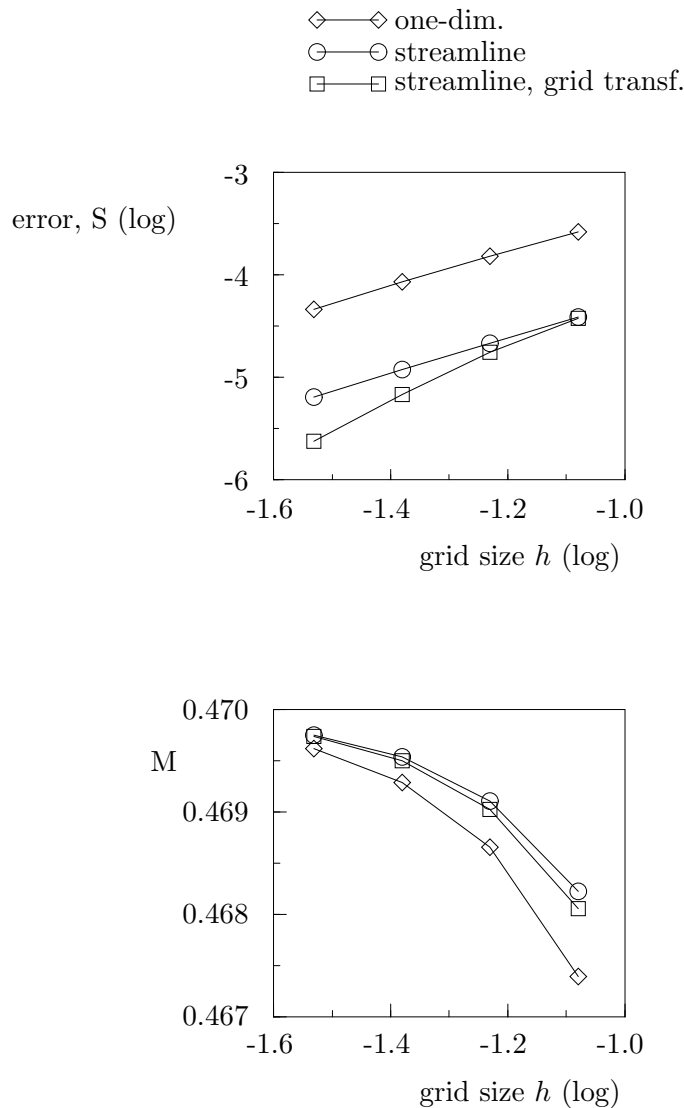


Figure 8.6. The log of the extremum of the entropy  $S$  and the extremum of the Mach number as function of the log of the grid size  $h$  for the three central second order approximations.

## 9. Conclusion.

In this paper, we have described methods to construct approximations for advection equations on an extended stencil, which include nodes which lie beyond the grid axes passing through the node of discretization.

A basis of stencils expresses the most general approximation to a derivative. The basis follows from a Taylor series expansion of the nodes present in the stencil. Tuning the degrees of freedom leads to optimization of the error of the approximation, or of the stability. The number of degrees of freedom is large. It is possible, and sometimes necessary, to make approximations a function of the advection direction. Continuity of the approximation when switching stencils is important.

We can classify the new approximations in the following groups :

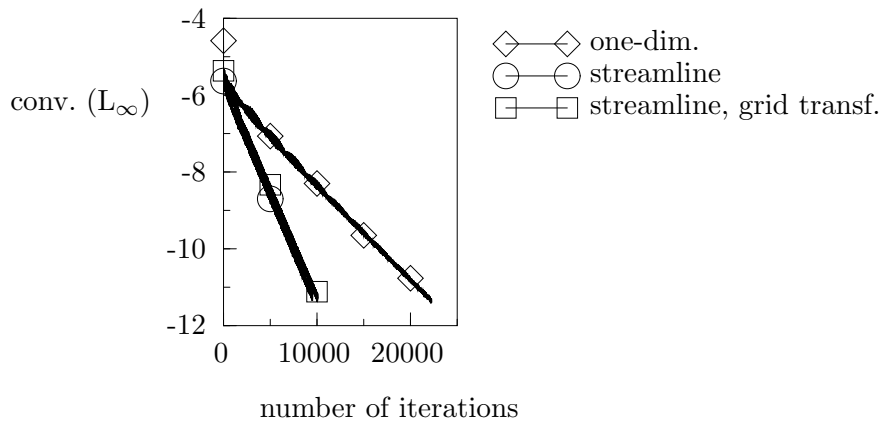


Figure 8.7. The convergence in the  $L_\infty$  norm for the three central approximations for the channel flow problem with grid size  $1/34$ , with global time step.

*Diagonal discretizations* use only nodes on grid lines and diagonals which are passing through the point of discretization. For the flow direction along those lines they reduce to a stream-wise approximation.

This class of discretizations exhibits the optimal stability and time step. We find in any number of space dimensions the same stability limit as in one dimension. In three dimension, this means an improvement of a factor of three in time step compared to the currently available discretizations.

The diagonal approximation depends piece wise on the flow angle and is continuous in the FD method, but not in the FV method. The latter method can be accommodated when making the approximation continuously dependent on the advection direction.

The dependency on the flow angle makes this approximation suited for scalar equations, or for systems of equations with commuting Jacobian matrices. The Jacobian matrices for the Euler equations do not commute. Solving these equations requires a flux splitting, a procedure currently used in upwind schemes.

*Streamline approximations* focus on eliminating the leading error term normal to the streamline. At steady state this leads to an increase in the order of accuracy of the approximation. Unsteady computations benefit also from this improvement. The stencil of the approximation includes nodes outside the diagonals and grid lines passing through the node of discretization.

The streamline property is based on a careful elimination of error terms, and is very sensitive to grid quality. The accuracy of a FV streamline approximation suffers on a deformed grid, but shows still an improvement over the currently available approximations. A FD approximation can take into account the actual position of the nodes, and retain accuracy on a deformed mesh.

In upwind approximations, the streamline condition is in conflict with continuity of the approximations. A first order streamline method also breaches the monotonicity condition. Limiting is needed to reconcile these properties in case of non-monotone solutions.

Streamline boundary stencils for the central second order approximation occupy a stencil which protrudes one layer deeper in the interior domain.

*General approximations* combine some of the above optimizations, on a stencil includ-

ing nodes outside the diagonals and grid lines passing through the node of discretization.

A second order central approximation exists which has almost the optimal stability, while being flow-angle independent. The price of the fixed stencil is a significantly larger truncation error.

A fourth order central approximation on a fixed stencil has been found in two dimensions which combines the streamline property with the optimal time step.

The Lax-Wendroff scheme is a combination of a first and a second derivative. The new approximations result in a time step which is 95% of the optimal time step in three dimensions, and the optimal time step in two dimensions. There is no regular diagonal second derivative in three dimensions.

Degrees of freedom can be used for improving smoothing properties in a multi-grid application.

The method of Hildebrand for generating discretizations is extended to more than one space dimension. This includes approximations for higher derivatives and the diagonal discretizations. Approximations which are produced this way have to be verified afterwards for truncation error and stability.

The basis of stencils applies also to unstructured grids. The inherently varying number of surrounding elements on an unstructured grid limits the use of a basis of stencils to a FD application. The natural surrounding of a node in three dimensions with twenty tetrahedra is insufficient to permit a central streamline approximation. There are enough nodes in two dimensions, and remarkably, FV approximation are streamline discretizations.

Restricting a higher order approximation to a monotone first order approximation requires limiters. Due to the coupling of the various grid-based derivatives in the approximation, an implicit solution of the limiting function is needed, which may be costly. If strict monotonicity cannot reasonably be obtained, a second best choice is approximate limiters or artificial viscosity. Application to problems with strong discontinuities will have to reveal the practical value of the new discretizations in non smooth flow.

The discretizations presented in this paper need further analysis. This concerns especially application to discontinuous problems, systems of equations, the damping of the schemes for multi-grid application, behavior with preconditioning of the equations, multi-level and implicit discretizations, application to equations in entropy or symmetrizing variables and so on.

We can state with confidence that the schemes are more accurate and stable than those nowadays available, but the major contribution may be the improvement of the time step. The implementation in existing codes is trivial, and the extent of the stencils of directional discretizations does not exceed the extent of the stencils which are currently in use.

The actual gain in computational efficiency will only be known after rigorous testing using multi-block codes in an industrial environment.

**Acknowledgement.** I wish to thank Mr. C. Lassaille of Cabinet Barré Laforgue, Toulouse, France for stimulating discussions on directional discretizations. The use of the program *dplot* of D. DeZeeuw, university of Michigan, has been very helpful.

**Property.** The author claims the intellectual property rights of directional discretizations [28].

### Appendix A. Limiters for diagonal discretizations.

We extend the limiters of grid-aligned one-dimensional discretizations to the diagonal discretizations of §2 in two dimensions. We apply the method of Spekreijse [29] for the case  $a\Delta y > b\Delta x > 0$ , and write a general update of node  $u_{i,j}$  involving the nodes  $u_{k,l}$  with  $k \in \dots, i-1, i, i+1, \dots$  and  $l \in \dots, j-1, j, j+1, \dots$  as

$$u_{i,j}^{n+1} - u_{i,j}^n = -a \frac{\Delta t}{\Delta x} A_{i,j}^n (u_{i,j}^n - u_{i-1,j}^n) - b \frac{\Delta t}{\Delta y} B_{i,j}^n (u_{i-1,j}^n - u_{i-1,j-1}^n). \quad (\text{A.1})$$

The monotonicity coefficients  $A_{i,j}^n$  and  $B_{i,j}^n$  are a function of all the unknowns  $u_{k,l}$ . Monotonicity for the steady state can easily be shown with the aid of (A.1) by taking  $u_{i,j}^{n+1} = u_{i,j}^n$ , which gives the convex average

$$u_{i,j} = \frac{\left( \frac{a}{\Delta x} A_{i,j} - \frac{b}{\Delta y} B_{i,j} \right) u_{i-1,j} + \frac{b}{\Delta y} B_{i,j} u_{i-1,j-1}}{\frac{a}{\Delta x} A_{i,j}}. \quad (\text{A.2})$$

The scheme is monotone under the conditions that the monotonicity coefficients  $A_{i,j}^n$  and  $B_{i,j}^n$  are positive and bounded,

$$0 \leq \frac{a}{\Delta x} A_{i,j} - \frac{b}{\Delta y} B_{i,j} \leq L, \quad 0 \leq B_{i,j}^n \leq L, \quad L > 0. \quad (\text{A.3})$$

This means that the steady state solution will be monotone, but it will be possible to find initial data for which the scheme is not TVD [29]. For the first order diagonal upwind discretization, (2.5), the monotonicity coefficients are

$$A_{i,j}^n = 1, \quad B_{i,j}^n = 1, \quad (\text{A.4})$$

and the discretization is monotone.

Let us derive the monotonicity conditions for the second order diagonal upwind discretization, (2.7), and the linear advection equation. The FV framework is used where the unknowns at the edges are limited for monotonicity. We define limiter functions  $\phi^x$  and  $\phi^y$ , and the limited variables as follows:

$$\begin{aligned} u_{i+1/2,j}^L &= u_{i,j} + \frac{1}{2} \phi_{i,j}^x (u_{i,j} - u_{i-1,j}), \\ u_{i,j+1/2}^L &= u_{i-1,j} + \frac{1}{2} \phi_{i,j}^y (2u_{i-1,j} - u_{i-2,j} - u_{i-2,j-1}), \end{aligned} \quad (\text{A.5})$$

where we don't specify yet on which variables the limiting functions depend. The update in case of the Euler backward scheme becomes

$$\begin{aligned} u_{i,j}^{n+1} - u_{i,j}^n &= -a \frac{\Delta t}{\Delta x} (u_{i,j} - u_{i-1,j} + \frac{1}{2} \phi_{i,j}^x (u_{i,j} - u_{i-1,j}) - \frac{1}{2} \phi_{i-1,j}^x (u_{i-1,j} - u_{i-2,j})) \\ &\quad - b \frac{\Delta t}{\Delta y} (u_{i-1,j} - u_{i-1,j-1} + \frac{1}{2} \phi_{i,j}^y (2u_{i-1,j} - u_{i-2,j} - u_{i-2,j-1}) \\ &\quad \quad - \frac{1}{2} \phi_{i,j-1}^y (2u_{i-1,j-1} - u_{i-2,j-1} - u_{i-2,j-2})). \end{aligned} \quad (\text{A.6})$$

Therefore, the monotonicity coefficients  $A_{i,j}^n$  and  $B_{i,j}^n$  of eq. (A.1) are

$$A_{i,j}^n = 1 + \frac{1}{2} \phi_{i,j}^x - \frac{1}{2} \phi_{i-1,j}^x \frac{u_{i-1,j} - u_{i-2,j}}{u_{i,j} - u_{i-1,j}} = 1 + \frac{1}{2} \phi_{i,j}^x - \frac{1}{2} \frac{\phi_{i-1,j}^x}{R_{i-1,j}^*},$$

$$\begin{aligned}
B_{i,j}^n &= 1 + \frac{1}{2}\phi_{i,j}^y \frac{2u_{i-1,j} - u_{i-2,j} - u_{i-2,j-1}}{u_{i-1,j} - u_{i-1,j-1}} - \frac{1}{2}\phi_{i,j-1}^y \frac{2u_{i-1,j-1} - u_{i-2,j-1} - u_{i-2,j-2}}{u_{i-1,j} - u_{i-1,j-1}} \\
&= 1 + \frac{1}{2}s_{i,j}\phi_{i,j}^y - \frac{\phi_{i,j-1}^y}{S_{i,j-1}}, \tag{A.7}
\end{aligned}$$

where

$$\begin{aligned}
s_{i,j} &= \frac{2u_{i-1,j} - u_{i-2,j} - u_{i-2,j-1}}{u_{i-1,j} - u_{i-1,j-1}}, \quad S_{i,j} = \frac{u_{i-1,j} - u_{i-1,j-1}}{2u_{i-1,j-1} - u_{i-2,j-1} - u_{i-2,j-2}}, \\
R_{i,j} &= \frac{u_{i,j} - u_{i-1,j}}{u_{i+1,j} - u_{i,j}}. \tag{A.8}
\end{aligned}$$

These expressions show similarities with the monotonicity coefficients of one-dimensional theory [30, 31], where

$$A_{i,j}^n = 1 + \frac{1}{2}\phi_{i,j}^x - \frac{1}{2}\frac{\phi_{i-1,j}^x}{R_{i-1,j}} \quad \text{with} \quad R_{i,j} = \frac{u_{i,j} - u_{i-1,j}}{u_{i-1,j} - u_{i-2,j}}, \tag{A.9}$$

in which case the limiter  $\phi$  is a function of the ratio of successive differences of the unknowns in a one-dimensional direction. In the ratios of (A.9), the successive differences involve different directions.

For smooth flow, the one-dimensional ratio of differences  $R_{i,j}$  is equal to 1, and for a second order solution, we need  $\phi(1) = 1$ . Let us consider a one-dimensional flow solution,

$$u_{i,j}^{\text{1D}} = u_0 + u_a(\vec{r}_{i,j} \cdot \vec{n}) = u_0 + u_a(i\Delta x n_x + j\Delta y n_y), \tag{A.10}$$

where  $u_0$  is constant,  $u_a$  is a function of the position  $\vec{r}_{i,j}$  and  $\vec{n}/\|\vec{\nabla}u$  is the direction of the gradient of the one-dimensional solution. For a linear solution,  $u_a(\vec{r}_{i,j} \cdot \vec{n}) = u_a \cdot (\vec{r}_{i,j} \cdot \vec{n})$ , where  $u_a$  is a constant, see fig. A.1.

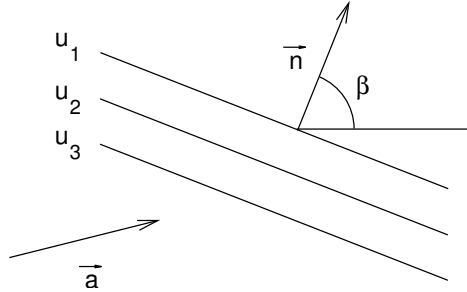


Figure A.1. A linear solution with the gradient in direction  $\vec{n}$ .

The smooth one-dimensional flow solution applied to the monotonicity ratios of (A.9) gives at steady state, when  $\vec{n} = \pm \begin{pmatrix} b \\ -a \end{pmatrix}$ ,

$$R_{i,j} = 1, \quad s_{i,j} = \frac{2n_x\Delta x + n_y\Delta y}{n_y\Delta y}, \quad S_{i,j} = \frac{n_y\Delta y}{2n_x\Delta x + n_y\Delta y}. \tag{A.11}$$

The ratios  $s_{i,j}$  and  $S_{i,j}$  do not have a value of one in smooth flow at steady state. We introduce therefore the scaled ratios with

$$c = \frac{a\Delta x - 2b\Delta y}{a\Delta y} = 1 - 2\gamma, \quad \text{where} \quad \gamma = \frac{b\Delta x}{a\Delta y}, \quad 0 \leq \gamma \leq 1, \quad \tilde{s} = \frac{s}{c}, \quad \text{and} \quad \tilde{S} = S * c. \tag{A.12}$$

In these new variables, the monotonicity condition of (A.3) can be rewritten as  $L \geq A_{i,j} \geq \gamma B_{i,j} \geq 0$ , or

$$L \geq 1 + \frac{1}{2}\phi_{i,j}^x - \frac{1}{2}\frac{\phi_{i-1,j}^x}{R_{i-1,j}} \geq \gamma \left\{ 1 + c \left( \frac{1}{2}\tilde{s}_{i,j}\phi_{i,j}^y - \frac{1}{2}\frac{\phi_{i,j-1}^y}{\tilde{S}_{i,j-1}} \right) \right\} \geq 0. \quad (\text{A.13})$$

The limiter function  $\phi^y$  poses no problem. Any of the classical limiters will do. It is the coupling of the limiting functions  $\phi^x$  and  $\phi^y$  in (A.13) which creates a complication. For  $\gamma \leq 1/2$ , an independent solution for  $\phi^x$  can be found, but for values of  $\gamma \geq 1/2$ , the limiting values of  $\phi^x$  and  $\phi^y$  have to be found simultaneously. Due to this coupling, the solution of the limiting values requires an implicit step, even in an explicit scheme. The problem is of the class of constraint optimization, and solution methods can be found in the book of Strang [22].

For the central scheme of (2.6) the relevant variables are

$$s_{i,j} = \frac{u_{i+1,j+1} - u_{i-1,j}}{u_{i-1,j} - u_{i-1,j-1}}, \quad S_{i,j} = \frac{u_{i-1,j} - u_{i-1,j-1}}{(u_{i+1,j} - u_{i-1,j-1})}. \quad (\text{A.14})$$

Again, the limiter values are coupled.

When limiters become impractical, the pragmatic choice of artificial viscosity could be considered.

## Appendix B. An overview of the number of basis stencils.

Grid-based derivatives are in this paper expressed as the sum of a fixed stencil and a basis of stencils. We present the number of stencils on a domain  $[-m, n]^N$  with  $N = 1, 2, 3$  the number of dimensions, and  $m + n$  the number of nodes along each grid coordinate. The derivatives are used in the approximation of the first, second and third stream-wise derivatives  $\partial u / \partial e_1$ ,  $\partial^2 u / \partial e_1^2$ , and  $\partial^3 u / \partial e_1^3$ . The number of stencils in the tables B.1, B.2, and B.3 corresponds to the number of degrees of freedom for each of the grid-based derivatives which contributes to the stream-wise derivative. The number of degrees of freedom is large, even on relatively small grids, especially in three dimensions. The number of basis stencils is proportional to  $(m + n)^N$ . Only in one dimension there are approximations which consist of the fixed stencil only, and for which the basis is empty. The computation of large bases in three dimensions is time consuming, which explains the missing numbers in table B.3.

The basis can be transformed to one which contains only antisymmetric and symmetric stencils. The symmetry is with respect to the gravity center of the domain,  $1/2(n - m)$  in each coordinate direction. This has the effect that a part of the basis has a truncation error which is an order higher than the remaining part, and therefore becomes of secondary importance. Other constraints like regularity of the basis described in §5.2 further reduce the degrees of freedom.

There is redundancy in the tables since for given  $m + n$ , the basis for the approximation of the first derivative of order  $M$  is also the basis for the approximation of the second derivative of order  $M - 1$  on the same domain. This pattern continues for higher derivatives. The number of antisymmetric and symmetric stencils is therefore only given for the first derivative, with the exception of some of the second derivatives. The bases for second order approximations of second derivatives on  $3^N$  nodes, fourth order on  $5^N$  nodes and so on have no first derivative counterpart.

Also the splitting in antisymmetric and symmetric basis stencils exhibits a pattern. For a given number of nodes  $m + n$  and approximations of order  $M$  and  $M - 1$ , either the number of antisymmetric basis stencils or the number of symmetric basis stencils are the same. The same holds for given  $m + n$  and  $M$  between the a derivative and the next higher derivative. An example is §6.3 where the symmetric part of the basis of §6.2 is used.

The most interesting parts of the tables concern three to five nodes in each direction in three dimensions, which are often encountered in industrial applications.

The degrees of freedom permit to optimize the error. Suppression of the highest derivative(s) normal to the streamline in an advection equation has the effect of increasing the order of accuracy, as is explained in this paper. The optimization in the Fourier domain leads to discretizations with improved stability, which in optimal cases gives the time step restriction of diagonal discretizations.

Table B.1. The number of stencils in one dimension for a given number of nodes and order of the error in the approximation. The numbers in the table are the degrees of freedom for each grid-based derivative which contributes to the derivative  $d^1 = \partial u / \partial e_1$ ,  $d^2 = \partial^2 u / \partial e_1^2$ , or  $d^3 = \partial^3 u / \partial e_1^3$  respectively. The total number of stencils is given, and for  $d^1$  the number of asymmetric and symmetric basis stencils.

	order	1	2	3	4	5	6	7	8
nodes									
2	$d^1$	0							
3	$d^1$	1	0						
		0, 1							
	$d^2$	0	0						
4	$d^1$	2	1	0					
		1, 1	1, 0						
	$d^2$	1	0						
	$d^3$	0							
5	$d^1$	3	2	1	0				
		1, 2	1, 1	0, 1					
	$d^2$	2	1	0	0				
	$d^3$	1	0						
6	$d^1$	4	3	2	1	0			
		2, 2	2, 1	1, 1	1, 0				
	$d^2$	3	2	1	0				
	$d^3$	2	1	0					
7	$d^1$	5	4	3	2	1	0		
		2, 3	2, 2	1, 2	1, 1	0, 1			
	$d^2$	4	3	2	1	0	0		
	$d^3$	3	2	1	0				
8	$d^1$	6	5	4	3	2	1	0	
		3, 3	3, 2	2, 2	2, 1	1, 1	1, 0		
	$d^2$	5	4	3	2	1	0		
	$d^3$	4	3	2	1	0			
9	$d^1$	7	6	5	4	3	2	1	0
		3, 4	3, 3	2, 3	2, 2	1, 2	1, 1	0, 1	
	$d^2$	6	5	4	3	2	1	0	0
	$d^3$	5	4	3	2	1	0		

Table B.2. The number of stencils in two dimensions for a given number of nodes and order of the error in the approximation. The numbers are the degrees of freedom for each grid-based derivative which contributes to the derivative  $d^1 = \partial u / \partial e_1$ ,  $d^2 = \partial^2 u / \partial e_1^2$ , or  $d^3 = \partial^3 u / \partial e_1^3$  respectively. The total number of stencils is given, and for  $d^1$  and some  $d^2$  bases the number of asymmetric and symmetric basis stencils.

	order	1	2	3	4	5	6	7	8
nodes									
2	$d^1$	1 <sup>(1)</sup> 0, 1							
3	$d^1$	6 <sup>(3)</sup> 2, 4	3 <sup>(2)</sup> 2, 1						
	$d^2$		1 <sup>(4)</sup> 0, 1						
4	$d^1$	13 6, 7	10 6, 4	6 <sup>(7)</sup> 2, 4					
	$d^2$	10	6						
	$d^3$	6							
5	$d^1$	22 10, 12	19 <sup>(8)</sup> 10, 9	15 <sup>(6)</sup> 6, 9	10 <sup>(5)</sup> 6, 4				
	$d^2$	19	15	10	6 2, 4				
	$d^3$	15	10						
6	$d^1$	33 16, 17	30 16, 14	26 12, 14	21 12, 9	15 6, 9			
	$d^2$	30	26	21	15				
	$d^3$	26	21	15					
7	$d^1$	46 22, 24	43 22, 21	39 18, 21	34 18, 16	28 12, 16	21 12, 9		
	$d^2$	43	39	34	28	21	15 6, 9		
	$d^3$	39	34	28	21				
8	$d^1$	61 30, 31	58 30, 28	54 26, 28	49 26, 23	43 20, 23	36 20, 16	28 12, 16	
	$d^2$	58	54	49	43	36	28		
	$d^3$	54	49	43	36	28			
9	$d^1$	78 38, 40	75 38, 37	71 34, 37	66 34, 32	60 28, 32	53 28, 25	45 20, 25	36
	$d^2$	75	71	66	60	53	45	36	28 12, 16
	$d^3$	71	66	60	53	45	36		

(1) : see §5.1.

(2) : see §5.2.

(3) : see §5.3.

(4) : see §5.4.

(5) : see §5.6.

(6,7,8) : see §5.7.

Table B.3. The number of stencils in three dimensions for a given number of nodes and order of the error in the approximation. The numbers are the degrees of freedom for each grid-based derivative which contributes to the derivative  $d^1 = \partial u / \partial e_1$ ,  $d^2 = \partial^2 u / \partial e_1^2$ , or  $d^3 = \partial^3 u / \partial e_1^3$  respectively. The total number of stencils is given, and for  $d^1$  and some  $d^2$  some bases the number of asymmetric and symmetric basis stencils.

	order	1	2	3	4	5	6	7	8
nodes									
2	$d^1$	4 <sup>(1)</sup>							
		1, 3							
3	$d^1$	23	17 <sup>(2)</sup>						
		10, 13	10, 7						
	$d^2$	17	10 <sup>(3)</sup>						
			3, 7						
4	$d^1$	60	54	44					
		29, 31	29, 25	19, 25					
	$d^2$	54	44						
	$d^3$	44							
5	$d^1$	121	115	105	90				
		59, 62	59, 56	49, 56	49, 41				
	$d^2$	115	105	90	72				
					31, 41				
	$d^3$	105	90						
6	$d^1$	212	206	196	181	160			
		105, 107	105, 101	95, 101	95, 86	74, 86			
	$d^2$	206	196	181	160				
	$d^3$	196	181	160					
7	$d^1$	339	333	323	308	287	259		
		168, 171	168, 165	158, 165	158, 150	137, 150	137, 122		
	$d^2$	333	323	308	287	259	226		
							104, 122		
	$d^3$	323	308	287	259				
8	$d^1$	508	502	492	477	456	428	392	
		253, 255	253, 249	243, 249	243, 234	222, 234	222, 206	186, 206	
	$d^2$	502	492	477	456	428	392		
9	$d^1$	725	719	709	694	673	645	609	564
		361, 364	361, 358	351, 358	351, 343	330, 343	330, 315	294, 315	294, 270

(1) : see §6.1.

(2) : see §6.2.

(3) : see §6.3.

## References

- [1] G.D. Raithby. Skew upstream differencing schemes for problems involving fluid flow. *Comput. Meth. Appl. Mech. Eng.*, 9:153–164, 1976. Citation on p. 1.
- [2] R.H. Ni. A multiple-grid scheme for solving the Euler equations. *AIAA J.*, 20:1565–1571, 1982. Citation on p. 1.
- [3] S.F. Davis. A rotationally biased upwind difference scheme for the Euler equations. *J. Comp. Phys.*, 56:65–92, 1984. Citation on p. 1.
- [4] J.G. Rice and R.J. Schnipke. A monotone streamline upwind finite element method for convection-dominated flows. *Comp. Meth. in Appl. Mech. and Eng.*, 48:313–327, 1985. Citations on p. 1, 6, and 86.
- [5] T.J.R. Hughes, M. Mallet, and A. Mizukami. A new finite-element formulation for computational fluid dynamics, II. Beyond SUPG. *Comp. Meth. Appl. Mech. & Eng.*, 84, 1986. Citation on p. 1.
- [6] B. van Leer. Progress in multidimensional upwind differencing. Technical Report 92-43, ICASE, NASA Langley Research Center, Hampton, Virginia, sep 1992. Citations on p. 1 and 81.
- [7] R. Struijs. Flux vector distribution. Available at [http://www.ma.utexas.edu/mp\\_arc](http://www.ma.utexas.edu/mp_arc), January 2010. Citations on p. 1, 6, 14, 18, 48, 49, 53, 54, 81, and 84.
- [8] D. Sidilkover. *Numerical solution to steady-state problems with discontinuities*. PhD thesis, The Weizmann Institute of Science, Rehovot, Israel, 1989. Citations on p. 2, 6, 12, 14, 15, 21, 22, 23, 36, 39, 45, and 86.
- [9] G. Dahlquist and A. Bjork. *Numerical Methods*. Prentice Hall, Englewood Cliffs, NJ, 1974. Citations on p. 2 and 42.
- [10] P.L. Roe and D. Sidilkover. Optimum positive linear schemes for advection in two and three dimensions. *SIAM J. Num. Anal.*, 29(6):1505–1825, 1992. Citations on p. 6, 12, 23, 56, 57, 59, and 86.
- [11] F.B. Hildebrand. *Introduction to numerical analysis*. McGraw-Hill, New York, 1956. Citation on p. 10.
- [12] B. Taylor. *Methodus Incrementorum Directa & Inversa*. London, 1715. Citation on p. 10.
- [13] C. Hirsch. Compact schemes for two-dimensional convection problems. In *Von Karman Institute Lecture Series 1991-04*, Computational Fluid Dynamics. Von Karman Institute, Brussels, February 18-22 1991. Citations on p. 12, 14, 21, 22, 25, and 26.
- [14] B. Koren. Low-diffusion rotated upwind schemes, multigrid and defect correction for steady, multi-dimensional Euler flows. In *International Series of Numerical Mathematics*, volume 98. Birkhäuser Verlag, Basel, 1991. Citations on p. 12, 14, 15, 21, 22, 36, and 39.
- [15] For information see <http://www.sciface.com>. Citation on p. 14.
- [16] A. Harten, P.D. Lax, and B. van Leer. On upstream differencing and Godunov-type schemes for hyperbolic conservation laws. *SIAM Review.*, 25:35–61, January 1983. Citation on p. 19.

- [17] T.J.R. Hughes and A. Brooks. A multi-dimensional upwind scheme with no crosswind diffusion. In T.J.R. Hughes, editor, *Finite Elements for Convection Dominated Flows*, AMD, volume 34. ASME, New York, 1979. Citation on p. 22.
- [18] A. Mizukami and T.J.R. Hughes. An accurate upwinding technique for satisfying the maximum principle. *Comp. Meth. Appl. Mech. and Eng.*, 50:181–194, 1985. Citation on p. 22.
- [19] D. Sidilkover and P.L. Roe. Unification of some advection schemes in two dimensions. Technical Report 95-10, ICASE, NASA Langley Research Center, Hampton, Virginia, feb 1995. Citation on p. 23.
- [20] H. Deconinck, R. Struijs, and P.L. Roe. Fluctuation splitting for multidimensional convection problems: an alternative to finite volume and finite element methods. In *Von Karman Institute Lecture Series 1990-03*, Computational Fluid Dynamics. Von Karman Institute, Brussels, March 5-9 1990. Citation on p. 23.
- [21] R. Struijs. *A multidimensional upwind discretization method for the Euler equations on unstructured grids*. PhD thesis, University of Delft, the Netherlands, 1994. Citation on p. 23.
- [22] G. Strang. *Introduction to Applied Mathematics*. Wellesley, 1986. Citations on p. 39 and 94.
- [23] The code HOPDM is available at <http://www.netlib.org>. Citations on p. 39 and 52.
- [24] Bases of stencils are available at <http://www.discretization.basis.heliohost.org>. Citations on p. 45, 51, 65, and 70.
- [25] P.D. Lax and B. Wendroff. Systems of conservation laws. *Comm. Pure and Appl. Math.*, 13:217–317., 1960. Citation on p. 55.
- [26] C. Hirsch. *Numerical computation of internal and external flow*. Vol. 2, Computational methods for inviscid and viscous flows. J. Wiley & Sons, New York, 1990. Citation on p. 55.
- [27] E. van der Maarel. *A local grid refinement method for the Euler equations*. PhD thesis, Universiteit van Amsterdam, feb 1993. Citation on p. 87.
- [28] The related application can be consulted on the web site <http://www.uspto.gov>, patent # 7,239,990. Citation on p. 91.
- [29] S.P. Spekreijse. *Multigrid solution of the steady Euler equations*. PhD thesis, Delft, The Netherlands, 1987. Citation on p. 92.
- [30] B. van Leer. Towards the ultimate conservative difference scheme. II. Monotonicity and conservation combined in a second-order scheme. *J. Comp. Phys.*, 14:361–370, 1974. Citation on p. 93.
- [31] P. K. Sweby. High resolution schemes using flux limiters for hyperbolic conservation laws. *SIAM J. Num. Anal.*, 21(5):995–1011, 1984. Citation on p. 93.